GENE THERAPY FOR AMYOTROPHIC LATERAL SCLEROSIS: AN AAV MEDIATED RNAi APPROACH FOR AUTOSOMAL DOMINANT *C9ORF72* ASSOCIATED ALS

A Dissertation Presented

By

GABRIELA TORO CABRERA

Submitted to the Faculty of the

University of Massachusetts Graduate School of Biomedical Sciences, Worcester

In partial fulfillment of the requirements for the degree of

DOCTOR OF PHILOSOPHY

(March 28th, 2019)

GENE THERAPY FOR AMYOTROPHIC LATERAL SCLEROSIS: AN AAV MEDIATED RNAi APPROACH FOR AUTOSOMAL DOMINANT *C9ORF72* ASSOCIATED ALS

A Dissertation Presented

By

GABRIELA TORO CABRERA

This work was undertaken in the Graduate School of Biomedical Sciences

Interdisciplinary Graduate Program

Under the mentorship of

_____

Christian Mueller Ph.D., Thesis Advisor

_____

Robert H. Brown Jr., DPhil, MD, Thesis Advisor

_____

Guangping Gao, Ph.D., Member of Committee

_____

Victor Ambros Ph.D., Member of Committee

_____

Miguel Sena-Esteves Ph.D., Member of Committee

_____

Christopher Shaw, MBChB, MD, FRACP, FRCP(Hon), FMEDSci, FANA., External Member of Committee

_____

Terence Flotte, MD, Chair of Committee

_____

Mary Ellen Lane Ph.D., Dean of the Graduate School of Biomedical Sciences

March 28th, 2019

Dedication

I dedicate this thesis to my mom Anita, my abuelita Elsita and my son Matteo

Thank you for your love and unconditional support

I couldn’t have done this without you

Acknowledgements

I would like to thank my family for their love and support. Especially my mom who has always been there for me in every possible way. I have achieved my dreams because she has always encouraged me and pushed me to be a better person. My grandma who always believed in me, I know she's watching over me every day. My brother who also always supported me. My aunt Elsie, my uncle Jim and my cousins Cristina and Stephanie who always stood by me and helped me make Massachusetts my second home.

I would like to thank my mentors Chris Mueller and Robert Brown, for always supporting me and guiding me to become a successful scientist. Especially Chris who worked with me closely teaching me to manage my projects and solve problems on a daily basis.

I am also very thankful to all the members in my committees: Dr. David Weaver, Dr. Daryl Bosco, Dr. Guangping Gao, Dr. Victor Ambros, Dr. Miguel Sena Esteves and Dr. Terry Flotte who has remained as Chair in my committees these past 6 years. Thank you all, for always finding the time to meet and discuss with me; new findings, failed experiments, troubleshooting issues and how to improve as a scientist. I would also like to extend my gratitude to my external member Chris Shaw for overseeing my dissertation. I am truly honored to have had such amazing scientists lead me through this path.

I would like to thank all the members of the Brown lab especially Alex Weiss, Nick Wightman, Ozgun Uyan, Dr. Helen Tran and Zack Kennedy for support, guidance and being great friends. Extreme gratitude towards Zachariah Foster thank you for your hard work, commitment and friendship.

Especial thanks to all the members and former members of the Mueller Lab. Huaming Sun, Hiroko Nagase, Nirmal Singh and Kailai Duan. As well as former members from the Esteves lab: Sourav Choudhury and Lorelei Stoica, thank you for being great friends and teachers. Thank you to all the members and former members of the Gene Therapy Center, working with everyone was a wonderful experience.

Finally, I need to thank my friends, I could not have completed my PhD. without your encouragement. Alisha Gruntman, I am so thankful for being able to call you my friend. I love you like a sister, thank you for everything! Sara Lewandowsky, thank you for being such a great friend, we were so lucky to be roommates throughout most of this journey! Allison Keeler and Meghan Blackwood, I will miss you guys so much, and all the motherly advice. Abbas Abdallah thank you amigo for all the support. Janine Rojas, Luke Myotte, Andrea Arauz, Carolina Herrera, Guinevere Lourenco, and Lina Song, thank you for letting me lean on you during difficult times. Every single one of you holds a special place in my heart.

Abstract

Amyotrophic lateral sclerosis (ALS) is a terminal neurodegenerative disease that affects motor neurons causing progressive muscle weakness and respiratory failure. In 2011, the presence of a hexanucleotide repeat expansion within chromosome 9 open reading frame 72(*C9ORF72*) was identified in ALS patient samples, becoming the major known genetic cause for ALS and frontotemporal dementia (FTD). Carriers of this mutation present reduced levels of *C9ORF72* mRNA, RNA foci produced by the aggregating expansion and toxic dipeptides generated through repeat-associated non-ATG translation. These findings have led to multiple hypotheses on the pathogenesis of C9ORF72: 1) Haploinsufficiency, 2) RNA gain-of-function, 3) RAN Translation, and 4) Disrupted nucleocytoplasmic trafficking. Due to lack of treatments for this disease, we have pursued an AAV-RNAi dependent gene therapy approach, using an artificial microRNA (amiR) packaged in a recombinant adeno-associated virus (rAAV). After validating our *in vitro* results, we advanced to *in vivo* experiments using transgenic mice that recapitulate the major histopathological features seen in human ALS/FTD patients. Adult and neonate mice were injected through clinically relevant routes and our results indicate that AAV9-mediated amiR silencing not only reduced mRNA and protein levels of *C9ORF72* but also the expansion derived toxic GP dipeptides. Although our amiR is not targeting the expansion itself but exon 3, we illustrate here that the evident dipeptide decrease is achievable due to the presence of aberrant transcripts in the cytoplasm containing miss-spliced Intron-HRE-*C9ORF72* species. These encouraging results have led to the continued testing of this treatment as a therapeutic option for *C9ORF72* - ALS patients.

Table of Contents

Chapter **Page**

List of Tables

Table **Page**

List of Figures

Table **Page**

Appendix

List of Copyrighted Materials Produced by the Author

1. Toro Cabrera G., Mueller C. (2016) Design of shRNA and miRNA for Delivery to the CNS. In: Manfredsson F. (eds) Gene Therapy for Neurological Disorders. Methods in Molecular Biology, vol 1382. Humana Press, New York, NY.

2. Peters, O. M., Cabrera, G. T., Tran, H., Gendron, T. F., McKeon, J. E., Metterville, J., Weiss, A., Wightman, N., Salameh, J., Kim, J., Sun, H., Boylan, K. B., Dickson, D., Kennedy, Z., Lin, Z., Zhang, Y. J., Daughrity, L., Jung, C., Gao, F. B., Sapp, P. C., Horvitz, H. R., Bosco, D. A., Brown, S. P., de Jong, P., Petrucelli, L., Mueller, C., … Brown, R. H. (2015). *Human C9ORF72* Hexanucleotide Expansion Reproduces RNA Foci and Dipeptide Repeat Proteins but Not Neurodegeneration in BAC Transgenic Mice. Neuron, *88*(5), 902-909.

3. Esanov, R., Cabrera, G. T., Andrade, N. S., Gendron, T. F., Brown, R. H., Benatar, M., Wahlestedt, C., Mueller, C., … Zeier, Z. (2017). A C9ORF72 BAC mouse model recapitulates key epigenetic perturbations of ALS/FTD. Molecular neurodegeneration, 12(1), 46. doi:10.1186/s13024-017-0185-9

PREFACE

Chapter II
Certain paragraphs were modified from: unpublished manuscript

Chapter III
Formatted and modified from: Toro Cabrera G., Mueller C. (2016) Design of shRNA and miRNA for Delivery to the CNS. In: Manfredsson F. (eds) Gene Therapy for Neurological Disorders. Methods in Molecular Biology, vol 1382. Humana Press, New York, NY.

Chapter IV
Figures formatted from Peters, O. M., Cabrera, G. T., Tran, H., Gendron, T. F., McKeon, J. E., Metterville, J., Weiss, A., Wightman, N., Salameh, J., Kim, J., Sun, H., Boylan, K. B., Dickson, D., Kennedy, Z., Lin, Z., Zhang, Y. J., Daughrity, L., Jung, C., Gao, F. B., Sapp, P. C., Horvitz, H. R., Bosco, D. A., Brown, S. P., de Jong, P., Petrucelli, L., Mueller, C., … Brown, R. H. (2015). Human C9ORF72 Hexanucleotide Expansion Reproduces RNA Foci and Dipeptide Repeat Proteins but Not Neurodegeneration in BAC Transgenic Mice. Neuron, 88(5), 902-909.

Chapter V
Formatted and modified from manuscript to be submitted as: Gabriela Toro Cabrera Abbas Abdallah, Helene Tran, Zachariah Foster, Alexandra Weiss, Nicholas Wightman, Rachel Stock, Tania Gendron, Alisha Gruntman, Anthony Giampetruzzi, Leonard Petrucelli, Robert Brown, Christian Mueller. (2019). "Artificial microRNA silences *C9ORF72* variants and decreases toxic dipeptides *in vivo*"

Appendix I
Excerpts and figures modified from publication: Esanov, R., Cabrera, G. T., Andrade, N. S., Gendron, T. F., Brown, R. H., Benatar, M., Wahlestedt, C., Mueller, C., … Zeier, Z. (2017). A C9ORF72 BAC mouse model recapitulates key epigenetic perturbations of ALS/FTD. Molecular neurodegeneration, 12(1), 46. doi:10.1186/s13024-017-0185-9

CHAPTER I

Overall Introduction

In 2011 a newly discovered gene mutation was shown to be the major cause for not only (ALS) but also for Frontotemporal dementia (FTD). At the time there were only 2 publications describing the presence of a hexanucleotide repeat located in the first intron of chromosome 9 open reading frame 72 (*C9ORF72*). Since then ~three thousand papers have been published referencing this mutation and the importance of finding a therapeutic strategy for the leading genetic cause of ALS and FTD.

In my thesis I will address a possible therapeutic strategy using recombinant adeno-associated virus (rAAV) mediated RNA interference (RNAi) to silence the toxic gene products produced by *C9ORF72*. In Chapter II, I will initially describe ALS and the *C9ORF72* mutation. I will then summarize in Chapter III, the RNAi pathway and how to design artificial microRNAs or shRNAs for delivery to the central nervous system (CNS).

As a group, we also generated a BAC transgenic mouse model containing the human *C9ORF72 gene* with approximately 500 repeats of the GGGGCC motif. The mice showed no overt behavioral phenotype but recapitulated distinctive histopathological features of *C9ORF72* linked ALS/FTD, including sense and antisense intranuclear RNA foci and poly (glycine-proline) dipeptide repeat proteins. In addition to creating this mouse model we sought to prove that this model could be a valuable tool in the study of ALS/FTD pathobiology and therapeutic testing. In doing so, an AAV mediated artificial microRNA (amiR) was designed and tested targeting *C9ORF72* in primary cortical cultures obtained from this mouse. In Chapter IV, I will not only describe the characterization of the C9BAC

mouse model, but also that gene therapy could be used as an approach to attenuate expression of the C9BAC transgene and decrease the poly GP dipeptides *in vitro*.

Chapter V will encompass the pipeline illustrated in **Figure 1.1**, for the *in vitro* screening and *in vivo* validation as well as relevant peripheral and CSF surrogate injection routes for therapeutic delivery in mice.

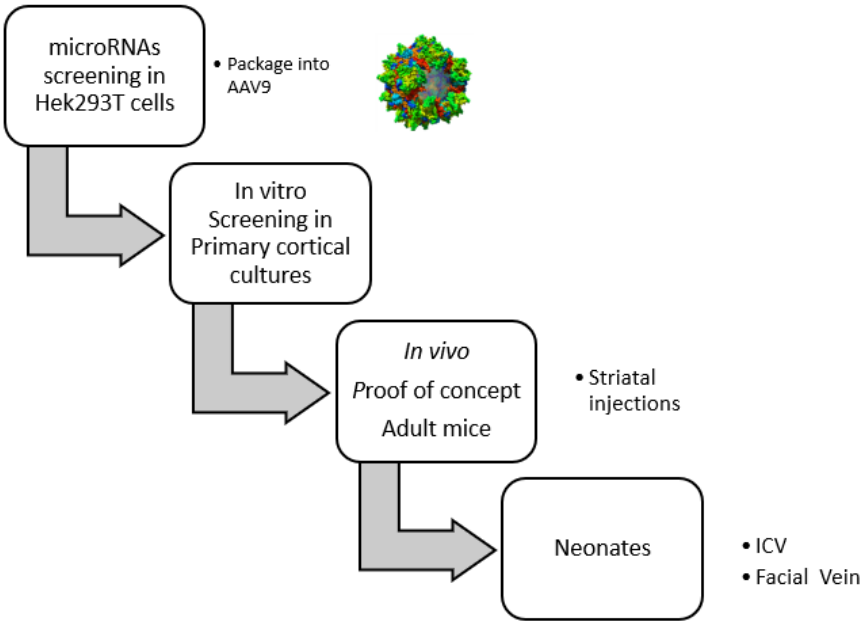

Figure 1.1 Pipeline for microRNA screening and validation

After a preliminary screening in HEK293T cells, the selected microRNAS are packaged into recombinant adeno associated virus (rAAV) serotype 9, which crosses the blood brain barrier (BBB). *In vitro* screening will take place in cortical primary neurons from a BAC transgenic ALS mouse model. *In vivo* proof of concept studies will entail striatal injections in adult mice, followed by local and systemic deliveries to neonate mice.

I hypothesized that AAV mediated amiR silencing of *C9ORF72* could decrease *C9ORF72* toxic mRNA levels and the corresponding protein. To achieve this several amiRs were designed to target all three variants of *C9ORF72*. Knowing that microRNAs primarily act in the cytoplasm as post-transcriptional gene repressors we expected to see an overall

decrease of all *C9ORF72* gene products, with the exception of the nuclear RNA aggregates (foci). After screening, the best amiR candidate was packaged into AAV9 vector for *in vitro* and *in vivo* delivery to adult and neonatal mice through various injection routes. Here I demonstrate that an AAV9 mediated delivery of a H1-amiRC9 against *C9ORF72* effectively leads to a decrease of mRNA, protein and more importantly the most abundant dipeptide (GP) in the brain and spinal cords of *C9ORF72* BAC transgenic mice. These findings suggest that amiRs delivered by AAV9 vector are a potentially viable therapeutic strategy for C9 linked ALS/FTD cases.

In collaboration with a group at the University of Miami we identified key ALS/FTD epigenetic factors present in the *C9ORF72* BAC mouse model. Similar to what is observed in patient populations we found that a subset of C9BAC mice had epigenetic perturbations caused by the hexanucleotide repeat, such as DNA histone methylation. These findings suggested that epigenetic aberrations in the presence of the expansion may lead to repression of the *C9ORF72* gene and delay of disease progression. This research will be discussed in appendix I.

In addition to working with ALS as a neurodegenerative disease we also sought to use AAV mediated RNAi as an approach to treat other neuronal diseases such as hereditary sensory and autonomic neuropathy 1 (HSAN). This disease is the most common neuropathy known to affect peripheral sensory nerves, the main mutation linked to HSAN1 is a lack of function of the *SPTLC1* gene. In appendix II, I will describe a summary and preliminary data from an in *vitro* screening of artificial microRNAs targeting the *SPTLC1* gene for silencing and the potential use of gene replacement therapy to restore normal *SPTLC1*.

CHAPTER II

C9ORF72 hexanucleotide repeat expansion, the major cause for ALS/FTD

Introduction

Amyotrophic lateral sclerosis (ALS), is a lethal neurodegenerative disease that affects approximately 2 in every 100,000 persons worldwide [1, 2]. Patients suffering from this disease have an average life expectancy of 2-5 years after symptom onset. Over time, they develop progressive muscle wasting and shortness of breath, losing their ability to move freely or breathe on their own [3]. Although ALS was first described in the early 1800's as a motor neuron disease the root cause or prediction of a degeneration pattern still remains to be identified. [1,2] Nonetheless, ALS has been further classified as sporadic or familial ALS depending on genetic inheritance with only 5% of all cases being of known origin. [4-7]

Recently, two independent groups [8, 9] conducting genomics studies of ALS and frontotemporal dementia (FTD) patient samples found an expanded hexanucleotide repeat expansion (HRE) of (GGGGCC) located in the non-coding intronic region of chromosome 9 open reading frame 72(*C9ORF72*). These expanded repeats, hundreds to thousands compared to healthy variation of 23-30, differ in number depending on the tissue; so far, the most substantial repeats are observed in the brain. [8, 9]. To date, *C9ORF72* HRE accounts for the majority of familial and sporadic ALS (**Figure 2.1**) as well as 20% of familial and 6% of sporadic (FTD) cases [8, 9] [10]

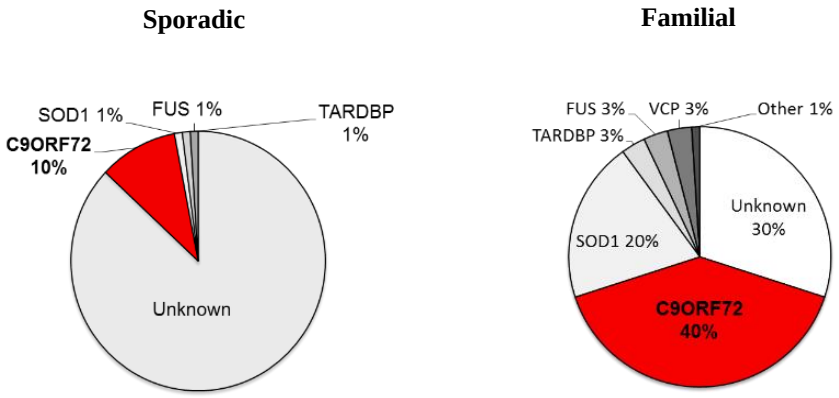

Figure 2.1 Familial and Sporadic ALS gene architecture

The Sporadic ALS pie chart is indicating that most cases are considered unknown with 10% accounting for *C9ORF72* cases. The Familial ALS pie chart shows *C9ORF72* as the prevalent mutation accounting for 40% of the cases followed by Unknown, SOD1, TARDBP, FUS, VCP, Others.

Three main splice variants have been validated by NCBI as the major products of the *C9ORF72 gene:* Variant 1 (NM_145005.5), Variant 2 (NM_018325.3), and Variant 3 (NM_001256054.1). Variants 1 and 3 containing the expansion are the least abundant, contrary to V2, which is the more abundant variant **(Figure 2.2)**. While the function of the *C9ORF72* protein isoforms remains to be determined they have been linked to (differentially expressed in normal and neoplastic cells) DENN proteins which interact with Rab GTPases in membrane trafficking , endosomal trafficking and nucleocytoplasmic transport.[11-13]

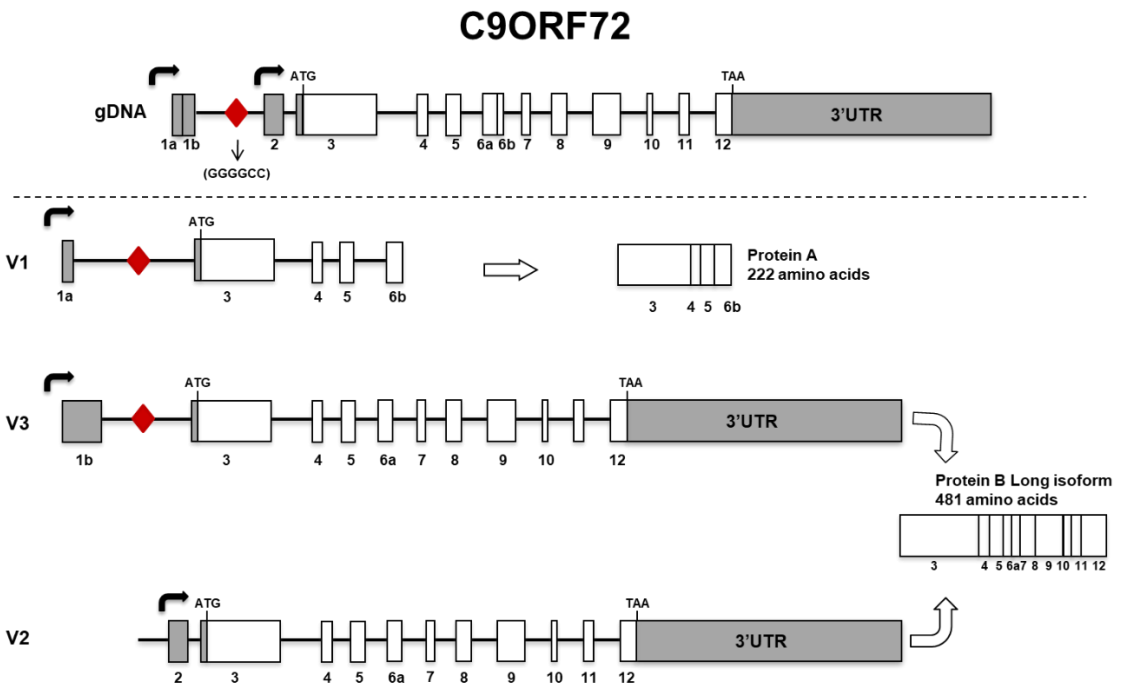

Figure 2.2. Schematic of the *C9ORF72* gene

Following the NCBI nomenclature the *C9ORF72* gene is 28kb long and has 12 exons. The hexanucleotide repeat expansion (HRE) depicted by the red diamond in located in the first intron exons 1-2. Two different promoters and alternative splicing give rise to 3 variants, V1 is the short isoform that codes a 222 aa protein and variants 2 -3 code for the same 481 aa protein. Only V1-V3 carry the expansion along with the 80 bp non coding Exon 1a and 158bp long Exon 1b respectively.

The presence of the HRE causes a series of consequential effects including an overall reduction of *C9ORF72* mRNA, an accumulation of *C9ORF72* sense and antisense transcripts resulting in nuclear RNA foci, and the presence of long dipeptide chains generated by repeat-associated non-ATG translation (RAN) in the cytoplasm. [11, 14] These findings led to three hypotheses on the pathogenesis of *C9ORF72:* **(Figure 2.3)**: (1) Haploinsufficiency, where decreased levels of mRNA lead to insufficient gene product. [15-17] (2) RNA gain-of-function, where the expanded RNA foci sequester RNA binding

and/or splicing proteins [18] (3) RAN translation of the hexanucleotide expansion, in which all reading frames of both a sense and antisense RNA is translated, generating toxic poly-dipeptide protein inclusions [19-22] (3)

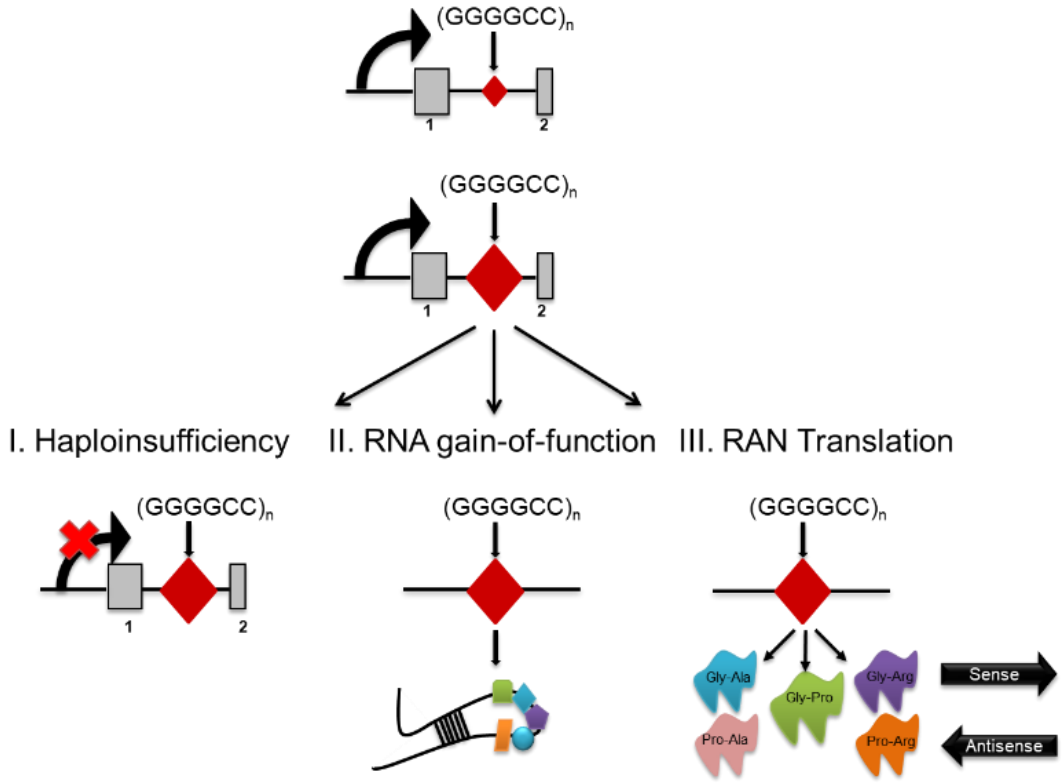

Figure 2.3 Hypotheses for *C9ORF72* disease pathology

There are 3 major putative mechanisms underlying *C9ORF72* (HRE). (1) Involves a loss on function of *C9ORF72*, (2) an RNA gain of function and (3) RAN translation of toxic dipeptides.

Glycine Proline (GP) dipeptides are the most abundant since it is translated from both sense and antisense reading frames, and Arginine containing dipeptides, Glycine Arginine (GR) and Proline Arginine (PR) are the most toxic to the cells when overexpressed *in vitro* and

in *drosophila* fly models [12, 14]. A recent (PR) mouse model was used to show that this dipeptide was bound to DNA within heterochromatin resulting in cellular aberrations [13]. These dipeptides can co-localize with p62 staining yet do not form TDP43 inclusions. A series of recent publications have also proposed that *C9ORF72* HRE may disrupt nucleocytoplasmic transport. [11, 12, 14, 23, 24] While the main cause for motor neuron death is still unclear, it may simply be the result of several of these molecular hallmarks simultaneously compounding and overwhelming the cell.

Due to the intricacy of this disease, finding an effective therapeutic strategy has not been feasible. Currently, patient treatment is limited to palliative care or two main medications approved by the food and drug administration (FDA); Riluzole (Rilutek) [25] and Edaravone (Radicava) [26, 27]. Riluzole is a pharmacological agent that blocks sodium channels and impedes the release of glutamate from nerve terminals protecting neurons from overstimulation, human clinical trials have shown prolonged survival for only a few months[25]. Radicava alternatively acts by reducing oxidative stress leading to neuronal protection. This treatment requires intravenous administration of the drug for 14 days in 28-day cycles for a minimal reduction in disease progression. [26, 27] Thus, the need for a new and enhanced therapeutic approach has encouraged the scientific community to devise new means to target and safely deliver agents. We developed an approach using RNA interference (RNAi) molecules to target *C9ORF72* for post-transcriptional silencing.

The major concern while developing a therapeutic strategy other than the effectiveness of said technology, is finding a way to deliver it safely and to the desired target tissue. Specifically, when working with diseases that affect the CNS, the main obstacle is getting

the therapeutic across the blood brain barrier (BBB). This barrier serves as a defense mechanism against pathogens and toxins, while allowing certain ions, molecules and cells to pass in a controlled manner.[28] Previous attempts for protein replacement therapy would not only be thwarted by the presence of the BBB but also by limitations in protein half-life, dose and possible toxicity. Although the BBB can be bypassed by direct injections, in patients' however, repetitive brain or intrathecal injections can lead to a higher risk of contracting cerebral infections. Reagents such as nanoparticles or antisense oligos can deliver or express a therapeutic agent however toxicity and recurrent injections to deliver said therapeutics over time can become overwhelmeing and dangerous for patients.[29] [30] [31] The use of recombinant adeno-associated vectors (rAAV) as tools to mediate transgene delivery has overcome these hurtles and become the safest and most reliable path to obtain sustained expression of a transgene in mice, non-human primates and in clinical trial patients.

Recombinant adeno-associated virus (rAAV) as a vehicle for therapeutic delivery

Initially wild type (WT) AAV was found as a contaminant of adenovirus (Ad) cultures. This single stranded 4.7kb DNA virus contains two genes (*rep) replication* and (*cap) capsid*. *Rep* genes produce four proteins, two involved in genome replication (78-68) and two involved in genome packaging (52-40). *Cap* genes produce 3 proteins VP1-VP2-VP3 at a 1:1:10 ratio, these proteins are involved in capsid production and generating an icosahedral structure.In addition to the assembly activating protein (*AAP*) gene, coded within cap has also been linked to vector construction. These genes are flanked by 125 nt palindromic sequences called inverted terminal repeats (ITRs) which are crucial for genome replication and packaging [32].

As a member of the *Parvovirinae* family it is non-pathogenic and replication deficient, requiring the aid of a helper virus such as Adenovirus(AD), Herpes simples virus (HSV) type I,II, Baculovirus, Cytomegalovirus or Pseudorabies in order to replicate. Other non common paths involve making the virus susceptible by using agents such as Ultraviolet irradiation (UV), cycloheximide, hydroxyurea, topoisomerase inhibitors and chemical carcinogens. [30] However for the purpose of packaging rAAV as a therapeutic vehicle addition of a helper virus along with a plasmid containing the rep and cap genes, is the standard approach also known as triple tranfection. [33-35]

To use AAV for gene delivery the plasmid is modified to retain only the wild type ITRs and the *rep* and *cap* gene are replaced with the transgene of interest [36]. The packaging capacity is ~4.7 kb of single stranded DNA for which expression can be detected three to four weeks post delivery. The delay in expression results from the time needed to generate the complentary strand [37]. This can be bypassed by packaging double straned or self complementary DNA ~2.3kb where gene expression can be detected two weeks post injection. This is a limiting factor for genes too large to be packaged within AAV, however new strategies have evolved, using shorter promoters or truncated versions of the transgenes in order to fit the transgene in the vector. Other studies involve trans-splicing AAV vectors by using the recombination capabilities of the ITRs. A desired ~9kb transgene cassette can be split between two vectors, each containing the appropriate donor and acceptor sites and can be re-combined to create a full message once inside the cell [38].

Because the AAV capsid will determine the cell tropism, multiple capsids have been discovered, modified or generated to improve cell tropism, infectivity and specificity. This vast library of vectors is available for researchers to test the more adequate capsid for each

therapeutic purpose. [28]. For my thesis work we have chosen to use rAAV9. This capsid crosses the BBB and transduces a wide neuronal population including astrocytes, and motor neurons in the brain and spinal cord of rodents and non-human primates[39-46] An additional benefit of using rAAV9 as a delivery tool for the CNS, is that motor neurons are non-dividing cells, so once the cells are transduced they will sustain transgene expression indefinitely. Keeping in mind that although rAAV9 will transduce cell populations in the CNS it will also leak systemically and transduce the liver, heart, muscle. Luckily there are ways to use tissue specific promoters to restrict this moving forward. [28, 47]

A common concern when treating diseases where the targeted cells will continue to replicate is loss of rAAV expression overtime. Since rAAV remains episomal it will not replicate along with the host cell. Depending on the turnover rate of the cells, rAAV will go through a dillution effect which will then lead to a decrease of overall transgene expression. Whoever as long as a significant population of cells continue to express the transgene of interest, the expression levels produced may be sufficient to maintain normal cell function for an extended period of time. [42, 48, 49]

Another concern when using rAAV as a vehicle is generating an immune response towards either the capsid or to transgene within it. Because AAVs are common within the human population the presence of neutralizing antibodies (nab) is a complication which can be managed to a degree using immunosupressors [50]. However pre-screening of possible gene therapy candidates can provide information inregards to the presence of neutralizing antibodies against specific serotypes. In which case using a different serotype may be the simplest solution [50].

Understanding the biology of AAV, the immunological response to rAAV and finding ways to improve rAAV capsids, production and their purification is a continued goal that further provides confidence in the use of this technology as a means for therapeutic delivery.

CHAPTER III

Design of shRNA and microRNA for delivery to the Central Nervous System

Introduction

There are many well-known human neurodegenerative diseases, such as Parkinson's, Alzheimer's and Huntington's, that specifically affect neurons [51]. Neuronal cells, unlike other cells in the body are non-regenerating; therefore if they suffer damage they may deteriorate and die without being replaced [52]. Neuronal loss can lead to many symptoms of neurologic disease such as ataxia (uncoordinated movements) and/or dementia (loss of mental health and higher thought processing) [51-56]. Every year the number of patients diagnosed with one of these illnesses increases [57, 58]. Currently there is an increased interest in neuroscience research a lot of which is focused in pursuit of a treatment that will slow the progression and/or cure these diseases. To this end many approaches are constantly being developed. The discovery of RNA interference (RNAi) as well as the use of viral vectors as mediators for delivery has given gene therapy the possibility to treat diseases caused by a toxic gain of function, such as Huntington's and ALS [59].

The RNAi mechanism entails the transcription of sequence specific small RNAs that bind in a complementary manner to their target messenger RNA (mRNA) forming double strand RNA (dsRNA). The cells innate defense response to dsRNA is to induce its degradation [60]. This response evolved to regulate gene expression or as protection against exogenous, single stranded DNA seen, for example, from viruses [61, 62].

RNAi was first observed in plants in 1990, followed by its description in the nematode *Caenorhabditis elegans* in 1998 by Craig Mello and Andrew Fire [63]. Small RNAs such

as short hairpin RNAs (shRNAs) and micro RNAs (miRNAs) enter the RNAi pathway and act as post-transcriptional gene regulators [59, 60, 63]. Researchers have designed artificial short hairpin RNAs (shRNAs) and micro RNAs (miRNAs) to target specific gene sequences.

Engineered miRNAs are designed based on the endogenous miRNA biogenesis. They are commonly transcribed from genes by RNA polymerase II (pol II) or less frequently by RNA polymerase III (pol III). Pol II promoters transcribe precursors for small RNAs, mRNA, snRNA and microRNAs. Pol III are strong promoters that not only synthesize small RNAs but are also transcribing housekeeping genes that are expressed abundantly throughout different cell types.[64]

After being transcribed, miRNAs transcripts are capped at the 5’ end, and polyadenylated at the 3’ end. This structure is termed primary miRNA (pri-miRNA). Pri-miRNAs will then be recognized by the protein/enzyme complex DGCR8/Drosha and further cleaved to precursor miRNAs (pre-miRNAs)[65]. Pre-miRNA hairpins are then structurally recognized by the nuclear receptor Exportin-5, which will guide it to the cytoplasm [65]. In the cytoplasm the RNase III enzyme Dicer serves as a molecular ruler that will recognize dsRNA and cleave a specified distance from the 3’end overhang[66], or 5’ end phosphate group[67] resulting in a 22-nucleotide miRNA: miRNA duplex[66]. This duplex is made up of a guide strand, which will enter the RNA- induced silencing complex (RISC), and a passenger strand, which will be degraded. Once in the RISC complex the guide strand will bind to its target mRNA. If the guide strand, is perfectly complementary to the target sequence the result will be cleavage by the catalytic component of RISC, argonaut 2

(AGO2)[59, 65, 68]. However, if there is only partial complementarity at the seed sequence (2-8 nt) with the target sequence the result will be translational repression.

Short hairpin RNAs are commonly transcribed from pol III promoters (e.g. U6 or H1) however, pol II and cell specific promoters can be an alternative option though scarcely used [69]. Unlike miRNAs they enter the RNAi pathway as hairpins skipping cleavage by Drosha and being shuttled through Exportin-5 to the cytoplasm where they follow the same miRNA Dicer- RISC route. A diagram of the RNAi pathway can be found in (Borel. 2013) [59]. Although these molecules are designed to only bind to their target, there may be instances where there are off target effects. Given that miRNAs can regulate translation by just binding at the seed sequence it's difficult to repress all off-target effects [70]. However, the engagement of the slicer activity from AGO2 relies on more extensive base pairing as mentioned above, the off-target effects for this can be more easily controlled. Several bioinformatics tools and websites exist that will allow the user to query their sequence to find theoretical targets to minimize the off-target effects. [71]

A debatable issue regarding shRNAs driven by strong pol III promoters has been cell toxicity caused by overload of the RNAi machinery. Saturation occurs when artificial molecules and endogenous microRNAs compete to enter this pathway and exit it through Exportin-5 [59, 72]. Researchers have compared toxicity levels between miRNAs driven by pol III promoters and shRNAs; they found that although miRNAs have an extra saturable step in the nucleus in addition to the cytoplasmic, they cause less toxicity than shRNAs. Results by Maczuga, P., et al. (2012) also show that although using a pol II (CMV) promoter lead to reduced toxicity compared to pol III driven shRNAs, the overall effectiveness of miRNAs was more consistent than that of shRNAs [73].

Additionally, vector-derived genes can transcribe artificial miRNAs by either pol II or pol III; allowing researchers to use pol II tissue specific promoters. These factors have encouraged investigators to opt for the use of miRNAs for long-term expression and silencing rather than using shRNAs for therapeutic purposes.

In this chapter detailed instructions for the proper design of miRNA and an shRNA will be discussed in addition to guidance on how to design an *in vitro* screen prior to packaging these constructs in either recombinant Adeno Associated Viruses (rAAV) or lenti-virus for an *in vivo* delivery. The main goal is to design molecules with the potential of being delivered to the CNS for therapeutic purposes.

Methods

Selection of RNA target sites and design of miRNA or shRNA

First, one selects the target sequence to be silenced. Both miRNAs and shRNAs can be designed to be species specific, or to target a region conserved across various species. In addition, these molecules can also be tailored to target a single variant or multiple variants produce by a gene. The sequences can be obtained at the National Center for Biotechnology Information (NCBI) http://www.ncbi.nlm.nih.gov/refseq/.

With the aid of an RNA folding software [74] , which computes an algorithm for base pair probabilities, thermodynamics and circular RNA folding; the structure of the target sequence can be analyzed. The prediction software will allow the visualization of the secondary structure of the target sequence and all looped areas of single stranded RNA that are at least 22 nucleotides long will serve as target sites.

microRNA design

The 22-nucleotide sequence from the loops identified can be selected and copied into a microsoft word document. Within each sequence the 5' end should contain an A or a U as the first base of the microRNA, this will improve thermodynamic stability, and allow for enhanced AGO2 loading.[75]. The following 19-21 nucleotides selected should be unique to the intended target. To verify this, the BLAST database from NCBI (http://blast.be-md.ncbi.nlm.nih.gov/Blast.cgi) can be used as a tool to ensure there are no mistargeting effects.

Another feature to consider is the GC content of the selected sequence, the preferential range should lie between 20-70%. An example of a target sequence is shown in **(Figure 3.1)** this sequence has a GC content of 57.1%. The GC calculation can be done manually by counting the number of G's, C's and dividing by the total number of nucleotides in the sequence. Or online calculators are available on the web https://molbiol-tools.ca/DNA_composition.htm

The addition of a basal UG motif immediately after the stem-loop at position 14 can also be added to the microRNA design, it has been shown to enhance Dicer binding [75]. At least 5 different possible target regions should be designed and screened.

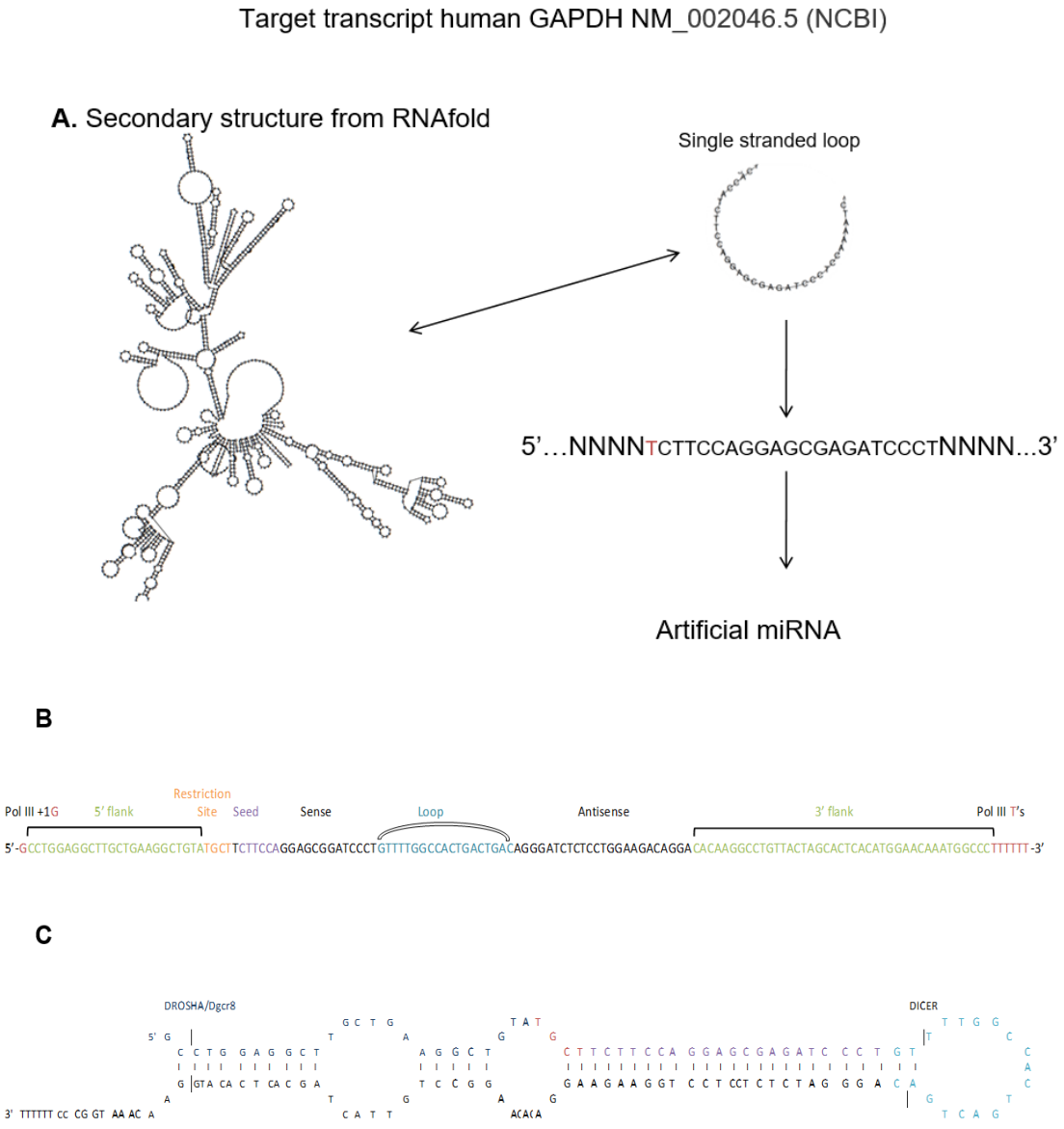

Figure 3.1: An example of a microRNA designed against the human housekeeping gene GAPDH NM_002046.5 (NCBI)

Both flanks and loop have been modified and adapted from human miR155. A) Indicates the folding structure of GAPDH obtained from the software, zoomed into the loop to be targeted. B) Starting from the 5' end the microRNA contains flank sequences, which will form part of the structure and cleavage sites recognized by Drosha. The 5' flank is followed by the 22-nucleotide sequence that contains a seed sequences from nucleotides 2-8, and a mismatched loop. The antisense sequence is the reverse compliment of the sense sequence with nucleotides from positions 10-11 deleted to form an unpaired bulge. The sequence has a +G modification that should be added if cloning into a plasmid with a U6 promoter, and a tail of 6 T's as the terminator. C) Depicts the folding structure of the designed microRNA.

shRNA Design

After identifying and selecting the 22-nucleotide target sequence the following 19-nucleotides comprise a loop structure adapted from an endogenous microRNA (human miR155 in this case). After the loop the reverse complement of the 22 nucleotides will be added to form a hairpin structure. The conserved loop structure will contain the cleavage sites needed for Dicer to cleave it and leave a dsRNA duplex. Adding a multiple cloning site to the construct design is a useful tool, when cloning into different expression cassettes. Selection of a pol III U6 or H1 promoter would be at the discretion of the designer. Nonetheless if a U6 promoter is selected an additional +1-G must be added at the 3' end of the promoter. **(Figure 3.2)**

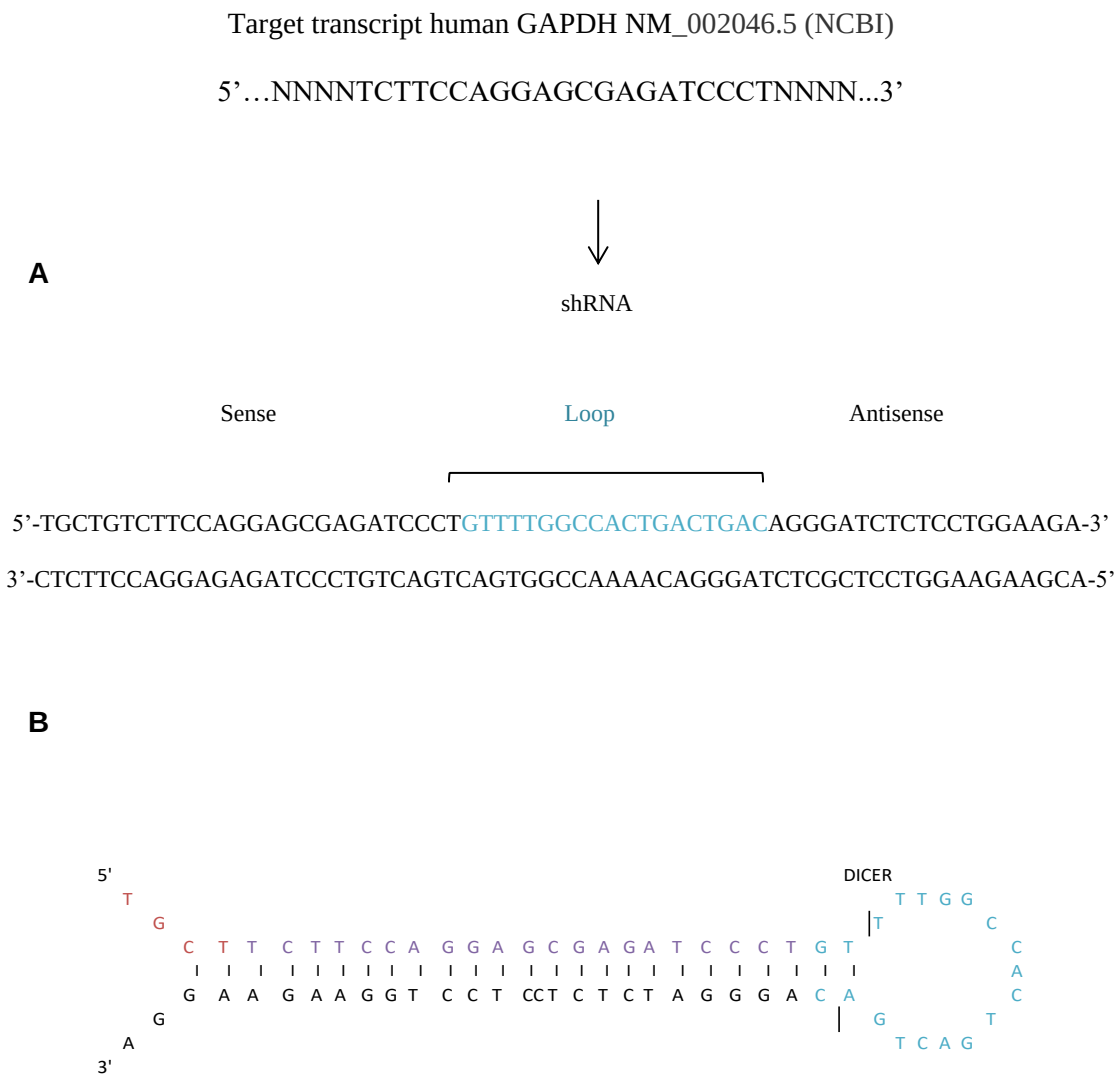

Figure 3.2: An example of an shRNA designed to target the human housekeeping gene GAPDH NM_002046.5 (NCBI)

The loop has been modified and adapted from hsa-miR155. In panel A) starting from the 5' end is a restriction site for cloning; followed by the sense 22-nucleotide sequence, then a 19-nucleotide loop that contains the 2nt- 3'overhang site for Dicer cleavage, and finally the antisense 22-nucleotide sequences with bases in positions 10-11 deleted to form a bulge. The bottom strand is the reverse complementarity of the top strand. In panel B) is an image of the folding structure of the shRNA.

Backbone design

Either endogenous miR155 or miR30 are commonly used as backbones to design the artificial microRNA and shRNA. For the microRNA design both the 3' and 5' flanks, as well as the loop region are adapted from the endogenous miRNA of choice **(Figure 3.1)**. For the shRNA design only the loop region is adapted as the backbone **(Figure 3.2)**. The 5' and 3' flank sequences of 50-100nts, from the endogenous microRNA of choice should contain the structural cleavage areas for the Drosha-DGCR8 machinery to bind. Drosha will sit 40nt upstream and downstream of the pre-miRNA hairpin, these flanking sequences complement each other and leave single stranded areas at the base of the stem loop that the microprocessor will recognize as substrate. Refer to [68, 76-78]. In addition to the flanks a loop from a naturally occurring microRNA should be selected. Dicer will recognize the hairpin shaped pre-mRNA. Refer to (Gu et al., 2012) [79] on specific details for loop design and (Lewis et al., 2003 , and Siolas et al., 2003) for problems concerning improper Dicer cleavage [80, 81].

Introduction of the 20-22-nucleotide sequence into the backbone

Immediately after 5' flank sequence, the 20-22-nucleotide sequence that is perfectly complementary to the target sequence can be added, this stretch of nucleotides will also contain the seed located in positions 2-8. A common problem when designing is not finding a 21-22-nucleotide single stranded sequence. In that case the seed sequence should be enough, although the specificity and efficiency might vary. Prediction programs other than the mentioned above, can be used and might result in alternative secondary structures. After the 22 nucleotides, the loop sequence adapted from the naturally occurring microRNA can

be added followed by the reverse complement of the 22 nucleotides modified by having a deletion in positions 10-11 creating a bulge. The presence of the bulge will allow for the sense strand to be preferentially loaded into AGO2. The whole sequence described above can then reverse complemented to create the bottom strand 3'-5'.

If a pol III promoter such as U6 is being used addition of a +1 G at the 3'end of the U6 promoter sequence is needed, before the 5'flank sequence of the miRNA. [82] After the 3' flank sequence the pol III terminator formed by 4-6 T's (TTTTTT) and the restriction site of choice for cloning should be the last components added to the design. This stretch of T's will create an overhang at the 3'end necessary for Dicer recognition [82]. Stretches of AAAA or TTTTT's, should be generally avoided for these are common terminator sites for pol III promoters.

When designing the experiment proper controls should include a microRNA targeting an unrelated non essential sequence or gene . A scramble for proof of concept and to control for saturation of the RNAi machinery, promoter or reporter toxicity. An example of U6 and CB-A entry plasmids is shown in **(Figure 3.3)**

A) U6 Promoter entry plasmid

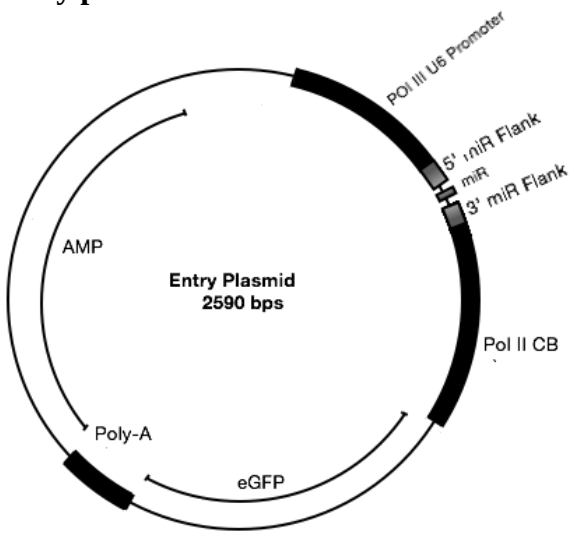

B) CB Promoter entry plasmid

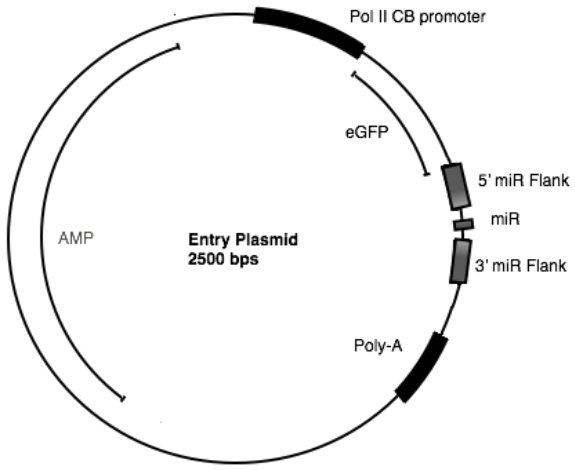

Figure 3.3: An example of the entry plasmid used for cloning a microRNA/ shRNA

A) U6 entry plasmid contains a U6 promoter followed by either the miR155 endogenous flanks or the shRNA directly. AN additional Chicken beta actin (CB-A) promoter driving the expression of a reporter gene (GFP) can be added. B) CB entry plasmid contains a CB promoter driving GFP, followed by the miR155 endogenous flanks or the shRNA directly.

Cloning of the miRNA or shRNA

Oligonucleotides must be reconstituted with nuclease-free water to 100-µMolar concentration. The oligo annealing reaction will then take place in a beaker with boiling water at 95^{o}C, each eppendorf 1.5ml tube containing the annealing reaction **(Table 3.1)** will be kept at 95^{o}C for 5 minutes, then the heat will be shut off and the beaker will be allowed to cool to room temperature. Oligos can then be stored at -20 ^{o}C indefinetly.

Table 3.1. Annealing reaction

Component	Volume
5'-3' oligo	2 µl
3'-5' oligo	2 µl
Annealing buffer (IDT)	196 µl

The plasmid containing the promoter of choice, reporter etc. must be verified prior to starting any cloning experiments. The plasmid should be digested with the enzyme selected for cloning to confirm the presence of the expected cut site and size of the band. the annealed oligonucleotides and the vector should be run side by side in a 1% agarose gel to observe and quantify the relative abundance of each to ensure a 1:1 ratio to then perform an adequate ligation. The ligation mixture described in **(Table 3.2)** can be left at 16^{0}C overnight in a PCR thermocycler.

Table 3.2. Ligation reaction

Reagent	Volume
Vector	1 µl
Insert	1 µl
Quick T4 DNA ligase	1 µl
Buffer	2 µl
Nuclease-free water	15 µl
Volume reaction	20 µl

The transformation protocol should be followed as instructed by the manufacturers. For our intented purposes we used SURE2 super-competent cells. The transformations were plated and incubated overnight at 37^0C. The next day, multiple colonies were selencted and grown in 5ml tubes containing terrific broth media and the antibiotic used for selection at 37^0C, shaking. Cultures should no be grown for more than 13 hours . A 2ml aliquot of bacterial growth media was taken to extract the plasmid DNA using a commerical miniprep kit. And the leftover was stored in a 50:50 ratio solution of glycerol for -80^0C long term storage. Based on the designed restriction site digests of the DNA should allow for clear distinction of the vector and the insert when run in a 1% agarose gel.

Once the correct clones have been verified, they should be sent to be sequence verified to confirm the insert (miRNA/shRNA) is properly cloned into the plasmid. Once the sequencing results are received the sequences can be compared and aligned to a cloning map. Software such as snapgene or clonemanager should be purchased for ease of plasmid contruction and data analysis.

Screening of miRNA or shRNA

An adequeate cell line shown to have detectable levels of expression of your gene of interest should be selected for the screening process. This cell line should also be amenable to tranfections and easy to maintain such as human embryonic kidney cells (HEK293) which are commonly used for these purposes. A transfection optimization prior to the experiment is recommended, where different tranfection reagents, volumes, media changes, plasmid concentrations and incubation times can be adjusted. Reagents for transient tranfections such as Lipofectamine2000 or Jet Prime are the more frequently used. An additional way to assess the tranfection efficiency and verify the presence of the transgene includes the use of reporter genes such as Green fluorescent protein (GFP). These can either be cloned into the same construct with the miRNA/ShRNA or can be co-transfected at a 1:1 ratio. Twenty four to seventy two hours post transfection the cells can be collected for RNA extraction. The experimental design should include the proper controls: 1) A miRNA, that targets an unrelated sequence, which will control for saturation of the RNAi machinery and as a a guide for normalization. The use of a scrambled miRNA sequence is also very common however we discourage it since it may lead to uncknown misstargeting. 2) A control plasmid with only the selected promoter and reporter (i.e: CMV-GFP) to control for the reporter gene expression and possible toxicity. 3) A sham transfection, where all transfection components are added except for DNA. 4) And an un-transfected well, to control for cell growth, viability and contamination. To collect cells, cell media is removed and washed with 1x PBS solution, followed by Trizol reagent according to the manufactures instructions for RNA and/or protein extraction.

Silencing analysis by RT-qPCR or Western blot.

Following an RNA extraction, complementary DNA should be made using the RNA to cDNA kit from Qiagen with the reagents in **(Table 3.3)**. The reaction will be incubated at 37^0C for 60 minutes, then stopped by heating at 95^0C for 5 minutes and held at 4^0C or stored at -20^0C indefinitely. Primers and probes can be designed or made to order for the gene of interest.

Table 3.3 cDNA reaction

Component	**Component Volume /Reaction (µl)**	
	+ RT reaction	**-RT control**
2X RT Buffer	10	10
20X Enzyme Mix	1	-
RNA sample	2µg- up to 9µl	2µg- up to 9µl
Nuclease-free H_2O	Bring to 20 µl	Bring to 20 µl
Total Per Reaction	20	20

cDNA should be diluted in a 1:10 ratio with sterile water or serial dilutions should be run to assess the adequate concetration needed for an efficient qPCR. Additional controls for the qPCR include assessing the expression levels of a housekeeping gene such as GAPDH or HPRT which will then be used as references for relative expression quantification via the delta delta CT method [83]. If antibodies against the gene of interest are available a western blot may be used to measure the level of protein knockdown using Actin as loading control. Densitometry levels of each band can be quantified for silencing.

In vivo validation of miRNA and shRNA

To test the selected constructs *in vivo*, the artificial miRNAs/shRNAs can be packaged in either recombinant adeno associated virus (rAAV) or lentivirus. Something to be considered for the *in vivo* work is the nature of the constructs, if they are designed to be species specific to human sequences, then a transgenic model or human derived cell lines may be needed. Nonetheless,both miRNAs/shRNAs designed against human sequences might cross-react with other species if the target sequence or the seed is conserved.

Summary

The discovery of RNA interference (RNAi) has enabled scientist to design new therapeutic approaches based on specific gene silencing rather than the canonical gene therapy through gene augmentation. Two types of molecules can be used for viral vector-mediated gene silencing: short hairpin RNAs (shRNAs), and artificial microRNAs (miRNAs), that can enter the RNAi pathway. Although both shRNAs and miRNAs can be used to silence genes, they enter the RNAi pathway at different points. Unlike shRNAs, miRNAs require an additional cleavage step inside the nucleus before being exported to the cytoplasm. These molecules can then be incorporated into the RNA-induced silencing complex (RISC) which utilizes sequence complementarity to recognize target mRNAs and activate either translational repression, in the case of partial complementarity, or induce mRNA cleavage in the case of complete complementarity. Elevated amounts of shRNAs, which are commonly driven by strong polymerase III promoters, can cause saturation of the endogenous RNAi machinery due to competition between endogenous and artificial molecules. Switching to a DNA polymerase II promoter is an alternative to reduce shRNA production thereby reducing toxicity. Even though the molecules are designed to target

specific mRNAs there may be off-target effects due to non-specific binding that must be accounted for during the design process. If the microRNA is designed to target a mouse gene any off target effects can be further evaluated to ensure no essential gene is affected as a result of the therapeutic. We have shown here, how to properly design these artificial molecules so they can be used as a tool for modifying gene expression not only to target the CNS but also a wide variety of diseases. The AAV capsid can also be selected based on the cell tropism needed.

Chapter IV

Hexanucleotide Expansion Reproduces RNA Foci and Dipeptide Repeat Proteins but Not Neurodegeneration in BAC Transgenic Mice

Introduction

Model systems that recapitulate the pathobiology of the mutant *C9ORF72* gene are particularly helpful in understanding how such mutations cause neurodegeneration *in vivo*. Several invertebrate [84, 85], vertebrate [86] and patient-derived cell models [87-90] of *C9ORF72* motor neuron pathology have been reported. While each of these models have been instructive, it can be argued that a more informative model will permit studies of the *C9ORF72* expanded GGGGCC repeats in the context of stable expression in an intact mammalian nervous system. For that reason, we generated a novel transgenic mouse carrying an expanded form of the human *C9ORF72* gene with approximately 500 GGGGCC motifs.

We sought to assess if the model created would recapitulate the major molecular and motor hallmarks of the disease. If so, could this transgenic mouse be used as a model system to study the mechanism by which the hexanucleotide expansion causes toxicity or be an aid for testing possible treatments.

Results

BAC transgenic mice express the human mutant *C9ORF72* gene.

We generated a line of SJL/B6 transgenic mice using a 153.2kb bacterial artificial chromosome containing exons 1 through 6 of the human *C9ORF72* with about 500 GGGGCC repeat motifs, including approximately 140.5kb of upstream sequence **(Figure 4.1A)**. Hemizygous C9BAC mice were viable, producing progeny at expected Mendelian frequencies. Southern blot analysis of genomic DNA from these animals detected two distinct bands corresponding to about 500 and 300 GGGGCC repeat motifs, which were intergenerational, and tissue type stable **(Figure 4.1B, C)**. Using a human specific probe for all variants (Vall), *C9ORF72* mRNA transcripts were detected in the C9BAC mice in all tissues examined. The truncated human *C9ORF72* gene generates three transcript variants; V1 and V3 carry the repeat expansion (**Figure 4.1 D**). Human specific probes targeting human *C9ORF72* V1, V2 and V3 mRNAs detected all three transcripts in the C9BAC mice at expression levels comparable to their abundances in human frontal cortex having used the same RNA concentration input **(Figure 4.1 E).** Moreover, the total level of the transgenic human transcripts was roughly comparable to that of the endogenous mouse *C9ORF72* ortholog transcripts, and to levels of expression of human control and c9ALS/FTD cases **(Figure 4.1 E)**

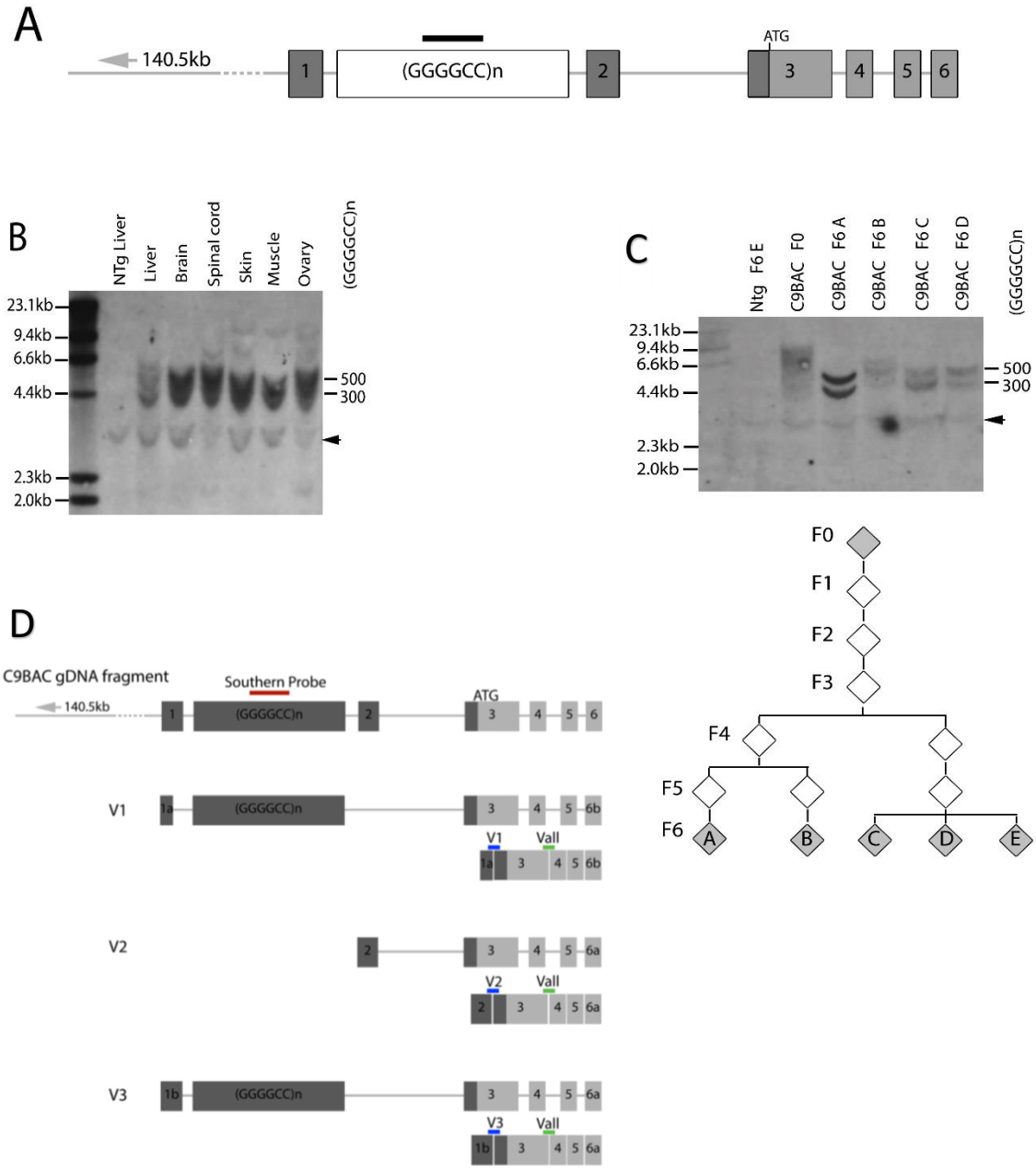
A
140.5kb
1
(GGGGCC)n
2
ATG
3
4
5
6
B
NTg Liver
Liver
Brain
Spinal cord
Skin
Muscle
Ovary
(GGGGCC)n
23.1kb
9.4kb
6.6kb
4.4kb
2.3kb
2.0kb
500
300
C
Ntg F6 E
C9BAC F0
C9BAC F6 A
C9BAC F6 B
C9BAC F6 C
C9BAC F6 D
(GGGGCC)n
23.1kb
9.4kb
6.6kb
4.4kb
2.3kb
2.0kb
500
300
F0
F1
F2
F3
F4
F5
F6
A
B
C
D
E
D
C9BAC gDNA fragment
Southern Probe
140.5kb
ATG
V1
V2
V3
ValI

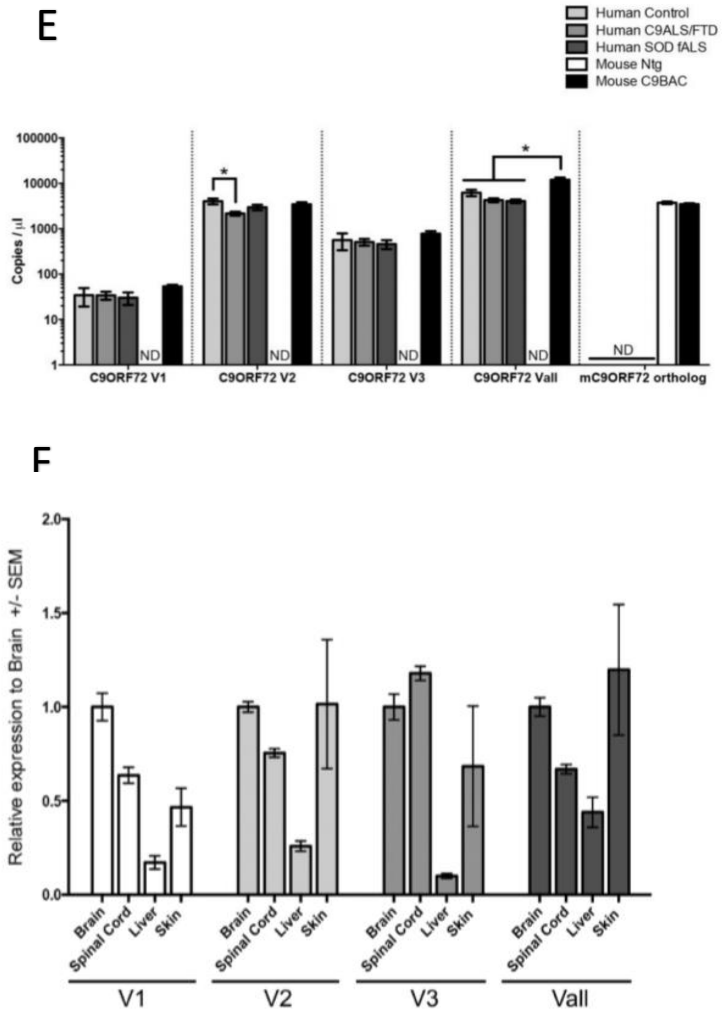

Figure 4.1: Construct design, expansion size and expression profile for the *C9ORF72* BAC transgene and phenotyping of C9BAC mice.

(A) Schematic of the bacterial artificial chromosome fragment used for generating the C9BAC mice. The 153.2kb construct contains (as shown from left to right) 140.5kb of human genomic DNA upstream of *C9ORF72*, the human *C9ORF72* promoter region, and exons 1 to partial exon 6 with a $(GGGGCC)_{500}$ repeat motif in *C9ORF72* intron 1. The black bar indicates the target region for the Southern blotting probe used in B. (B) Southern blot of genomic DNA extracted from various tissues digested with HindIII, SacI, and TaqI and probed with a 5'-DIG-$(GGGGCC)_5$-DIG-3' DNA probe. Two bands of ~4.4kb and ~6.0kb, are stable in size after 6 generations representing expansions of 300 and 500 repeats. The arrowhead indicates a non-specific band. No variation in expansion size was seen among tissues as assessed in liver, brain, spinal cord, skin, muscle and ovary. C) Southern blot of genomic DNA extracted from liver, digested with HindIII, SacI, and TaqI and probed with a 5'-DIG-$(GGGGCC)_5$-DIG-3' DNA probe. Two bands of ~4.4kb and ~6.0kb, are stable in size after 6 generations representing expansions of 300 and 500 repeats

respectively. Arrowhead indicates a non-specific band. (D) Schematic showing potential RNA transcript generated from the *C9ORF72* gene fragment used to generate the C9BAC mice. Three splice variant isoforms can be produced from the gene fragment, with V1 and V3 containing the hexanucleotide expansion. Nomenclature is based on NCBI reference sequences. For each isoform, the upper image shows unspliced pre-, while the lower image at the right is the spliced mRNA. The red bar denotes the presence of the southern blot probe used for determining expansion size. Blue bars show location of isoform specific TaqMan probes. Green bar shows location of TaqMan probe designed to recognize all isoforms (Vall). (E) ddPCR analysis of expression of all human *C9ORF72* variants (Vall), and variants V1, V2 and V3 and the mouse *C9ORF72* ortholog in human frontal cortex tissues from non-neurological disease control, c9ALS/FTD and SOD fALS patients, and whole brain homogenate from C9BAC and Ntg mice (mean±SEM, n=4, Kruskal-Wallis test, Mann-Whitney U-test, * $p<0.05$, ND = not detectable). (F) ddPCR analysis of expression of all isoforms.

Survival, motor and cognitive systems are normal in mice bearing the mutant *C9ORF72* gene.

A cohort of F1 generation male C9BAC mice was aged for phenotypic characterization and analysis of survival. At all ages, the C9BAC and control mice remained healthy. They trended towards a non-significantly elevated weight compared to Ntg littermates **(Figure 4.2A)** and lived beyond two years. Survival in the C9BAC and Ntg littermates was indistinguishable **(Figure 4.2B).**

We first tested for behavioral and histological abnormalities within the motor system of the C9BAC mouse. Overall, the C9BAC mice showed no significant motor deficits by rotarod performance and grip strength testing **(Figure 4.2 C, D)**. No difference was observed in motor or sensory spinal nerve root axon number and morphology **(Figure 4.2 E)**, nor was increased denervation of neuromuscular junctions seen in 24-month C9BAC mice **(Figure 4.2 F**). Motor unit number estimation (MUNE) recording in the hind limbs of 24-month C9BAC mice detected no changes in MUNE score, motor unit size or

compound motor action potential, although there was a trend towards a modestly increased denervation score, as gauged by electromyography **(Figure 4.2 G).** We also assessed several pathological features in the motor cortex and spinal cord that are common features of ALS. No significant changes were seen in activation of microgliosis or astrogliosis **(Figure 4.2 H)**. Cytoplasmic mislocalization and aggregation of TDP-43, both identified in the majority of ALS patients [91, 92], were not detected in the motor cortex of our C9BAC mice **(Figure 4.2 I, J**). To assess activation of programmed cell death within the spinal cord, we observed levels of cleaved capase-3 by Western blotting; levels in C9BAC and Ntg mice did not differ significantly. Because studies have demonstrated cortical hyperexcitability in patients and cell lines with *C9ORF72*-ALS hexanucleotide expansions [93], we next asked whether cortical neurons of neonatal C9BAC mice showed altered electrophysiological characteristics. We detected no changes in the electrophysiological properties of either pyramidal tract-type or intratelencephalically projecting neurons in L5 of motor cortex of these neonatal C9BAC mice **(Figure 4.2 K, L) (Table 4.1)**

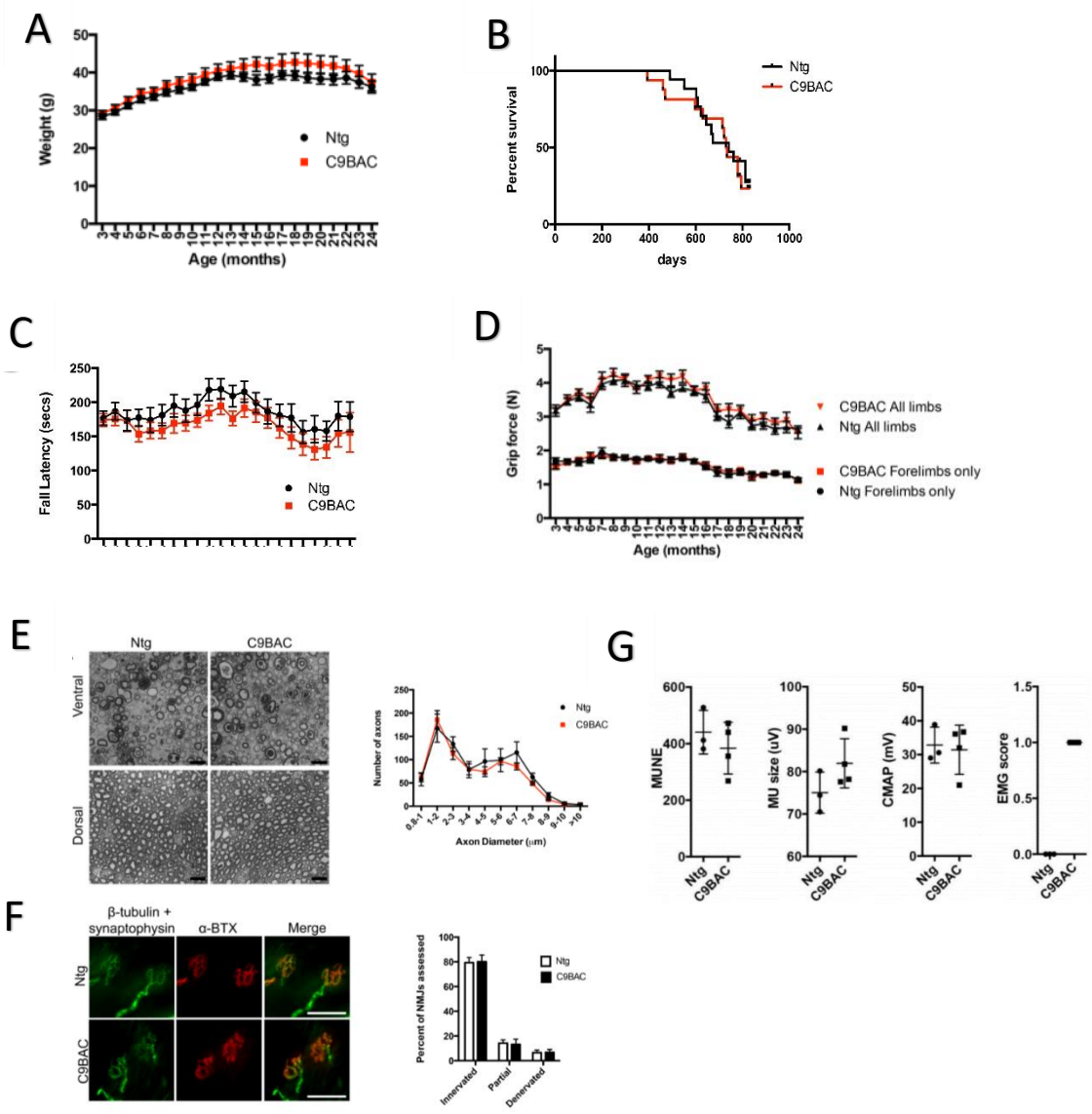
A
Weight (g)
Age (months)
Ntg
C9BAC
B
Percent survival
days
Ntg
C9BAC
C
Fall Latency (secs)
Ntg
C9BAC
D
Grip force (N)
Age (months)
C9BAC All limbs
Ntg All limbs
C9BAC Forelimbs only
Ntg Forelimbs only
E
Ntg
C9BAC
Ventral
Dorsal
Number of axons
Axon Diameter (μm)
Ntg
C9BAC
F
β-tubulin + synaptophysin
α-BTX
Merge
Ntg
C9BAC
Percent of NMJs assessed
Innervated
Partial
Denervated
Ntg
C9BAC
G
MUNE
MU size (uV)
CMAP (mV)
EMG score
Ntg
C9BAC

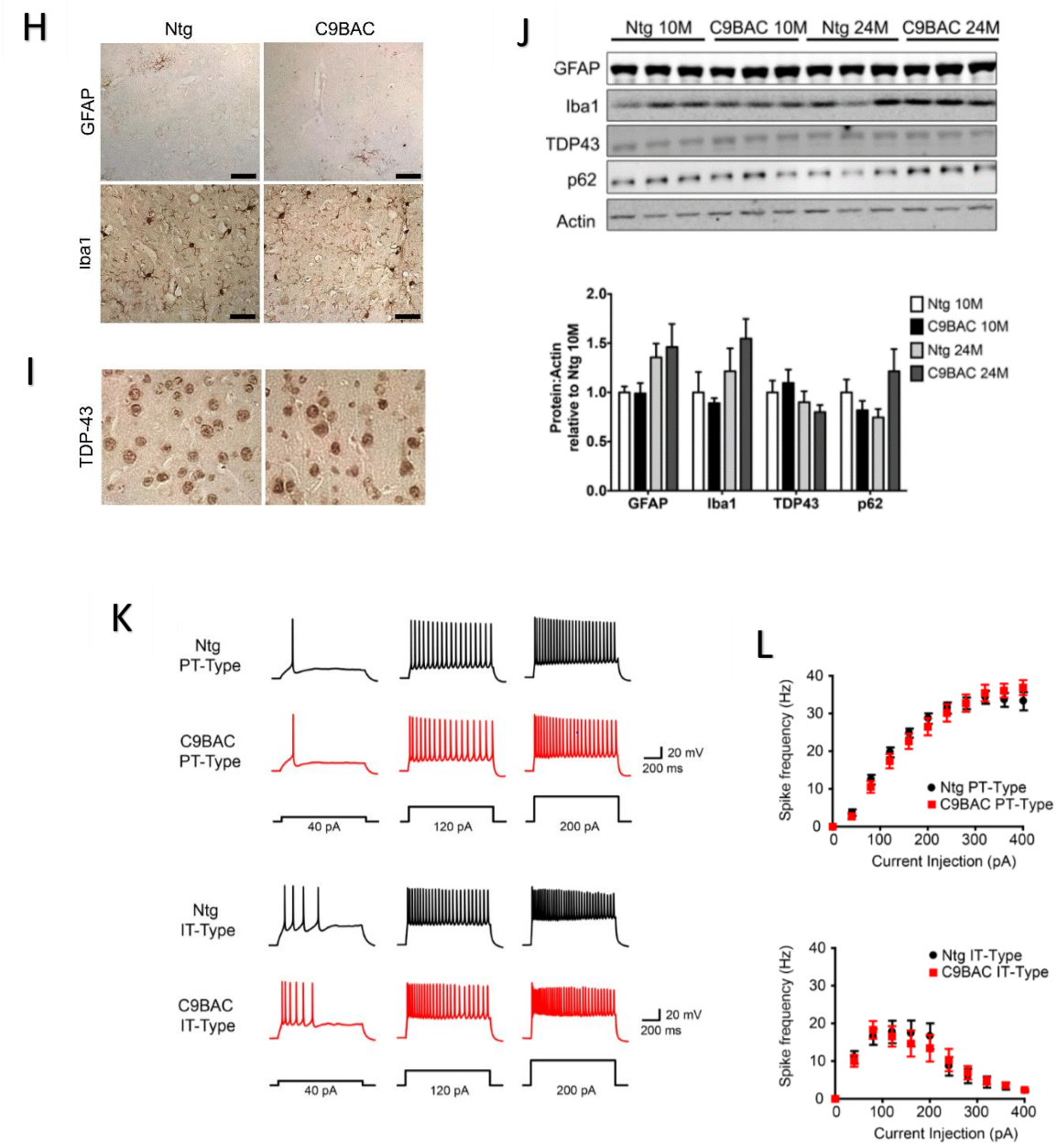

Figure 4.2 Aged C9Bac mice show no gross motor phenotypic abnormalities

A) C9BAC mice and Ntg littermates show no differences in weight from 3-24 months of age (mean±SEM, 2 -way ANOVA, Bonferroni's multiple comparison, Ntg n-17, C9BACn=15) B) Kaplan-Meier curve representing lifespan showing no significant difference in survival of C9BAC mice compared to Ntg littermates (Ntg n=17, C9BAC n=16, Mandel-Cox Log Rank, P=0.971). C) The performance of the C9BAC mice on a 5-minute accelerating rotarod task did not differ significantly from Ntg controls (mean±SEM, 2 -way ANOVA, Bonferroni's multiple comparison, Ntg n-17, C9BACn=15) D) The grip force of forelimb only and all limbs from 3-24- months of age showed no difference in mice of either genotype (mean±SEM, 2 -way ANOVA, Bonferroni's multiple comparison,

Ntg n-17, C9BACn=15) **.** (E) Toluidine blue stained semi-thin section of L5 ventral (upper panels) and dorsal (lower panels) nerve roots of 24-month old C9BAC mice and age-matched Ntg mice. Age-related alterations in axon and Schwann cell morphology were observed in motor fibers in both Ntg and C9BAC mice, while sensory fibers appeared normal. A plot of the numbers of myelinated motor axons in L5 ventral nerve roots as a function of axon diameter (µm) revealed no significant change in size distribution in 24-month old C9BAC mice compared to Ntg controls (mean±SEM, Ntg n=3, C9BAC n=4, 2 -way ANOVA, Bonferroni's multiple comparison) (F) Immunofluorescent staining (Green=synaptophysin, beta-III-tubulin, Red=alpha-bungarotoxin-alexa555) and quantification of neuromuscular junctions in the gastrocnemius muscle of 24-month old C9BAC mice revealed no significant change in innervation (mean±SEM, Ntg n=4, 699 NMJ assessed, C9BAC n=4, 675 NMJs assessed; 2 -way ANOVA) (G) Physiological studies reveal showed no significant change in motor unit number estimations (MUNE) motor unit's size or compound motor action potential, though a modest increase in electromyogram score was observed (mean±SEM, Ntg n=3, C9BAC n=4 unpaired t-test). (H) Immunostaining of motor cortex from 24-month old C9BAC mice revealed no pronounced increase in number of GFAP-labeled activated astrocytes or Iba1-labeled microglia, (I) nor was TDP-43 found to mislocalize in these neurons. (J) Quantitative western blotting revealed no difference in levels of GFAP, Iba1, TDP-43 or p62 in the spinal cord of age matched Ntg and C9BAC mice (mean±SEM, n=3, Kruskal-Wallis test (K) the top panels are representative voltage traces recorded from pyramidal tract (PT) type neurons in layer 5 of motor cortex from Ntg and C9BAC mice evoked by 40-120 and 200 pA current steps as indicated. (mean±SEM, Ntg=23 cells, 7 mice; C9BAC: 15 cells, 5 mice; P>0.4, 2-way ANOVA, Bonferroni corrected for multiple comparisons). And the lower panels are intratelencephalic (IT)-type neurons in later 5 of motor cortex. (mean±SEM, Ntg=19 cells, 7 mice; C9BAC: 13 cells, 5 mice; P>0.6, 2-way ANOVA, Bonferroni corrected for multiple comparisons) (L) A corresponding summary graph for the current spike frequency relationship for transgenic and control neurons. Scale bars E=20µm, F-H-I= 50µm

We next surveyed pathological findings that are common in FTD. No activation of gliosis was detected in the prefrontal cortex (PFC) or hippocampus **(Figure 4.3 A-B)** Changes in social interaction behavior have been described in rodent models of FTD [94, 95], however we found no change in social behavior of adult C9BAC in response an intruder mouse response assay. **(Figure 4.3 C).** Quantitative studies of Golgi preparations revealed no change in dendritic spine density of PFC layer 2-3 pyramidal neuron apical dendrites in aged C9BAC mice **(Figure 4.3 D)**. Finally, altered gene expression profiles have been shown in c9ALS/FTD patient derived cell lines [88-90] and tissues [96]. To determine

whether a specific *C9ORF72* RNA profile can be defined in our C9BAC transgenic mice, we sequenced total RNA extracted from the frontal cortex of six-month old C9BAC mice and littermate controls. Statistical analysis of differentially expressed genes did not reveal any change between the two groups, including several genes identified as differentially expressed in iPSC-derived motor neurons [88, 90] **(Figure 4.3 E-H)**

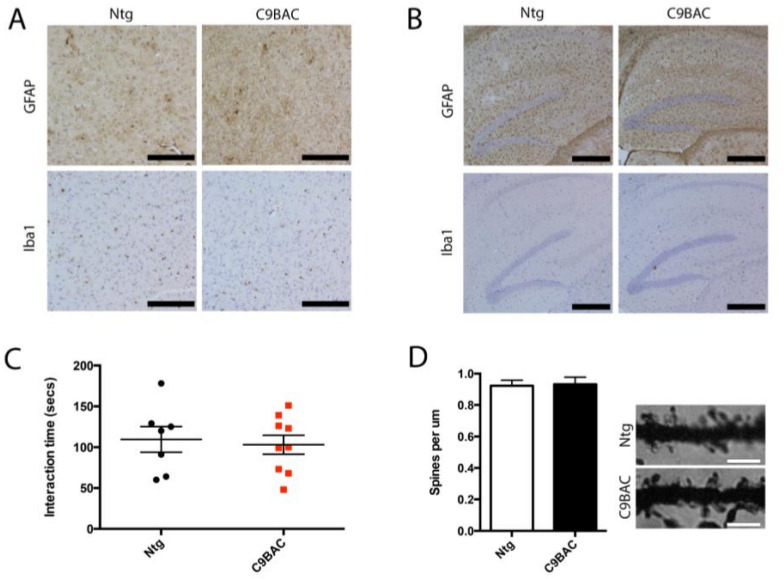

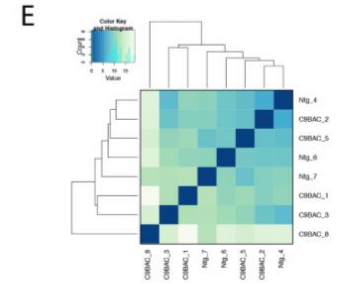

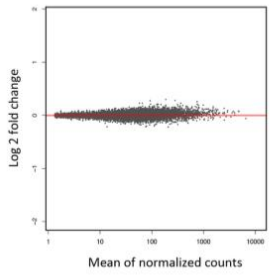

G

Gene	Log2 Fold Change	p-value (adjusted)
Donnelly et al 2013		
NEDD4L	-0.04337	0.99976
FAM3C	0.01679	0.99976
CHRDL1	-0.00654	0.99976
CP	-0.01729	0.99976
SEPP1	-0.12254	0.99976
SERPINE2	-0.04773	0.99976
Sareen et al 2013		
DPP6	0.00941	0.99976
KCNQ3	0.01161	0.99976
CBLN1	0.01184	0.99976
CBLN2	0.11578	0.99976
CBLN4	0.03093	0.99976
SLITRK2	0.00772	0.99976

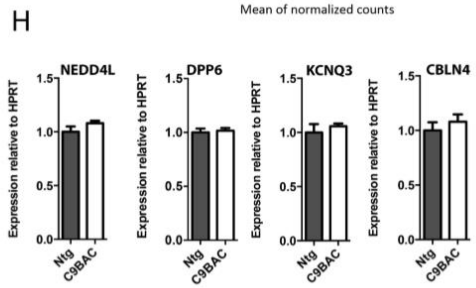

Figure 4.3: Aged C9BAC mice do not recapitulate FTD-like pathology nor show changes in cortical neuron electrophysiology.

(A) Immunostaining for markers of astrogliosis (GFAP) and microgliosis(iba1) in (A) prefrontal cortex and (B) hippocampus of 24-month old Ntg or C9BAC (C)During a 5-minute test period, the interaction times of 18-24 month olf Ntg or C9BAC mice with a juvenile male mouse were not different (mean±SEM, unpaired t-test, Ntg n=7, C9BAC n=9) (D) Golgi staining and quantification of dendritic spine density of layer 2-3 pyramidal neuron apical dendrites found no difference between 18- month old C9BAC and Ntg mice (mean±SEM, Mann-Whitney U- test, n=3 animals per genotype, 3-12dendrites per brain, total length of dendrite sampled: Ntg=1943.5 µm, C9BAC=1266.1 µm). (E) Heatmap showing the Euclidean distance between sample conditions and replicates (frontal cortex, 6month old, n=5 C9BAC and n=3 Ntg) as calculated from the regularized log transformation of the gene expression counts. Based on these values, no distinct hierarchical clustering was observed, indicating that the overall gene expression patterns of *C9BAC* and Ntg mice were similar. (F) Differentially expressed genes (DEG). MA-plot of log2 fold changes from the C9BAC over the mean of normalized counts. No DEG were identified using DESeq2 negative-binomial Wald test. (G) Table of genes of interest from (Donnelly, et al.,2013, Sareen et al., 2013) selected from the DESeq2 dataset showing adjusted p-value. (H) ddPCR quantification of NEDD4L, DPP6, KCNQ3 and CBLN4 from the RNA library used for RNAseq analysis (mean± SEM, Mann-Whitney U -test) Scale bars A=100µm, B=200µm, D=2µm

C9BAC mice recapitulate histopathological features of human *C9ORF72* ALS-FTD.

At autopsy, brains from c9ALS/FTD patients show several histopathological characteristics that are not detected in other forms of familial and sporadic ALS or FTD: (i) sense transcript nuclear and occasional cytoplasmic RNA foci, (ii) antisense transcript nuclear RNA foci and (iii) the generation of DPR proteins through RAN translation of the sense and antisense transcripts.

We used fluorescence *in situ* hybridization (FISH) to detect *C9ORF72* sense and antisense foci in the brain and spinal cords of C9BAC mice **(Figure 4.4**). Intranuclear, sense foci were detected at 3 months of age (data not shown) and by 10 and 24 months were abundant

throughout the CNS, including motor cortex and spinal cord **(Figure 4.4A**), present in both neurons **(Figure 4.4 B, C)** and glia (**Figure 4.4 D)**. Antisense foci were also detected in 10- and 24-month old mice **(Figure 4.4 A)** but were sparser throughout the brain than sense-foci. Quantification of numbers of sense foci in nuclei of the cortical external pyramidal layer **(Figure 4.4 E)** and spinal motor neurons **(Figure 4.4 F)** revealed that the majority of foci-positive nuclei contain one to five detectable sense foci, though in some cases greater than 20 foci were seen in individual nuclei. A trend towards a reduced number of nuclei containing foci was seen between 10 and 24-months, reaching statistical significance in the motor cortex external pyramidal layer, but not spinal cord motor neurons.

Because both sense and antisense *C9ORF72* transcripts were present in the C9BAC mice, we next sought evidence of RAN translation products, using a sandwich immunoassay for the detection of poly (Glycine-Proline) poly (GP), which is synthesized from both sense and antisense transcripts. Tissues from 4- and 24-month old Ntg and C9BAC mice, and frontal cortex from six c9ALS case, were homogenized in buffer containing 2% SDS, with the detergent soluble fraction analyzed for poly (GP) content. At 4 months of age, poly (GP) was detected throughout the brain of C9BAC mice, with levels highest in the cerebellum, the spinal cord, sciatic nerve and liver **(Figure 4.4 G)**. Though the mean concentration of poly (GP) levels in 4-month mice was lower than that observed in c9ALS frontal cortex, the 4-month C9BAC mean did fall within range of the lowest samples in the patient group **(Figure 4.4 G**). All tissues from 24-month old C9BAC mice showed a significant reduction in SDS-soluble poly (GP) levels. One hypothesis for the observed decline in soluble poly (GP) is that the DPR proteins show an age-dependent propensity to

form insoluble species. Immunostaining of brain tissues from 10- and 24-month old C9BAC mice revealed the presence of small perinuclear inclusion bodies stained for poly (GP) **(Figure 4.4 H)**. Such inclusions were detected throughout the brain, including cortex, cerebellum and striatum, and were more frequently observed in the brains of 24-month mice, suggesting a heightened deposition of insoluble poly (GP) species.

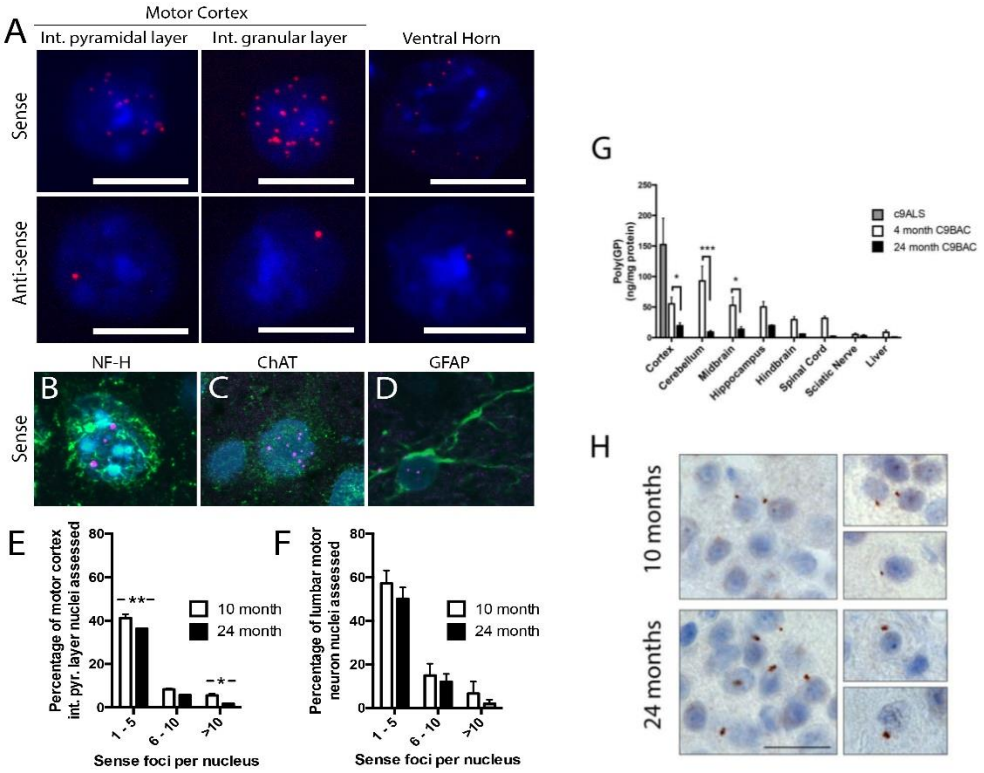

Figure 4.4: C9BAC mice recapitulate the histopathological hallmarks of *C9ORF72* ALS and FTD patients.

(A) Fluorescence *in situ* hybridization (FISH) using Cy3-tagged DNA probes against sense and anti-sense abnormally expanded *C9ORF72* transcripts (Red = probe, Blue = DAPI nuclear stain). The *C9ORF72* repeat containing sense or anti-sense transcripts form intranuclear RNA inclusions, or foci, throughout the brain, including motor cortex internal pyramidal layer and internal granular layer, and lumbar motor neurons of 24-month old C9BAC mice. FISH coupled with cell type specific immunostaining revealed sense transcript foci in neurofilament heavy positive neurons (B), choline acetyl transferase (ChAT) positive pyramidal neurons (C) and GFAP positive astrocytes (D). The number of sense transcript foci per nucleus in 10-month and 24-month old C9BAC mice in (E) motor cortex internal pyramidal layer and (F) lumbar motor neuron nuclei (Cortex: 10-month,

n=3, 821 nuclei; 24-month, n=3, 845 nuclei: Spinal cord: 10-month, n=3, 124 nuclei; 24-month, n=3, 100 nuclei: mean±SEM, 2-way ANOVA, Bonferroni multiple comparison * $p<0.05$, ** $p<0.001$). (G) Quantification of soluble poly (GP) proteins in various regions of the CNS and liver of 4- and 24-month old C9BAC mice and frontal cortex of C9ALS cases by immunoassay (mean±SEM, C9BAC groups n=3, c9ALS n=6, two-way ANOVA, Bonferroni's multiple comparison, * $p<0.05$, *** $p<0.001$). (H) Immunostaining for poly (GP) proteins in cortex of C9BAC mice. Staining revealed the presence of small perinuclear inclusion bodies throughout the brain at 10-months of age, with a pronounced elevation in the number observed in 24-month old mice. Such inclusions were not observed in age-matched Ntg mice. Scale bars A - D = 10 µm, H = 20 µm.

We established primary cortical neuron cultures from C9BAC and non-transgenic littermate embryos. At 10 days in vitro (DIV) both nuclear foci containing sense or antisense *C9ORF72* hexanucleotide expansion transcripts **(Figure 4.5 A**) and poly (GP) RAN-translation products could be detected **(Figure 4.5B**). We next tested whether neurons from C9BAC mice are hypersensitive to cellular stress. In a previous study, neurons differentiated from induced pluripotent stem cells (iPSCs) derived from FTD patients showed an increased sensitivity to cell death induced by inhibition of autophagy in vitro *[87]*. We treated 15 DIV primary cortical neuron cultures derived from individual embryos with two inhibitors of autophagy **(Figure 4.5C**), chloroquine and 3-methyladenine. Both compounds increased cell death to the same degree in the C9BAC and Ntg neurons, as determined by an LDH assay.

Silencing *C9ORF72* transcripts and poly (DP) production *in vitro*

Though lacking cognitive or motor deficits, the C9BAC mouse robustly recapitulates the molecular pathology of c9ALS/FTD, with readily quantifiable expression of all three *C9ORF72* transcripts, RNA foci and at least one of the poly (DP) RAN-translation products. Both read-outs rely on the expression of the *C9ORF72* gene transcripts. We have

therefore tested a gene therapy approach to silence expression of the *C9ORF72* transgene in our C9BAC mice. We generated recombinant adeno-associated virus (rAAV) serotype 9 expressing an artificial microRNA (miRC9) targeting exon three of human *C9ORF72* preceded by an eGFP reporter, under the transcriptional control of the CB-promoter and CMV-enhancer (rAAV-GFP-miRC9). For control groups, a vector expressing only the eGFP reporter was used (rAAV-GFP). We carried out two sets of experiments in DIV4 primary cortical neuron cultures **(Figure 4.6 D, E, F)**. In the first (Exp 1), individual cultures were generated from separate C9BAC hemizygous embryos from the same litter of C9BAC mice; in the second (Exp 2), all transgenic embryos from a C9BAC litter were pooled to generate a mixed population of cortical neurons from multiple transgenic embryos. In both experiments, transgene transcripts and poly (GP) were reduced by expression of the GFP control vector alone, in conjunction with some cell death; to account for this non-specific silencing, all silencing outcomes are normalized to this GFP control. In all experiments we consistently observed further depletion of *C9ORF72* products in groups expressing the microRNA. Relative to the rAAV-GFP group, *C9ORF72* mRNA transcript **(Figure 4.5D)** expression in individual embryo cultures (Exp 1) was decreased by 35% by rAAV-GFP-miRC9 (n=4, one-way ANOVA, Bonferroni's multiple comparison, $p<0.05$), and 24% in the pooled embryo cultures in Exp 2 (not statistically significant; n=3, one-way ANOVA, Bonferroni's multiple comparison). We detected mature miRNA only in the rAAV-GFP-miRC9 treated cultures and found that the percent silencing was proportional to levels of the expressed miRNA **(Figure 4.5E**). In two cultures derived from individual embryos (Exp 1), rAAV-GFP-miRC9 reduced levels of poly (GP) by ~60% (Fig. 3F). In mixed cultures (Exp 2), poly (GP) was reduced by 73% relative to

GFP. Though not significant by one-way ANOVA (n=3, Bonferroni multiple comparison test), we note that in Exp 2 statistical testing of the rAAV-GFP vs rAAV-GFP-miRC9 (independent of the untreated group) detected a significant decrease in poly (GP) levels (unpaired t-test, p=0.0008).

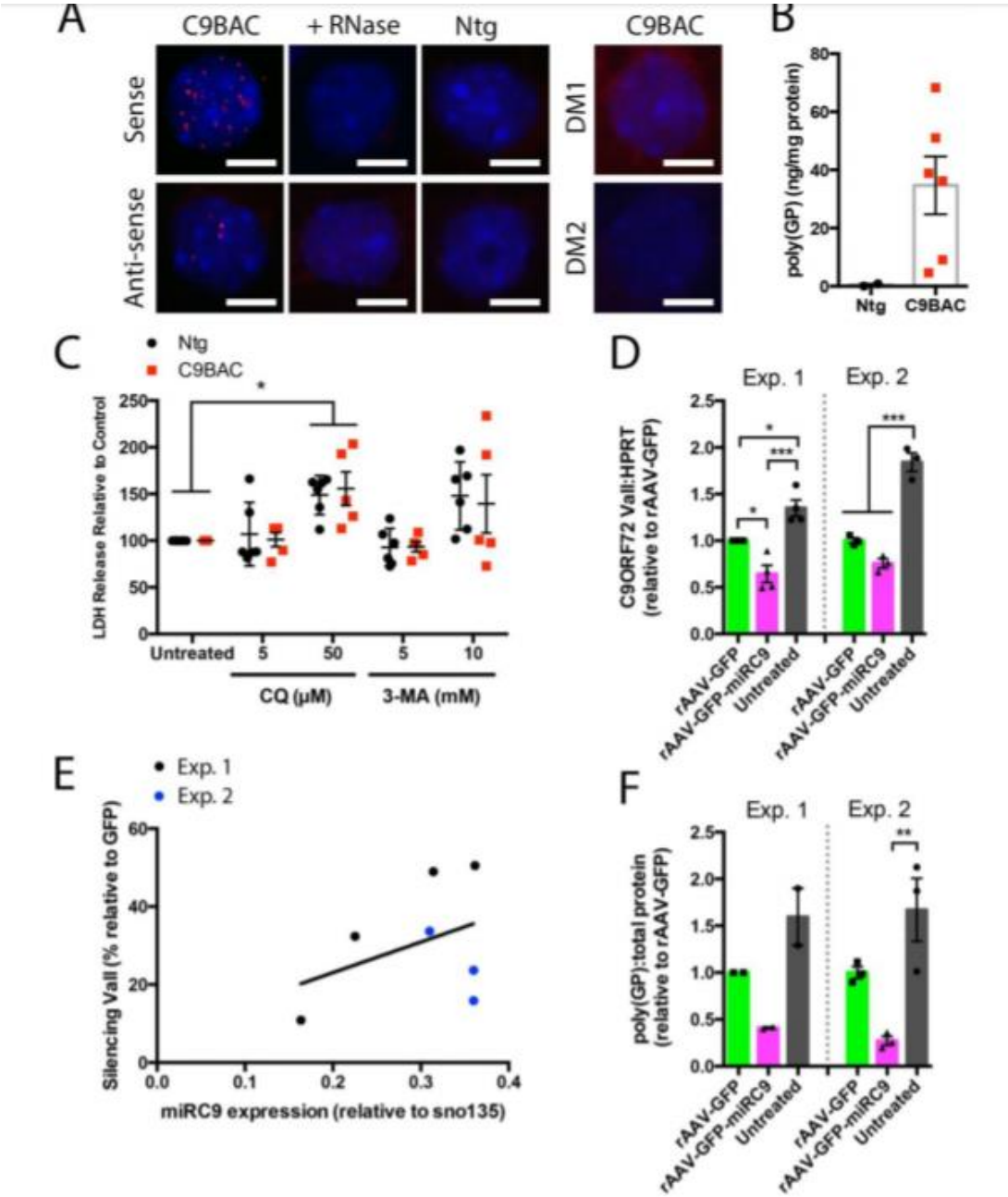

Figure 4.5: Silencing of *C9ORF72* in C9BAC mice and primary cortical neurons.

(A) Sense and antisense foci are detected in cultured cortical neurons of C9BAC embryos at 10 days *in vitro* (DIV). These foci were not visible following RNase treatment and were not detected in Ntg neurons, or by probes targeting the myotonic dystrophy associated type-1 (CTG)n or type-2 (CCTG)n expansions (DM1 and DM2 respectively, scale bar = 5 μm). (B). Concentration of poly (GP) in cultured cortical neurons derived from individual C9BAC or Ntg littermate embryos measured by ELISA (mean±SEM, Ntg n=2, C9BAC n=6, unpaired t-test). (C) No significant differences were detected in the response of cultured cortical neurons derived from individual C9BAC and Ntg embryos to the autophagy inhibitors chloroquine or 3-methyladenine (two independed experiments, individual embryos cultured; C9BAC n=6, Ntg n=5, mean±SEM, 2-way ANOVA, Bonferroni's multiple comparison, * $p<0.05$). (D) ddPCR analysis of all transcripts of *C9ORF72* (Vall) relative to HPRT in two independent experiments (Exp. 1. individual embryos n=4, mean±SEM, one-way ANOVA, Bonferroni's multiple comparison test, * $p<0.05$, *** $p<0.001$; Exp. 2. mixed embryo culture, n=3, one-way ANOVA, Bonferroni's multiple comparison test *** $p<0.001$). (E) Levels of the mature microRNA product (normalized to snoRNA135) of rAAV-GFP-miRC9 trended toward correlation with percent silencing of *C9ORF72* relative to rAAV-GFP from Exp. 1 (black) and Exp. 2 (blue). (F) Levels of poly(GP) quantified by ELISA from primary cortical neuron cultured derived from two independent experiments (Exp. 1. individual embryos n=2, mean±SEM, one-way ANOVA; Exp. 2. mixed embryo culture, n=3, one-way ANOVA, Bonferroni's multiple comparison test, ** $p<0.01$).

Discussion

We report here a novel line of transgenic mice that harbor a portion of the human *C9ORF72* gene with an expanded GGGGCC repeat motif. Though the mice do not develop an overt motor phenotype, they recapitulate distinctive histopathological features seen in c9ALS/FTD patients, including both sense and antisense intranuclear RNA foci and the presence of RAN-translated DPR proteins. These data indicate that the 300-500 GGGGCC repeat motifs are sufficient for the generation and deposition of abnormal tracts of RNA and DPR proteins but not to induce neurodegeneration. Why this is the case remains unclear. Possibly the pathology, seen quite clearly at the molecular level, is not sufficient to compromise motor neuron viability within the lifespan of the mice. Alternatively, some

other aspect of the model may be required to induce motor pathology. For example, if the pathology in humans entails sequestration of critical RNA binding proteins by intranuclear RNA aggregates, it is possible that these proteins are more abundant in the mouse, and thus less prone to be titrated to insufficiency in the RNA foci. Alternatively, it is possible that the DPR proteins are better tolerated in some manner in the mouse.

Two aspects of the histological findings in these mice are intriguing. First, there were distinctly more cells containing sense foci than anti-sense RNA foci. This is broadly analogous to data from human cortex [97]. It is also conceivable that the relative paucity of anti-sense RNA foci reflects the structure of the human BAC in our mice, which contains the full 5' expanse of the *C9ORF72* locus but only extends through exons 1-6 and thus might lack 3' regulatory regions necessary for generating anti-sense foci. Also, of interest in the C9BAC mice were age-dependent changes in the abundance of RNA foci and the levels of soluble RAN-translated poly (GP) proteins. Our data indicate that the numbers of intranuclear foci composed of *C9ORF72* RNA sense transcripts declined between 10 and 24 months, possibly reflecting an age-dependent increase in clearance of these foci, reduced expression of the offending transcripts with age, or loss of foci-containing cells.

There were also age-related shifts in the properties of poly (GP) DPR proteins. In 4-month C9BAC mice, SDS-soluble poly (GP) species were present at a concentration comparable to levels detected in frontal cortex of some c9ALS patients. Soluble poly (GP) levels in 24-month C9BAC mice were lower, a change that coincided with an increased presence of poly (GP)-positive inclusions, suggesting conversion of soluble poly (GP) into insoluble, aggregating species.

Finally, we note that although the C9BAC mouse does not develop a discernible abnormal behavioral phenotype, the histopathological and transcript variant expression profile matches well with that of c9ALS/FTD patients. In successful experiments *in vivo* and *in vitro* [88-90], the *C9ORF72* expression has been reduced following treatment with antisense oligonucleotides (ASO). In the present study we have conducted a proof-of-principle experiment to test whether a synthetic microRNA (miR) targeting exon 3 of *C9ORF72* delivered by recombinant adeno-associated virus (rAAV) might offer an alternative therapeutic strategy. With this intervention, primary cortical neuron cultures from the C9BAC transgenic mice demonstrated a consistent trend towards reduced expression of *C9ORF72* transcripts and decreased production of the poly (GP) DPR. These studies suggest that this strategy (AAV-mediated delivery of a synthetic miR) merits further investigation and that these C9BAC mice will be useful for assessing therapies that silence transcription or RAN translation across the expanded GGGGCC repeats or otherwise inhibit the formation of RNA foci and DPR proteins. Combined with accurate analytical techniques to quantify levels of aberrant RNA transcripts, RNA foci and DPR proteins, the C9BAC mouse will be of considerable use for investigating the pathophysiology of *C9ORF72*-mediated neurodegeneration and much needed therapeutic approaches.

Methods

Generation of *C9ORF72* transgenic mice

A BAC library was generated from a familial FTD/ALS patient from a *C9ORF72-linked* ALS/FTD pedigree. Transgenic animals were produced using a BAC carrying a 153.2kb

genomic DNA fragment including 140.5kb upstream of *C9ORF72*, exons 1 to exon 6 of the *C9ORF72* gene, including part of the 3'UTR of the short isoform V1 and ~500 GGGGCC motifs between exons 1 and 2. Mice were maintained on an SJL/B6 background. Circular construct injections generated 3 out of 49 positive animals; one (C9BAC) resulted in germline transmission. Presence of the C9BAC transgene was detected using forward primers 5' TTAATT TCC TAC CCC TGC CC 3' and reverse primers 5' AGG CCT TGA CAA ATG TAG CC 3', amplifying a 250bp fragment. F1 males used for longitudinal survival and behavior testing were housed individually The University of Massachusetts Medical School Institutional Animal Care and Use Committee approved all experiments involving animals.

Motor behavior testing

Motor function was assessed in F1 male C9BAC mice and non-transgenic (Ntg) littermates monthly from 3- to 24-months of age using rotarod (Med-Associates Inc., USA). Mice were tested three times on a 5-minute, 4-40rpm accelerating rotarod task with latency to fall for each individual test recorded. The mean score for each animal was used for statistical analysis. Limb grip strength was recorded using a digital force gauge (Mark-10, USA) fitted with a metal grid. Mice were placed on the grid, allowing either all paws to grip or forepaws only, followed by being gently pulled horizontal to the apparatus until grip was released. Each animal was tested 5 times for fore- or all limb grip, with peak strength for each recorded for statistical analysis. Data from longitudinal behavior testing was statistically analyzed by two-way ANOVA and Bonferroni 's multiple comparison test.

Intruder testing

To assess social interaction behavior, an unfamiliar 6-week-old, juvenile C57Bl6/J wild type mouse was introduced into the home cage of an individually housed 18-22-month-old male C9BAC or Ntg mouse. Direct physical interaction by the home cage male with the juvenile was recorded over a 5-minute period.

Electrophysiological recordings: Motor Unit Number Estimate

Electrophysiological recordings were as described [3]. Motor conduction studies and motor unit number estimate (MUNE) were performed using a portable electrodiagnostic system (Cardinal Synergy). For the motor nerve conduction studies, the lowpass filter was set at 30 HZ, and the high-pass filter was set at 10 kHZ. The nerve was stimulated with single square-wave pulses of 0.1-ms duration. Supramaximal responses were gradually generated, and maximal responses were obtained with stimulus currents <20 mA (most often <10 mA). The distal latency, distal and proximal compound motor action potential (CMAP) amplitudes, distal and proximal CMAP durations (measured from onset of initial negative deflection to initial return to baseline), and conduction velocity were determined for each nerve studied. For the MUNE recordings, the incremental technique was used [4-6]. For electromyography potentials were recorded from several sites of the hindlimb muscles with a concentric needle electrode (30G) [7].

Electrophysiological recordings: Whole-cell cortical neuron recordings

Brain slice preparation for electrophysiological recordings. After anesthetizing mice with isoflurane, brains were rapidly removed and chilled in an ice-cold sucrose solution containing 76mM NaCl, 25mM NaHCO3, 25mM glucose, 75mM sucrose, 2.5mM KCl,

1.25mM NaH2PO4, 0.5mM CaCl2, and 7mM MgSO4; pH 7.3. Acute brain slices (300 µm) were prepared (VT1200s, Leica) tilted anteriorally 15° in the coronal plane. Slices were then incubated in warm (32-35°C) sucrose solution for 30 minutes and then transferred to warm (32-34°C) artificial cerebrospinal fluid (aCSF) composed of 125mM NaCl, 26mM NaHCO3, 2.5mM KCl, 1.25mM NaH2PO4, 1mM MgSO4-7H2O, 20mM D-(+)-glucose, 2mM CaCl2-2H2O, 0.4mM ascorbic acid, 2mM pyruvic acid, and 4mM L-(+)-lactic acid; pH 7.3, 315 mOsm. All solutions were continuously bubbled with 95% O2/5% CO2. Slices were transferred to a submersion chamber on an upright microscope (Zeiss AxioExaminer, 5x and 40x objectives lenses, 0.16 and 1.015 NA respectively) and continuously superfused (2-4 ml/min) with warm oxygenated aCSF (32-34°C). Neurons were visualized with a digital camera (Sensicam QE, Cooke) using transmitted light with infrared differential interference contrast optics. PT-type neurons were distinguished by their large, pyramidal shaped cell bodies and thick apical dendrite. IT-type neurons were identified by their small oval shaped cell bodies and a thinner apical dendrite. The identity of each cell was further confirmed by analyzing its intrinsic membrane properties including sag amplitude, input resistance, and response to current injections as these are significantly different between the two **types (Table 4.1).** Glass recording electrodes (2-4 MΩ) were filled with internal solution containing 2.7mM KCl, 120mM KMeSO4, 9mM HEPES, 0.18mM EGTA, 4mM MgATP, 0.3mM NaGTP, 20mM phosphocreatine (Na), pH 7.3, 295 mOsm with 0.25% biocytin. Whole-cell patch clamp recordings were obtained using a Multiclamp 700B amplifier (Molecular Devices) and digitized using an ITC-18 (Instrutech) controlled by custom software written in Igor Pro (Wavemetrics). All signals were low-pass filtered at 10 kHz and sampled at 20-100 kHz. The access resistance

averaged 9.6 ± 0.7 MΩ. Cells with an Ra of 30 MΩ or more were eliminated from the analysis. The Ra was not compensated during recordings. To measure intrinsic excitability, cells were recorded in the presence of the synaptic blockers: NBQX (AMPA receptor antagonist, 5 μM), CPP (NMDA receptor antagonist, 5 μM), and SR95531 (GABAA receptor antagonist, 10 μM, all from Tocris). The resting membrane potential (RMP) was measured after whole-cell configuration was achieved. Neurons exhibiting an RMP greater than -60 mV were excluded from the analysis. The input resistance was determined by measuring the voltage change in response to hyperpolarizing current steps and the amplitude of the sag response was calculated as the difference in minimum potential at the early phase of a hyperpolarizing current step and the steady-state potential at the end of the 1 s step. The current-spike frequency relationship was measured with depolarizing current steps (1 s) applied in 40 pA increments. The rheobase was measured similarly using 2 pA increments. Action potential properties were measured from single spikes evoked by rheobase current injections. The amplitude of the afterhyperpolarizations (AHP) was measured from the spike threshold to the minimum membrane potential during the AHP.

All data analyses were performed in Igor Pro (Wavemetrics), Excel (Microsoft), and Origin (OriginLab). The Mann-Whitney test was used to compare the rheobase, input resistance, RMP, sag amplitude, and spike properties recorded from control and C9BAC mice. A 2-way ANOVA with Bonferroni correction was used to test statistical differences in the current-frequency relationships between groups.

Electrophysiological characteristics were tested in the presence of blockers of glutamatergic and GABAergic synaptic transmission (NBQX, 5 μM, AMPA receptor antagonist; CPP, 5 μM, NMDA receptor antagonist; and SR95531, 10 μM, GABAA

receptor antagonist). We found no significant differences in the resting membrane potential, input resistance, sag amplitude, or action potential properties between control and C9BAC neurons for PT- or IT-type neurons. To compare the intrinsic excitability of neurons we evoked action potentials with a series of depolarizing current steps. We found that neither neuron type showed a significant difference in the rheobase or the current-spike frequency relationship between control and mutant neurons.

Table 4.1. Electrophysiological properties of layer V neurons in cortical slice cultures from C9BAC mice.

PT-type neurons	**Ntg** (23 cells, 7 mice)	**C9BAC** (15 cells, 5 mice)	***P*-value**
Resting membrane potential (mV)	-66.69 ± 0.61	-67.42 ± 0.68	P > 0.3
Input resistance (mΩ)	218.34 ± 6.89	223.04 ± 14.5	P > 0.8
Sag amplitude (mV)	5.92 ± 0.29	5.35 ± 0.43	P > 0.09
Spike threshold (mV)	-37.84 ± 0.61	-37.96 ± 0.81	P > 0.7
Spike amplitude (mV)	69.43 ± 0.89	69.76 ± 1.4	P > 0.7
Spike half-width (ms)	1.85 ± 0.04	1.9 ± 0.05	P > 0.3
Afterhyperpolarization (mV)	21.62 ± 0.49	21.87 ± 0.76	P > 0.8
Rheobase (pA)	38.73 ± 3.07	40.6 ± 4.21	P > 0.7
IT-type neurons	**Ntg** (19 cells, 7 mice)	**C9BAC** (13 cells, 5 mice)	***P*-value**
Resting membrane potential (mV)	-69.01 ± 0.82	-68.5 ± 1.06	P > 0.7
Input resistance (mΩ)	840.71 ± 35.79	775.61 ± 53.62	P > 0.4
Sag amplitude (mV)	1.52 ± 0.27	1.51 ± 0.33	P > 0.8
Spike threshold (mV)	-33.02 ± 1.08	-32.37 ± 0.95	P > 0.5
Spike amplitude (mV)	50.11 ± 2.26	47.92 ± 2.18	P > 0.2
Spike half-width (ms)	2.21 ± 0.08	2.38 ± 0.13	P > 0.2
After hyperpolarization (mV)	18.62 ± 0.76	17.75 ± 0.79	P > 0.5
Rheobase (pA)	17.94 ± 2.32	19.84 ± 1.65	P > 0.3

Primary cortical culture and drug susceptibility analysis

Cortical neurons were harvested and cultured from individual E15 embryos generated from C9BAC x WT crosses. For Experiment 2 of the knock down experiment, all transgenic embryos from a litter were maintained in Hibernate media (Thermo-Fischer) at 4C for approximately 5 hours whilst genotypes were established and were subsequently pooled and cultured. Cells from individual embryos were seeded onto poly-L-ornithine coated plates or cc2 coated chamber slides at 50,000/cm2. Neurons were maintained in neurobasal media supplemented with Glutamax, B27, and pen/strep (all from Invitrogen) with one half of the media replaced every 3-4 days. To inhibit glial cell proliferation, the anti-mitotic AraC (1 µM, Sigma) was added at DIV3 to the cultures used for assessment of neuronal susceptibility to cytotoxic insult. Susceptibility of DIV15 neurons to 24 hr treatment with chloroquine (CQ) and 3-methyladenine (3-MA) (all from Sigma) at the indicated doses was assessed by lactate dehydrogenase release assay (Promega).

For treatment with silencing vectors, cells were plated in 6-well dishes at 50,000/cm2 and fed every fourth day. At day in vitro four, 18µl of rAAV-GFP (titre = 1.7 E13 viral particles /ml) or rAAV-GFP-miRC9 (titre = 1.2 E13 vp/ml) were added to 1.5 ml of media and the cultures were maintained for a further 6-days. For protein analysis, cells were scrapped from the well, washed with PBS and pelleted. For quantification of *C9ORF72* transcripts, total RNA was collected using Trizol as per the manufacturer's instructions.

RT-qPCR

Frozen tissue samples were homogenized in a gentleMACS Dissociator (Miltenyi Biotec, USA) before total RNA extraction with Trizol (Life Technologies). Reverse transcription

to cDNA was performed using random hexamers and MultiScribe reverse transcriptase (High capacity RNAto-cDNA Kit, Life Technologies). Real time quantitative PCR was performed on an Applied biosystems StepOnePlus Real-Time PCR system using the Fast TaqMan Advanced master mix following the manufacturer instructions. A commercial mouse HPRT assay (Life Technologies, Mm01545399_m1) was used as an endogenous control. Data was analyzed using the Delta Delta CT method. Probes used to detect each variant are as follows: Vall commercial assay (Life Technologies Hs00376619_m1), probe AGAATATGGATGCATAAGGAAAGAC; V1 commercial assay (Life Technologies Hs00331877_m1), probe AGATGACGCTTGATATCTCCGGAGC (Life Technologies assay, # Hs00331877_m1); V2 forward primer AGGCGGTGGCGAGTGGATA, reverse primer TTGGAGCCCAAATGTGCCTTA, probe CGACTCTTTGCCCACCG; V3 forward primer GCGGGGTCTAGCAAGAGCAG, reverse primer TTGGAGCCCAAATGTGCCTTA, probe CCACCGCCATCTC. Position of probes is shown in Figure 4.1D

Droplet Digital PCR (ddPCR)

To assess the absolute concentration of transcripts, droplet digital PCR (ddPCR Bio-rad) was performed on both mouse samples and human frontal cortex samples from c9ALS/FTD (age, 61.3±4.5 years; sex, 3 male, 1 female), SOD1 fALS (age, 46.8±3.5 years; sex, 3 male, 1 female), and non-neurological disease control patients (age, 62.8±7.2 years; sex, 2 male, 2 female). Mouse brain tissue was obtained from 2-month-old C9BAC transgenic mice (n=4) and wild type littermate controls (n=4). Total RNA was extracted by homogenization in Trizol (Life Technologies, USA) in a gentleMACS Dissociator (Miltenyi Biotec). cDNA was synthesized from 2µg/µl RNA using High-Capacity RNA-

to-cDNA Kit (Life Technologies, USA). For reactions, cDNA was diluted 1:5 in nuclease free water. 20µl reactions solution were prepared for each sample, containing ddPCR Supermix for Probes (Bio-Rad, USA), 2µl of diluted cDNA, 1µl of each primer and 1µl *C9ORF72* variant specific FAM-labeled probes. 20µl samples and 70µl of ddPCR-oil was loaded into a DG8 cartridge (Bio-Rad, USA) and droplet generated using the QX100 droplet generator (Bio-Rad, USA). PCR was then run using 40µl of the sample droplet solution on a standard thermocycler (Eppendorf, USA), and absolute quantification calculated using the QX100 ddPCR reader (Bio-Rad, USA). Primers and probes used to detect each variant are as follows: *C9ORF72* all variants (Vall) forward primer ATCCTTCGAAATGCAGAGAG, Vall reverse primer TGAAGTGGGAGGTAGAAACT, Vall probe CTGGAATGGGGATCGCAGCACA; *C9ORF72* variant 1 (NM_145005.6) commercial assay, probe AGATGACGCTTGATATCTCCGGAGC (Life Technologies assay, # Hs00331877_m1); *C9ORF72* variant 2 (NM_018325.4) forward primer AGGCGGTGGCGAGTGGATA, reverse primer TTGGAGCCCAAATGTGCCTTA, probe CGACTCTTTGCCCACCG; *C9ORF72* variant 3 (NM_001256054.2) forward primer GCGGGGTCTAGCAAGAGCAG, reverse primer TTGGAGCCCAAATGTGCCTTA, probe CCACCGCCATCTC. Position of probes is shown in Figure S1A. Endogenous mouse *C9ORF72* (Rik_3110043O21, NM_001081343.1) commercial assay, probe GCAGCGGCGAGTGGCTATTGCAAGC (Life Technologies Mm01216837_m1). Probes for detection of RNAseq candidate genes were Biorad PrimePCR ddPCR Expression Probe Assays: Cbln4, Mouse dMmuCPE5122216 DDPCR GEX FAM ASSAY 500R; Dpp6, Mouse dMmuCPE5105460 DDPCR GEX FAM ASSAY 500R; Kcnq3,

Mouse dMmuCPE5117670 DDPCR GEX FAM ASSAY 500R; Nedd4l, Mouse dMmuCPE5124352 DDPCR GEX FAM ASSAY 500R; Hprt, Mouse dMmuCPE5095493. For detection of the mature microRNA product of rAAV-GFP-miRC9, RNA was diluted to 10ng/µl and the Taqman microRNA reverse transcription kit (Life Technologies assay #4366597) was used to generate cDNA. A custom Taqman small RNA assay was designed to detect the mature microRNA product of rAAV-GFP-miRC9 (probe ATAGCACCACTCTCTGCATT, Life Technologies). Control RNA snoRNA135 was detected using a commercially available probe (Life Techonolgies # 4427975).

Western Blotting

Tissue samples were lysed in RIPA buffer containing Complete Protease Inhibitor Tablets (Roche, USA) using a Dounce homogenizer followed by sonication on ice. Samples were centrifuged for 10 min at 14,000×g at 4˚C and the supernatant collected. Total protein concentration was quantified using the BCA Protein Assay kit (Thermo, USA). Five micrograms of protein lysate were run on Novex 12% Tris-Glycine gels (Life Technologies, (USA) using Tris-Glycine SDS running buffer (Invitrogen, USA). Proteins were transferred to nitrocellulose membranes using an i-Blot transfer device (Invitrogen, USA). Membranes were blocked for 1 hour at room temperature with Odyssey Blocking Buffer (LiCor, USA) before being probed overnight with primary antibodies. IR labeled secondary antibodies (LiCor, USA) were applied, and blots visualized using the Odyssey Infrared imaging system (LiCor, USA).

Poly (GP) immunoassay

An immunoassay for poly (GP) dipeptides was performed as published [36]. Tissues were homogenized in 10% (w/v) buffer containing 50 mM Tris–HCl, pH 7.4, 300 mM NaCl,

1% Triton X-100, 5 mM EDTA, as well as protease (EMD Millipore, USA) and phosphatase inhibitors (Sigma-Aldrich, USA). Sodium dodecyl sulfate was then added to a portion of homogenate at a final concentration of 2% and samples were vortexed, re-homogenized and sonicated. After sonication, samples were centrifuged at 16,000 x g for 20 min and supernatants collected. The protein concentration of lysates was determined by BCA assay (Thermo Scientific, USA). Poly (GP) levels in lysates were measured using a previously described sandwich immunoassay that utilizes Meso Scale Discovery (MSD) electrochemiluminescence detection technology [9]. Lysates were diluted in Tris-buffered saline (TBS) and tested using 35µg of protein per well in duplicate wells. Serial dilutions of recombinant (GP)8 in TBS were used to prepare the standard curve. Response values corresponding to the intensity of emitted light upon electrochemical stimulation of the assay plate using the MSD QUICKPLEX SQ120 were acquired and background corrected using the average response from lysates obtained from non-transgenic mice prior to interpolation of poly (GP) levels using the standard curve.

Antibodies

Primary antibodies: Goat anti-beta Actin (Abcam, USA), Rabbit anti-Actin (Sigma, USA), Rabbit anti-GFAP (IHC 1:500 Abcam, USA), Rabbit anti-Beta-III-tubulin (IHC 1:1000, Covance, USA), rabbit anti-ChAT (IHC 1:100, Abcam, USA), rabbit anti-cleaved caspase-3 (AB3623, Millipore, (USA), Rabbit anti-IBA1 (IHC 1:1000, WAKO, Japan), mouse anti-NF200 (IHC 1:100, clone SMI32 Abcam, USA), Guinea Pig anti-P62 (Progen, Germany), Rabbit anti-Synaptophysin (IHC 1:5,Life Technologies, USA), Rabbit anti-TDP43 (IHC 1:500 Proteintech, USA), Rabbit anti-TDP43 N-terminus (IHC 1:500, kind gift from Zuoshang Xu) [8]. Secondary antibodies: Donkey antiRabbit Alexa Fluor-488 (IHC

1:1000, Life Technologies, USA), Donkey anti-Mouse Alexa Fluor488 (IHC 1:1000, Life Technologies, USA), Biotinylated Goat anti-Rabbit (IHC 1:1000, Vector Labs, USA), Biotinylated Horse anti-Mouse (IHC 1:1000, Vector Labs, USA). Stated dilutions are for immunohistochemistry or immunofluorescent staining. For western blotting all antibodies were used at the manufacturers recommended dilution.

Human tissues

Frozen frontal cortex tissues analyzed for poly (GP) via ELISA assay were obtained from the Brain Bank for Neurodegenerative Disorders at Mayo Clinic in Jacksonville, Florida, which operates under protocols approved by the Mayo Clinic Institutional Review Board, in accordance with Health Insurance Portability and Accountability Act guidelines. Frozen frontal cortex tissues for ddPCR were obtained from the UCLA Human Brain and Spinal Fluid Resource center and University of Massachusetts and were collected under protocols approved by the UMMS Institutional Review Board.

MicroRNA design and cloning

A 22-nucleotide artificial miRNA (targeting sequence AATGCAGAGAGTGGTGCTATA) in exon 3 of the *C9ORF72* gene was designed and cloned into the miR-155 backbone. This synthetic miR was cloned into the 3'UTR of a GFP encoding AAV proviral plasmid under the control of the chicken beta actin (CB) promoter with a CMV enhancer. The plasmid was used to package pseudotyped rAAV9 vectors. Plasmids and vectors can be requested for academic use at http://www.umassmed.edu/muellerlab

RNA fluorescence in situ hybridization (FISH)

Cryosections (20µm) were fixed in 4% PFA for 20 min, followed by five 20 min washes in DEPC-treated PBS containing 0.1% Tween-20. Sections were permeabilized with 0.5% Triton X100 before pre-hybridization for 1 hour at 55C in 2x saline sodium citrate (SSC) containing 0.1% Tween-20, 50% of dextran sulfate, 50µg/ml heparin, 1mg/ml heat-denatured salmon sperm and 40% formamide. For hybridization, samples were incubated overnight at 55°C in pre-hybridization buffer containing a 1:500 dilution of 1µM DNA probe (Sense: (GGCCCC)4, Antisense: (GGGGCC)4, DM1 (GAC)6, DM2 (GGAC)6) 5' end Cy3 labeled. After hybridization the samples were washed in a pre-warmed mix 1:1 of hybridization buffer and 2XSSC for 30 min at 55°C. Followed by 2 washes in pre-warmed 2XSSC for 30 min at 55°C, 2 washes with 0.2XSSC for 30 min at 55°C, and 2 washes in 1XPBS+ 0.1% Tween-20 for 30 min, at room temperature. Sections were stained with DAPI (1:10,000) for 5 min, and autofluorescence quenched by incubation in 0.5% Sudan Black in 70% ethanol for 7 min. Glass coverslips were mounted using Lab Vision PermaFluor (Thermo Scientific Shandon, USA)

For FISH coupled with fluorescent immunohistochemistry, after probe hybridization and washes, sections were blocked by incubation with 10% serum donkey-serum in PBS with 0.4% TritonX100 for 1hr, followed by incubation with primary antibodies diluted in blocking solution overnight at 4°C. After PBS washes, sections were incubated with an Alexa Fluor-488 conjugated secondary antibodies diluted 1:1000 in PBS for 1hr at room temperature. Autofluorescence was blocked by submersion in 0.5% Sudan black B in 70% ethanol for 7 mins, followed by staining of nuclei by incubation in DAPI (1:10,000). Glass coverslips were applied using ImmuMount (Thermo Scientific Shandon, USA). For

quantification of motor cortex external pyramidal layer nuclei 8-10 10µm z-stack images were collected from three sections per animal. Lumbar spinal motor neurons were identified by large nuclei, with 20-40 nuclei assessed from 8 sections per animal. The number of foci per nucleus was counted using ImageJ, with each nucleus categorized as containing 0 foci, 1-5 foci, 6-10 foci or >10.

Immunohistochemistry

For DAB immunohistochemistry, 8µm paraffin sections of 4% paraformaldehyde or formalin fixed sagittal brain or coronal spinal cord were dewaxed in xylene and brought to water through a graded alcohol series. Endogenous peroxidase activity was quenched by incubation in a solution of 3% H2O2 in 10% methanol for 20mins at 4oC. Non-specific antibody binding was blocked by incubation with 10% serum goat-serum in PBS with 0.4% TritonX-100 for 1hr. Primary antibodies were diluted in blocking solution and sections incubated overnight at 4oC. Following washing, biotinylated secondary antibodies diluted in PBS were applied for 1hr at room temperature. After washing sections were incubated with an avatin-HRP solution (Vector labs, USA) for 30 mins. Peroxidase labeling was visualized with chromogen solution 3, 3'diaminobenzidine (Sigma-Aldrich, USA). Sections were counterstained with hemotoxylin, dehydrated and a glass coverslip applied using DPX. For fluorescent immunohistochemistry, Alexa Fluor-488 or -546 conjugated secondary antibodies diluted in PBS for 1hr at room temperature. Autofluorescence was blocked by submersion in 0.5% Sudan black B in 70% ethanol for 7 mins, followed by staining of nuclei by incubation in DAPI (1:10,000). Glass coverslips were applied using ImmuMount (Thermo Scientific Shandon, USA).

Immunohistochemistry for poly (GP)

For immunostaining of poly (GP) dipeptide repeats, eight micron-thick sagittal slices of mouse hemibrain were cut from formalin-fixed, paraffin-embedded blocks and mounted on glass slides. After drying, slides were deparaffinized and rehydrated in xylene and alcohol washes before being steamed for 30 min in 1X Tris–EDTA (pH 9) buffer solution for antigen retrieval. All slides were processed on a Dako Autostainer with the Dako EnVision™+ system and 3'3diaminobenzidine chromogen. After staining with anti-GP serum (1:10,000) [10], slides were counterstained with Lerner hematoxylin and coverslipped with Cytoseal permanent mounting media.

Immunostaining for neuromuscular junctions

Mice were perfused first with a PBS prewash for 2mins followed by 4% PFA in PBS for 5mins. Gastrocnemius muscles were dissected and post-fixed overnight in 1.5% PFA at 4ºC. Muscles were washed in PBS, incubated in 25% sucrose in PBS overnight at 4ºC and embedded longitudinally in OCT (Thermo Scientific Shandon, USA). 35µm cryosections were collected, mounted on glass slides and stored at -80°C until use. Frozen sections were air dried for 30mins and washed with PBS, followed by blocking in 10% goat-serum in 10% tritonX100 for 3hrs. Sections were incubated for 24hrs at 4°C in a primary antibody solution containing a cocktail of rabbit anti-synaptophysin (1:5, Invitrogen) and rabbit anti-Neuronal Class III BetaTubulin (1:1000, Covance, USA) diluted in blocking solution. Following washing sections were incubated in PBS containing secondary antibodies Alexa Fluor-488 conjugated donkey antiRabbit (1:500) and Alexa Fluor-555 conjugated alpha-

bungarotoxin (1:500) overnight at 4°C. Sections were washed, counterstained with DAPI and coverslips mounted using Immumount (Thermo Scientific Shandon, USA).

For quantification, 15µm z-stacks were collected at 40x magnification from two non-adjacent section of gastrocnemius muscle. Approximately 150-200 NMJs were assessed per animal. NMJs were categorized as; innervated, with complete overlap of green and red signal; partial, with incomplete overlap of green and red signals; denervated, with no overlap of green and red signals.

Semi-thin sectioning, toluidine blue staining and axon quantification Mice were fixed by perfusion with 4% PFA in PBS and L5 ventral nerve roots dissected. Following overnight fixation in 2.5% gluteraldehyde in 0.1M cacodylate buffer nerves were washed and further post-fixed in 1% osmium tetroxide for 1hr. Samples were dehydrated through a graded ethanol series into propylene oxide, followed by overnight infiltration in 1:1 solution of propylene oxide and SPI-Pon 812 resin mixture. Following 3hrs of incubation in SPI Pon 812 resin samples were polymerized at 68°C for 4 days. Nerves were trimmed, reoriented and 0.6µm semi-thin sections collected. Semi-thin sections were mounted on glass slides, followed incubation in toluidine blue on a hot plate for 30 seconds. Following washing, sections were dried, and a coverslip mounted using DPX. Sections were imaged and axon number and diameter quantified using ImageJ.

Dendritic spine analysis

Brains from 18-month-old C9BAC and Ntg littermate controls (n=3 per genotype) were prepared for Golgi staining using the FD Rapid GolgiStain Kit (FD NeuroTechnologies Inc, USA) as per the manufacturer's instructions. Brains were embedded in low gelling

temperature agarose (Boston BioProducts, USA) and 100µm coronal sections were collected using a Leica VT1000 S vibratome (Leica Microsystems Inc, USA). Apical dendrites of layer 2-3 pyramidal neurons were imaged at 60x magnification with 1.5x optical zoom in the prefrontal cortex (3-12 per brain). Number of spines was counted along a recorded length of dendrite (total length of dendrite sampled: Ntg = 1943.5µm, C9BAC = 1266.1µm). Density of spines per dendrite was calculated by dividing the number of spines by the length of dendrite sampled.

RNAseq

Total RNA was extracted from dissected frontal cortex of six months old C9BAC and their Ntg littermate controls by Trizol (Life Technologies). 4µg of high-quality total RNA was treated with RiboZero magnetic beads (Epicentre) to remove most of the ribosomal RNA (rRNA). rRNA depleted total RNA was then treated with Turbo DNAse 1 (Ambion) for 30 min at 37°C to remove possible contamination from genomic DNA. Resulting RNA was purified with RNA clean and Concentrator 5 (Zymo Research), removing RNA fragments shorter than 200 nt and tRNA. Strand-specific libraries were then prepared as described [11]. Validation of cDNA libraries fragment size was performed using an Agilent Technologies 2100 Bioanalyzer. Four barcoded samples were pooled in a single lane and sequenced as 100nt paired-end reads on an Illumina HiSeq 2000 instrument. RNA seq generated greater than 34 million clean reads for each sample. Using TopHAT 2, at least 75% of this total clean read mapped at a single location of the mouse reference genome (mm10) for each replicate sample. RNA seq reads were then aligned to mouse reference transcripts and their abundance was estimated using RSEM software workflow (RSEM parameters: --bowtie-e 70 --bowtie-n 200 --forward-prob 0) [12]. Normalization and

differential expression gene analysis was performed with DEseq2 software package, based on the negative binomial model on R/bioconductor statistical framework [13]. RNAseq data are deposited in the NCBI GEO repository GSE74973

CHAPTER V

Artificial microRNA silences *C9ORF72* variants and decreases toxic dipeptides *in vivo*

Introduction

Amyotrophic lateral sclerosis (ALS), is a lethal neurodegenerative disease that affects approximately 2 in every 100,000 persons worldwide [1]. Patients suffering from this disease have an average life expectancy of 2-5 years after symptom onset. They develop progressive muscle wasting and shortness of breath, ultimately losing their ability to move freely or breathe on their own [3]. Although ALS was first described in the early 1800's as a motor neuron disease, the root cause or prediction of a degeneration pattern still remains to be identified. [1,2]

Recently two independent groups [8, 9] conducting genomics studies of samples from patients diagnosed with ALS and frontotemporal dementia (FTD), found an expanded hexanucleotide repeat expansion (HRE) of (GGGGCC) located in the intronic region of chromosome 9 open reading frame 72 (*C9ORF72*). These expanded repeats, ranging from 23-30 repeats in healthy individuals to hundreds or thousands in ALS patients, vary in number depending on the tissue. So far, the most extensive number of repeats are observed in the brain. [8, 9]. To date, *C9ORF72* HRE accounts for the majority of familial (FALS) and (FTD) cases with known origin [8, 9].

Three main splice variants have been annotated by NCBI as the major products of the *C9ORF72 gene:* Variant 1 (NM_145005.5), Variant 2 (NM_018325.3), and Variant 3 (NM_001256054.1). Variants 1 and 3 containing the expansion are the least abundant, in contrast to V2, which is the more abundant variant. While the function of the *C9ORF72* protein isoforms remains to be determined, they have been linked to endosomal trafficking and nucleocytoplasmic transport [11-13].

The presence of the HRE causes a series of consequential effects including an overall reduction of *C9ORF72* mRNA, an accumulation of *C9ORF72* sense and antisense transcripts resulting in nuclear RNA foci, and the presence of long dipeptide chains generated by repeat-associated non-ATG translation (RAN) in the cytoplasm. [11, 14] These findings led to three hypotheses on the pathogenesis of *C9ORF72:* (1) Haploinsufficiency, where decreased levels of mRNA lead to insufficient gene product [15-17]; (2) RNA gain-of-function, where the expanded RNA foci sequester RNA binding and/or splicing proteins [18]; and (3) RAN translation of the hexanucleotide expansion, in which all reading frames of both a sense and antisense RNA is translated, generating toxic poly-dipeptide protein inclusions [19-22]. Glycine Proline (GP) dipeptides are the most abundant because they are translated from both sense and antisense reading frames, and the Arginine-containing dipeptides, Glycine Arginine (GR) and Proline Arginine (PR), are the most toxic to the cells when overexpressed *in vitro* and in *drosophila* fly models [12, 14]. A recent mouse model designed to overexpress the poly (PR) dipeptide was used to show that this sole dipeptide was bound to DNA within heterochromatin, resulting in cellular aberrations [13]. In addition, a series of recent publications have proposed that the presence of the expansion may disrupt nucleocytoplasmic transport [11, 12, 14, 23, 24], as

well cause epigenetic aberrations that result in age-dependent gene repression seen in both patients and a BAC transgenic model [98]. While the main cause for motor neuron death is still unclear, it may simply be the result of several of these molecular hallmarks simultaneously compounding and overwhelming the cell.

Because the majority of ALS cases are sporadic and only ten percent are familial, finding an effective therapeutic strategy has been challenging. As previously mentioned in CHAPTER II, mainly two FDA approved medications are accessible, providing minor benefits to qualified patients [26, 27]. Thus, the need for a more effective and sustained therapeutic approach. We developed an approach using RNA interference (RNAi) molecules to target *C9ORF72* for post-transcriptional silencing using recombinant adeno associated vectors (AAV) as a means for delivery.

We hypothesize that AAV artificial microRNA (amiR) mediated silencing of *C9ORF72* would decrease mRNA, protein and the cytoplasmic misspliced *C9ORF72* resulting in the reduction of toxic dipeptides. Several amiRs were designed to target all three variants of *C9ORF72*, knowing that microRNAs acting in the cytoplasm as post-transcriptional gene repressors will most likely not affect the nuclear RNA aggregates (foci). After screening, the best amiR candidate was packaged into an AAV9 vector for *in vitro* and *in vivo* delivery to neonate and adult mice through various injection routes. We demonstrate that AAV9 mediated delivery of amiR against *C9ORF72* effectively leads to a decrease of mRNA, protein, and more importantly, the most abundant dipeptide (GP) in the brain and spinal cords of *C9ORF72* BAC112 transgenic mice [99]. Moreover, these findings offer a promising therapeutic strategy for cases of ALS and FTD using amiRs delivered by AAV9 vector.

Results

Newly designed artificial microRNAs target *C9ORF72* variants for silencing

Because the *C9ORF72*-HRE is the major mutation linked to ALS, targeting it for silencing is a practical approach to ameliorate the molecular hallmarks caused by the HRE. To this end, we designed four different artificial microRNAs (amiRs) that perfectly match areas within the *C9ORF72* gene. The constructs were cloned into two different plasmids. The first with a (Pol II) Chicken B-Actin promoter, and the second with a stronger (Pol III) H1 promoter, both containing enhanced Green Fluorescent Protein (eGFP) and ITR flanks **(Figure 5.1A)**

The target location for each amiR is depicted in **Figure 5.1B** and **Table 5.1** lists the amiR sequences. The amiRs were screened in HEK293T cells, and mRNA levels for each variant were evaluated by quantitative Droplet Digital PCR (ddPCR). The results were graphed as ratios of each variant to human endogenous HPRT levels and normalized to the GFP control **(Figure 5.1C).** After the selection process of amiRC9 and based on published data from Pfister, 2017 [100], we anticipated that the weaker CB promoter would not be strong enough for *in vivo* experiments in a mouse model with multiple copies of the transgene. To overcome this obstacle, we moved forward to the *in vivo* experiments using only the H1-amiRC9 construct packaged in AAV9.

H1-amiRC9 silences *C9ORF72 in vitro*

Prior to validating our candidate *in vivo,* we first sought to assess silencing actiity of the packaged AAV9-H1-amiRC9 in primary cortical cultures from the *C9ORF72*-BAC112 mouse model [99, 101]. Cells were dissected and plated as previously described [102]. Two

independent cultures were transduced with GFP control vector, a PBS-mock control, and the H1-amiRC9 vector at day *in vitro* four (DIV4) at a MOI of 50,000 vector particles and collected at DIV10, the transduction efficiency was visually assessed by GFP fluorescence of ~70% **(Figure 5.1D**). Total RNA extraction followed by ddPCR quantification indicated a significant decrease for each *C9ORF72* mRNA variant (**Figure 5.1E**).

To confirm that *C9ORF72* silencing was the result of post transcriptional regulation of gene expression by amiRC9, we designed a custom microRNA assay to quantify the mature form of amiRC9 levels by ddPCR. **(Figure 5.1F**) As expected, only treated samples had detectable levels of amiRC9. In addition to detecting amiRC9, we wanted to compare the expression levels to other endogenous miRs. Henceforth, we assayed for the presence of microRNA128a, a miR shown to be highly expressed in the brain [103, 104] as a guide for comparison. Results show that in treated samples the levels of miR128a are 19-25 times higher than the levels of amiRC9. Nonetheless, the high levels of miR128a detected provide insight that although amiRC9 levels are lower they have a significant biological effect and are most likely not saturating the RNAi pathway.

In CHAPTER IV we had similarly used AAV mediated amiRC9 driven by a Pol II CB promoter, in primary cultures from the BAC we were characterizing. We showed that amiRC9 decreased *C9ORF72* mRNA and the most abundant poly GP depeptide [102]. To determine if we could attain a similar reduction in a second mouse model (BAC112) containting a non-truncated version of the gene, we repeated said experiment and quantified the GP levels in treated and control samples. Notably, an ELISA assay showed the GP dipeptides were significantly lower compared to controls (**Figure 5.1G**)**,** thereby further validating previous results from our group [102].

While microRNAs primarily act in the cytoplasm [80, 105, 106], we suspected based on a some publications [107-109], that they could be shuttled back into the nucleus and decrease the number of RNA foci[23]. To test this, we used fluorescent in situ hybridization (FISH) to detect sense foci. Multiple 4-well chamber slides were scored for foci number per nucleus (**Figure 5.1H**). Quantification revealed no significant differences in foci presence between treated and control samples.

Figure 1

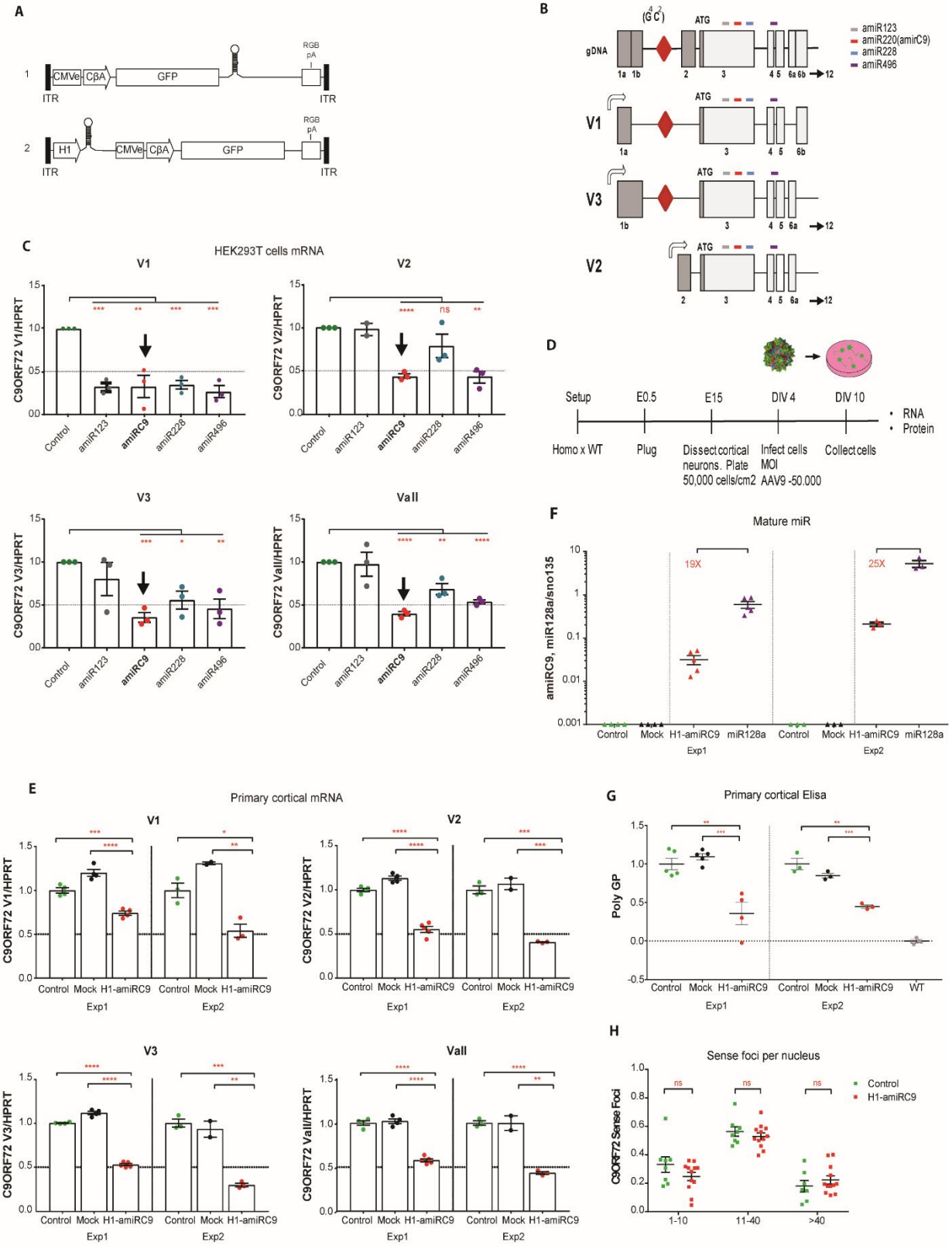
A
1
CMVe-CβA
GFP
RGB pA
ITR
ITR
2
H1
CMVe-CβA
GFP
RGB pA
ITR
ITR
B
gDNA
(G4C2)
ATG
amiR123
amiR220(amirC9)
amiR228
amiR496
1a 1b 2 3 4 5 6a 6b 12
V1
1a 3 4 5 6b
V3
1b 3 4 5 6a 12
V2
2 3 4 5 6a 12
C
HEK293T cells mRNA
V1
C9ORF72 V1/HPRT
V2
C9ORF72 V2/HPRT
V3
C9ORF72 V3/HPRT
VaII
C9ORF72 VaII/HPRT
Control
amiR123
amiRC9
amiR228
amiR496
D
Setup
E0.5
E15
DIV 4
DIV 10
RNA
Protein
Homo x WT
Plug
Dissect cortical neurons. Plate 50,000 cells/cm2
Infect cells MOI AAV9 -50.000
Collect cells
E
Primary cortical mRNA
V1
C9ORF72 V1/HPRT
V2
C9ORF72 V2/HPRT
V3
C9ORF72 V3/HPRT
VaII
C9ORF72 VaII/HPRT
Control Mock H1-amiRC9 Control Mock H1-amiRC9
Exp1 Exp2
F
Mature miR
amiRC9, miR128a/sno135
19X
25X
Control Mock H1-amiRC9 miR128a Control Mock H1-amiRC9 miR128a
Exp1 Exp2
G
Primary cortical Elisa
Poly GP
Control Mock H1-amiRC9 Control Mock H1-amiRC9 WT
Exp1 Exp2
H
Sense foci per nucleus
C9ORF72 Sense Foci
ns
Control
H1-amiRC9
1-10 11-40 >40

Figure 5.1: Artificial microRNA plasmid constructs, HEK293T screening, microRNA silencing validation in cortical primary cultures from BAC112 transgenic model

(A) Schematic of the artificial microRNA plasmid constructs: The first plasmid was used for preliminary screening in HEK293T and the second for further experiments *in vivo* 1.) Chicken beta actin promoter driving enhanced Green Fluorescent Protein (eGFP) and the artificial microRNA, followed by a PolyA tail and flanked by inverted terminal repeats (ITRs). 2.) H1 promoter driving the expression of the artificial microRNA followed by a CBA promoter driving eGFP a PolyA tail and flanking ITRs. (B) Target location of each artificial microRNA: amiRs labeled by the nucleotide target position in regard to each variant. (C) Screening of microRNAs in human HEK293T cell line.: HEK293T cells were transfected with 4 artificial microRNA plasmids driven by CBA promoter 1.) Digital PCR analysis of expression of each individual variant V1, V2, V3 as well an assay detecting all variants jointly Vall, normalized to Human HPRT and in reference to GFP control. Top silencing amiRC9 marked with a black arrow (mean ±SEM, n=3, biological replicates, Student-T test ($p \geq 0.05$ not significant; p* 0.01-0.05; p** 0.001-0.01; p*** 0.0001-0.001; p****<0.0001). (D) Primary culture timeline: Male homozygous mice were crossed with Wild Type female C57/BL6 mice. Cortical neurons were dissected from multiple embryos at embryonic day 15, pooled and plated at 50,000cells/cm2. Infected with each vector at day *in vitro* 4 (DIV4) at a MOI of 50,000 AAV, in 3-5 technical replicates per condition and collected at (DIV10). (E) Digital PCR analysis of expression of each individual variant V1, V2, V3 as well an assay detecting all variants jointly Vall, normalized to mouse HPRT and in reference to GFP control. amiRC9 effectively decreases each variant by~50% in 2 independent experiments with 3-4 technical replicates each. (mean ±SEM, n=2, biological replicates, Student-T test (p* 0.01-0.05; p** 0.001-0.01; p*** 0.0001-0.001; p****<0.0001) (F) Detection of mature amiRC9 product, ratio to small nuclear RNA135. (Mean ±SEM), and compared to endogenous microRNA128a, this miR is highly expressed in the brain. (G) Concentration of poly (GP) measured by Elisa in mixed cortical neurons from the same 2 biological experiments in (E) consistent decrease in treated samples (Mean ±SEM, n=2, biological experiments, Student-T test (p** 0.001-0.01; p*** 0.0001-0.001) (H) Fluorescent in situ hybridization quantification for the sense foci in 4 well chamber slides from the second set of primary cultures (Exp2). The graph shows quantification of 2-3 chambers with ~300 cells counted. Grouped into cells with 1-10 foci, 11-40 or greater than 40. No significant differences between treated and untreated groups.

Striatal brain injections silence *C9ORF72* variants *in vivo*

Since the discovery of *C9ORF72*, a variety of transgenic mouse models were generated by multiple groups [13, 99, 101, 102, 110] with each model differing with respect to mouse background, expansion size, transgene insertion site, copy number and *C9ORF72* expression levels. These mouse models mostly recapitulate the human molecular hallmarks of RNA foci and toxic dipeptides of *C9ORF72*-linked ALS, but do not recapitulate the loss of motor function. Moving forward with the *in vivo* studies, we used the non-truncated transgenic mouse model BAC112 from O'Rourke [99], available at Jackson Laboratories. This mouse model, with a C57BL/6 background and containing the full-length human *C9ORF72* gene and an expansion that ranges from 100-1,000 repeats, recapitulates the pathological aspects of the disease-producing abundant RNA foci and poly-dipeptides. Heterozygous mice have ~16-20 copies of the transgene and homozygous ~38-40 copies [101] (**Figure 5.2 A**)

To determine *in vivo* efficacy of the vector, we first delivered our AAV9-H1-amiRC9 vector into adult heterozygous mice via tail vein injection. Two weeks post injection, liver tissue was collected and analyzed for mRNA silencing by ddPCR (**Figure 5.2 B**). After confirming the vector's effectiveness, we next delivered our vector to the striatum of adult homozygous mice. Striatal injections are a comparatively easy method to inject a large volume to a broad area in the brain.

Homozygous 4-month-old mice were gender and copy-number matched, and separated into three injection groups (PBS-mock, AAV9-CB-GFP-control, and AAV9-H1-amiRC9). We performed bilateral striatal injections, delivering 5 µl of vector per side for a final dose

of 5E10 GC/ml per mouse (**Figure 5.2 C**). Mice were culled 16 weeks post injection, PBS-perfused, and dissected. Two-millimeter punches were taken from each hemisphere for RNA and protein extraction. In accordance with our primary culture experiments, we found significant silencing of each *C9ORF72* mRNA variant by 50% when compared to GFP-control and PBS mock (**Figure 5.2 D**). This was consistent with significant levels of the mature form of amiRC9 in treated samples only (**Figure 5.2 E**).

To quantify the protein levels of *C9ORF72*, we used what was advertised as a human specific antibody. However, we were still able to detect the mouse *C9ORF72* ortholog, which was not detected in knockout control brain samples. To control for this non- species-specific detection, we ran 3 (WT) C57BL/6 brain samples side by side with our controls and treated samples. Densitometry was used to quantify protein levels and the average of the WT samples were subtracted as background. Results showed protein levels of the long isoform (481 aa~ 51kDa) (**Figure 5.2 F, G**) were significantly decreased by more than 80%.

Unlike previously described AAV based therapeutic strategies [35, 49], RNase-H based therapeutic strategies for *C9ORF72* linked ALS, involve decreasing the toxic *C9ORF72* dipeptides, here we tested whether an RNAi based approach could engage RAN translation-RNA templates and achieve sustained dipeptide reduction. To quantify the toxic dipeptide levels, we ran an immunoassay designed to detect the most abundant dipeptide poly GP. After a single striatal AAV injection of H1-amiRC9 at a dose of 5E10 GC/ml we detected ~50% reduction of poly GP dipeptides in all treated mice compared to controls **(Figure 5.2 H**)

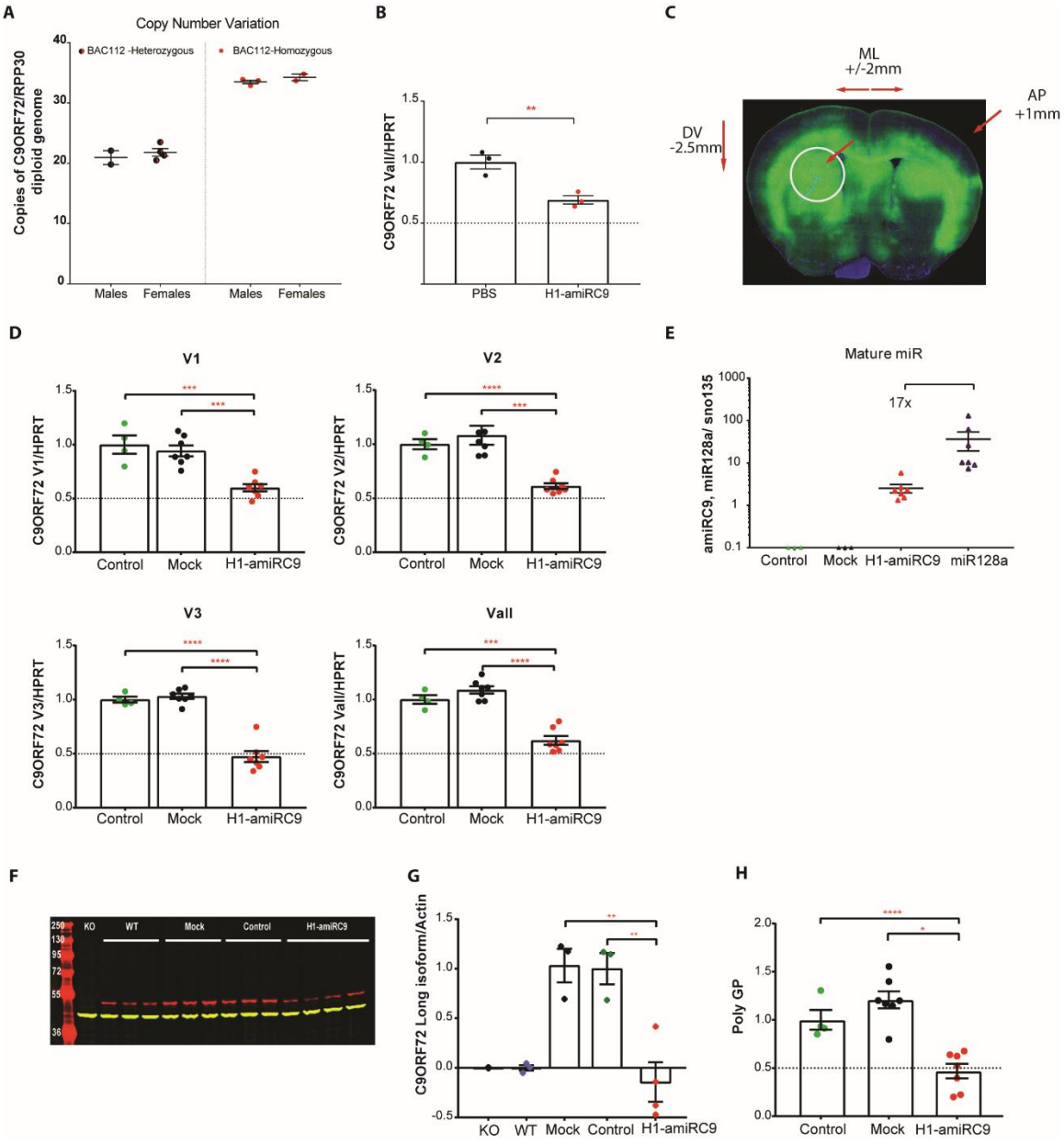

Figure 5.2: AAV9 mediated artificial microRNA silences in the striatum: Adult bilateral striatal injections in BAC112 transgenic model

(A) DNA from ear tissue was used for ddPCR analysis of copy number variation for all animals injected. Samples normalized to either EiF2C1 or RPP30 reference gene for diploid genome. Homozygote and Heterozygote controls at ~40 and ~20 CNV correspondingly. (B) Adult heterozygous mice were injected via tail vein injection with

200µl of vector at a dose of 5E11vg/ml. Mice were collected 2 weeks post injection, RNA from the liver tissue was extracted and ddPCR showed a significant decrease of Vall of~40%. Samples were normalized to mouse HPRT and in reference to GFP control. (mean ±SEM, mice n=3 PBS, n=3 H1-amiRC9) Student-T test (p** 0.001-0.01) (C) Striatal Brain image from an injected mouse depicting the coordinates; medial- lateral +/- 2mm, dorsal – ventral -2.5mm, anterior-posterior +1mm. Arrow depicts ~2mm punch location. (D) Starting from a 2mm punch dissected from the striatum we ran ddPCR analysis of expression of each individual variant V1, V2, V3 as well an assay detecting all variants jointly Vall, normalized to mouse HPRT and in reference to GFP control. Approximately ~50% silencing is observed in H1-amiRC9 treated mice. (mean ±SEM, mice n=4 CB-GFP, n=7 PBS, n=7 H1-amiRC9), (p* 0.01-0.05; p** 0.001-0.01; p*** 0.0001-0.001; p****<0.0001) (E) Detection of mature H1-amiRC9 product, ratio to small nuclear RNA135. (Mean ±SEM), and compared to endogenous microRNA128a, this miR is highly expressed in the brain. (F) Western Blot image for the long isoform of *C9ORF72*, 55kDA protein, normalized to Actin ~42kDA. From left to right KO mouse samples used as a negative control, n= 3 C57 WT mouse controls, n=3 PBS and GFP controls and n=4 H1-amiRC9 treated mice. There is a clear decrease of signal in mice treated with H1-amiRC9. (G) Densitometry quantification of western blot in F); n=3 Wild type mice were used to average and subtract as background signal. Significant silencing is detected compared to untreated controls. Student-T test (p** 0.001-0.01) (H) Concentration of poly (GP) from corresponding groups were measured by Elisa, a similar ~50% decrease in the treated H1-amiRC9 group (Mean ±SEM, Brain punch corresponding to the opposite side of all mice for each group described in A), (p** 0.001-0.01; p****<0.0001)

CSF based delivery outperform peripheral based delivery for transduction of the frontal lobe of the brain

In order to deliver this therapy to patients, multiple delivery options need to be considered to obtain a thorough distribution of the vector to all target sites. The main goal in treating ALS is to reach the brain and central nervous system (CNS). However, when using mouse models to test vector delivery and distribution certain procedures such as intrathecal injections, which in patients is a common delivery route, are considered challenging due to the small size of the animals. To overcome this, we tested both an intracerebroventricular

(ICV) injection as surrogate for efficient cerebrospinal fluid (CSF) delivery and a peripheral facial intravenous (IV) injection in neonate mice.

An ICV delivery is a local injection to the cerebral lateral ventricles. The result predicted is sustained silencing of *C9ORF72* in the frontal lobe of the brain, close to the injection site. Heterozygous P1 pups were injected bilaterally [43] with 2µl of vector (**Figure 5.3 A**) AAV9-CB-GFP~ 8.5E12 GC/ml; AAV9-H1-amiRC9 ~ 5E12 GC/ml and a PBS control. Animals were culled 16 weeks post injection, when PBS-perfused, and whole brain and spinal cords were extracted. Frontal lobes were dissected and fresh frozen for RNA extraction. We assessed knockdown for each variant as described above. As expected, there was significant silencing in the treated samples (**Figure 5.3 B**). We validated the presence of the mature H1- amiRC9 in all injected animals and quantitated levels via ddPCR (**Figure 5.3 C**). We also detected a decrease in toxic poly GP dipeptides by ELISA (**Figure 5.3 D**). FISH was used to assay for sense RNA foci in layer V of the frontal cortex; total quantification showed no significant differences in size or number of foci between treated and control brains. Tranduction efficiency in the frontal lobe was ~60% by visual assessment of GFP fluorescence (**Figure 5.3 E, F**).

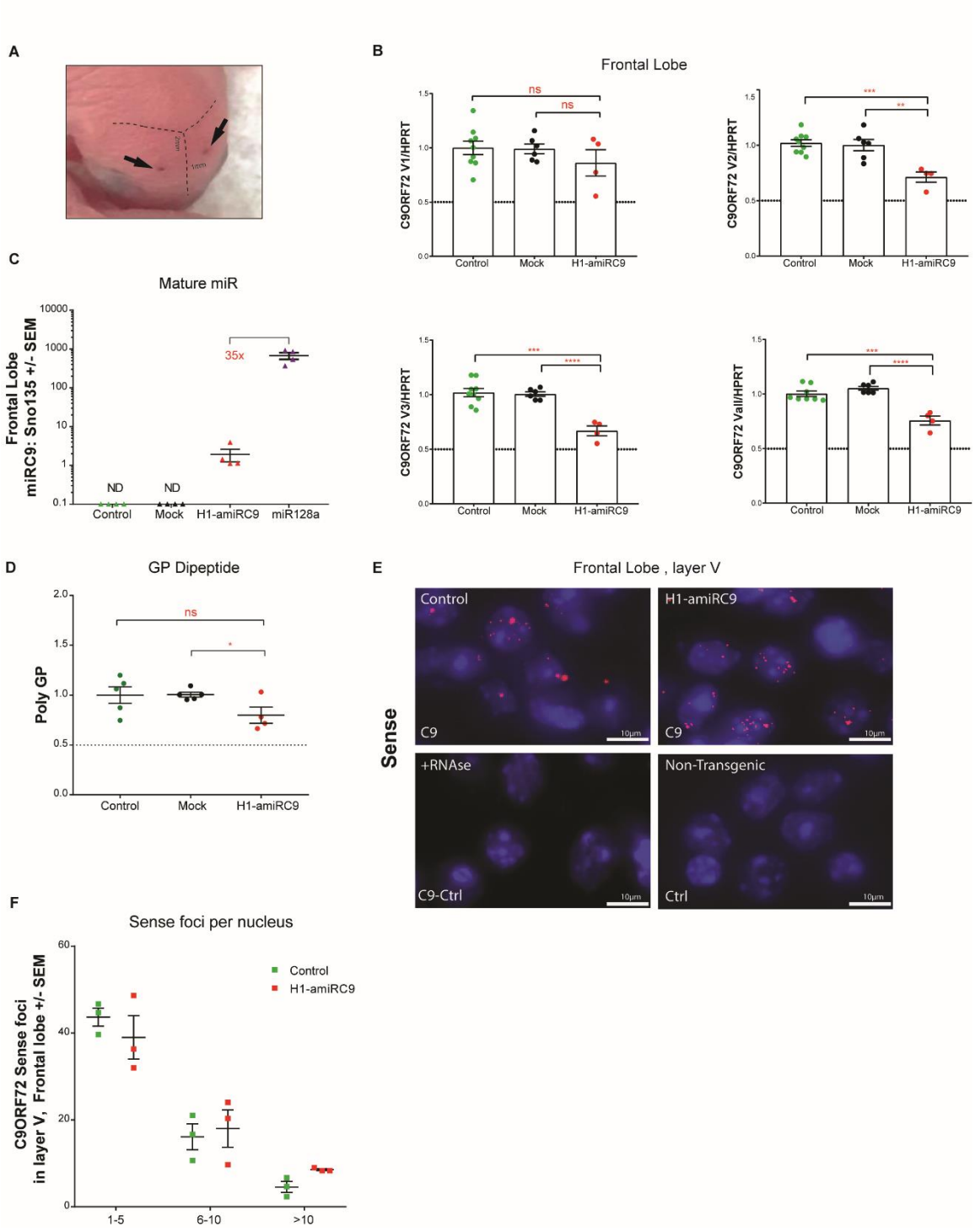
A
B
Frontal Lobe
C9ORF72 V1/HPRT
C9ORF72 V2/HPRT
C9ORF72 V3/HPRT
C9ORF72 Val/HPRT
ns
Control
Mock
H1-amiRC9
C
Mature miR
Frontal Lobe
miRC9: Sno135 +/- SEM
35x
ND
miR128a
D
GP Dipeptide
Poly GP
E
Frontal Lobe , layer V
Sense
Control
H1-amiRC9
+RNAse
Non-Transgenic
C9
C9-Ctrl
Ctrl
10µm
F
Sense foci per nucleus
C9ORF72 Sense foci
in layer V, Frontal lobe +/- SEM
1-5
6-10
>10

Figure 5.3: Neonatal Intracerebroventricular ICV injections silence *C9ORF72* mRNA and dipeptides but not RNA foci in the frontal lobe of the brain

(A) Neonate ICV Injection site. (B) Neonate pups were injected bilaterally with 2µl of vector at ~1E13GC/ml. Mice were collected 16 weeks post injection. Total RNA from Frontal lobe tissue was used for Digital PCR analysis of expression of each individual variant V1, V2, V3 as well an assay detecting all variants jointly Vall, normalized to mouse HPRT and in reference to GFP control. Mice treated with H1 promoter had significant silencing (mean ±SEM, mice n=8 CB-GFP, n=6 PBS, n=4 H1-amiRC9), Student-T test Student-T test ($p \geq 0.05$ not significant; p* 0.01-0.05; p** 0.001-0.01; p*** 0.0001-0.001; p****<0.0001) (C) Detection of mature H1-amiRC9 product, ratio to small nuclear RNA135. (Mean ±SEM) and compared to endogenous microRNA128a. (D) Concentration of poly (GP) from corresponding groups measured by Elisa showed no significant decrease when compared to GFP, although there is a slight decrease in the H1 treated group. Significant silencing is detected when compared to PBS controls. Student-T test ($p \geq 0.05$ not significant; p* 0.01-0.05) (E) Fluorescent in situ hybridization confirms the presence of sense foci in frontal lobe Layer V of treated and control mice. RNA foci were not detected following RNAse treatment or in non-Transgenic controls. (F) Quantification of RNA foci in the frontal lobe layer V, showed no significant differences between treated and untreated groups. The graph shows quantification of an average of 3 mice per group, ~500 cells counted per 3 images. Grouped into cells with 1-5 foci, 6-10 or greater than 10.

Facial (IV) injections slightly outperform (ICV) injections for delivering therapeutic to the spinal cord

Because ALS affects both upper (brain) and lower (spinal cord) motor neurons, we next sought to seek the best surrogate delivery route for our therapeutic in mice. We compared both a systemic and a local route for their ability to spread to the frontal lobe and the spinal cord, an important consideration for clinical settings. P1 pups were injected with 50µl of vector at a dose of 2E11GC/ml (**Figure 5.4 A**). We used the same vectors as previously mentioned. At 16 weeks post injection, tissue collection was followed in the same manner as for ICV samples. We extracted RNA from the frontal lobe and assessed silencing for each variant. Though there was a decrease in *C9ORF72* mRNA and detectable levels of the mature H1-amirRC9, there were no statistically significant differences between treated and control groups (**Figure 5.4 B, C)** Frontal lobe samples from both routes were processed simultaneously for comparison, silencing was only observed via the ICV route.

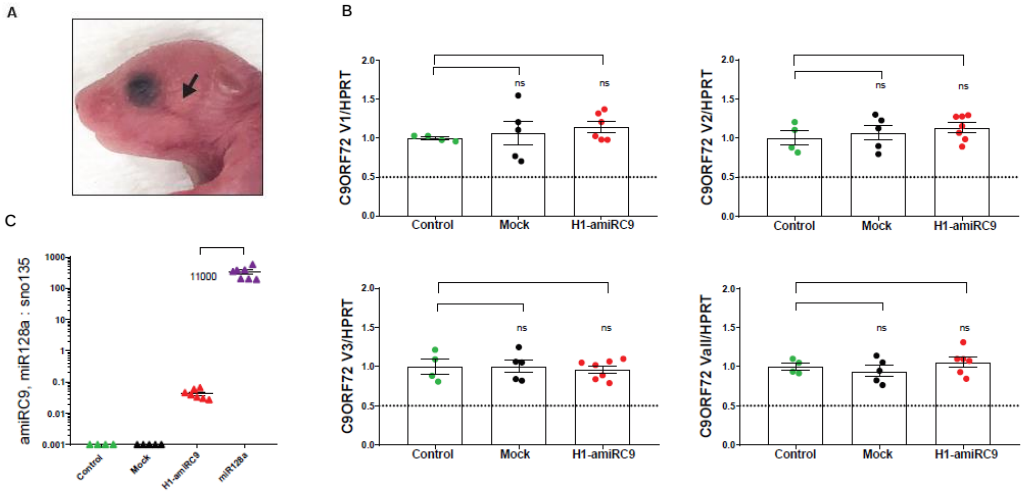

Figure 5.4: AAV9 mediated artificial microRNA silencing in the brain of facial vein injected mice.

(A) Injection site depicted in neonate temporal vein. (B) Neonate pups were injected 50µl of each vector at 2E11vp/ml into the temporal vein. Mice were collected 16 weeks post injection. Total RNA from Frontal lobe tissue was used for ddPCR analysis of expression of each individual variant V1, V2, V3 as well an assay detecting all variants jointly Vall, normalized to mouse HPRT and in reference to GFP control. There was no significant silencing (mean ±SEM, mice n=4 CB-GFP, n=5 PBS, n=7 H1-amiRC9), Student-T test Student-T test ($p \geq 0.05$ not significant) (C) Detection of mature amiRC9 product, ratio to small nuclear RNA135. (Mean ±SEM) and compared to endogenous microRNA128a.

Nonetheless, a systemic delivery was expected to be more efficacious at silencing mRNA in the spinal cord [40]. To verify this, we next compared our two delivery methods to determine which most efficiently silenced *C9ORF72* in the spinal cord. By using a laser capture microdissection (LCM) microscope, we specifically captured motor neurons within the ventral horn of cervical cord sections. We then quantified both the mRNA levels of the *C9ORF72* variants, and the presence of the mature H1-amiRC9. Indeed, a facial vein delivery knocked down *C9ORF72* by ~50% (**Figure 5.5 A, B**), which is slightly more efficient compared to an ICV delivery, where we detected a 30-35% decrease (**Figure 5.5 C, D**).

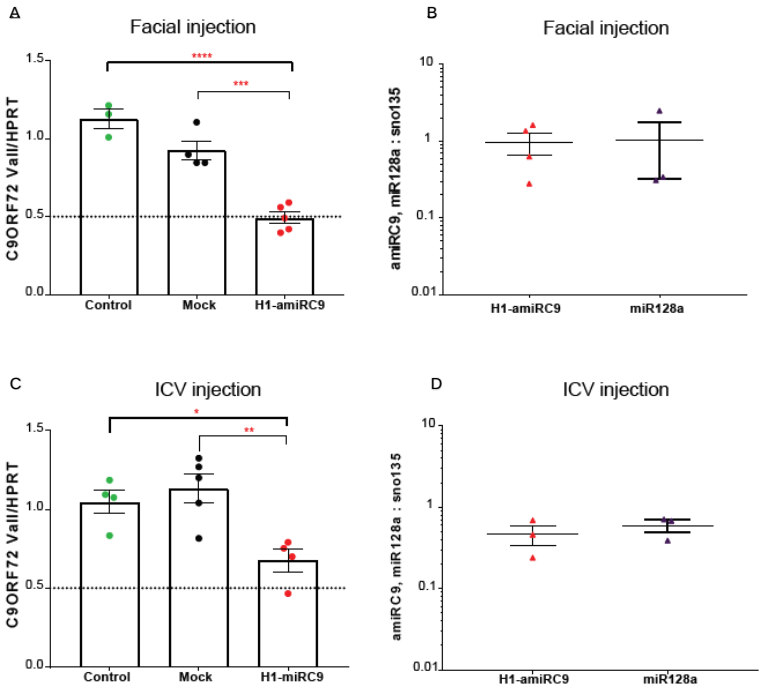

Figure 5.5: Comparison between a systemic and CSF based delivery of therapeutic for spinal cord silencing

(A) Total RNA from laser-captured motor neurons from the cervical portion of the cord showed significant silencing between treated groups for all the variants jointly. Samples were normalized to mouse HPRT and in reference to GFP control. (mean ±SEM, mice n=4 CB-GFP, n=4 PBS, n=6 H1-amiRC9) Student-T test (p** 0.001-0.01; p*** 0.0001-0.001; p****<0.0001) (B) Detection of mature H1-amiRC9 product in LCM cervical cords from temporal vein injections, ratio to small nuclear RNA135. (Mean ±SEM) and compared to endogenous microRNA128a. (C) ICV injected mice were described in Figure 5.3. Total RNA from laser-captured motor neurons from the cervical portion of the cord showed significant silencing between treated groups for all the variants jointly. Samples were normalized to mouse HPRT and in reference to GFP control. (mean ±SEM, mice n=4 CB-GFP, n=4 PBS, n=6 H1-amiRC9), Student-T test (p** 0.001-0.01; p*** 0.0001-0.001; p****<0.0001). (D) Detection of mature H1-amiRC9 product in LCM cervical cords from an ICV injection, ratio to small nuclear RNA135. (Mean ±SEM), and compared to endogenous microRNA128a

H1-amiRC9 targets misspliced transcript that produces the cytoplasmic toxic dipeptides

Although we were able to detect silencing of *C9ORF72* mRNA, protein and dipeptide, we sought to confirm the mechanism by which our H1-amiRC9 can decrease the toxic dipeptides. To this end, we used RNA in situ hybridization (RNAscope) on cervical cord sections from the facial vein injected group and designed two probes: the first targeting the intronic area just before the HRE (intron target) and the second targeting joint exons 3-6 (exon target) **(Figure 5.6 A)**. We predicted the presence of the intron and exon targets in both nuclear and cytoplasmic compartments. Under the assumption that the intron-HRE is retained within the misspliced transcript, we also expected to see these colocalize. In addition, we correctly anticipated a decrease of both targets in the cytoplasm of treated cervical cord samples compared to controls.

Henceforth, ventral horn motor neurons were imaged as Z-stacks and each puncta detected was quantified as an RNA target. Representative images in (**Figure 5.6 B**) illustrate the 3 different treated groups: mock, control and H1-amiRC9. The first column shows DAPI staining for the nucleus of the cell followed by the exon target in red, the intron target in green, and the overlay in yellow. Dotted areas on the top right corners emphasize magnified cytoplasmic regions containing colocalized targets. We scored for total exon targets, cytoplasmic intron targets, and colocalized targets (**Figure 5.6 C**). Treatment with AAV9-amiRC9 resulted in a decrease of ~40% total exon targets, ~60% cytoplasmic intron targets and ~50% of colocalized targets. We also identified the presence of cytoplasmic intron targets that did not colocalize with the exon target. Although we cannot assume this the

expansion lariat, we suspect this is likely the unaccompanied intron-HRE transcript, which cannot be targeted by H1-amiRC9.

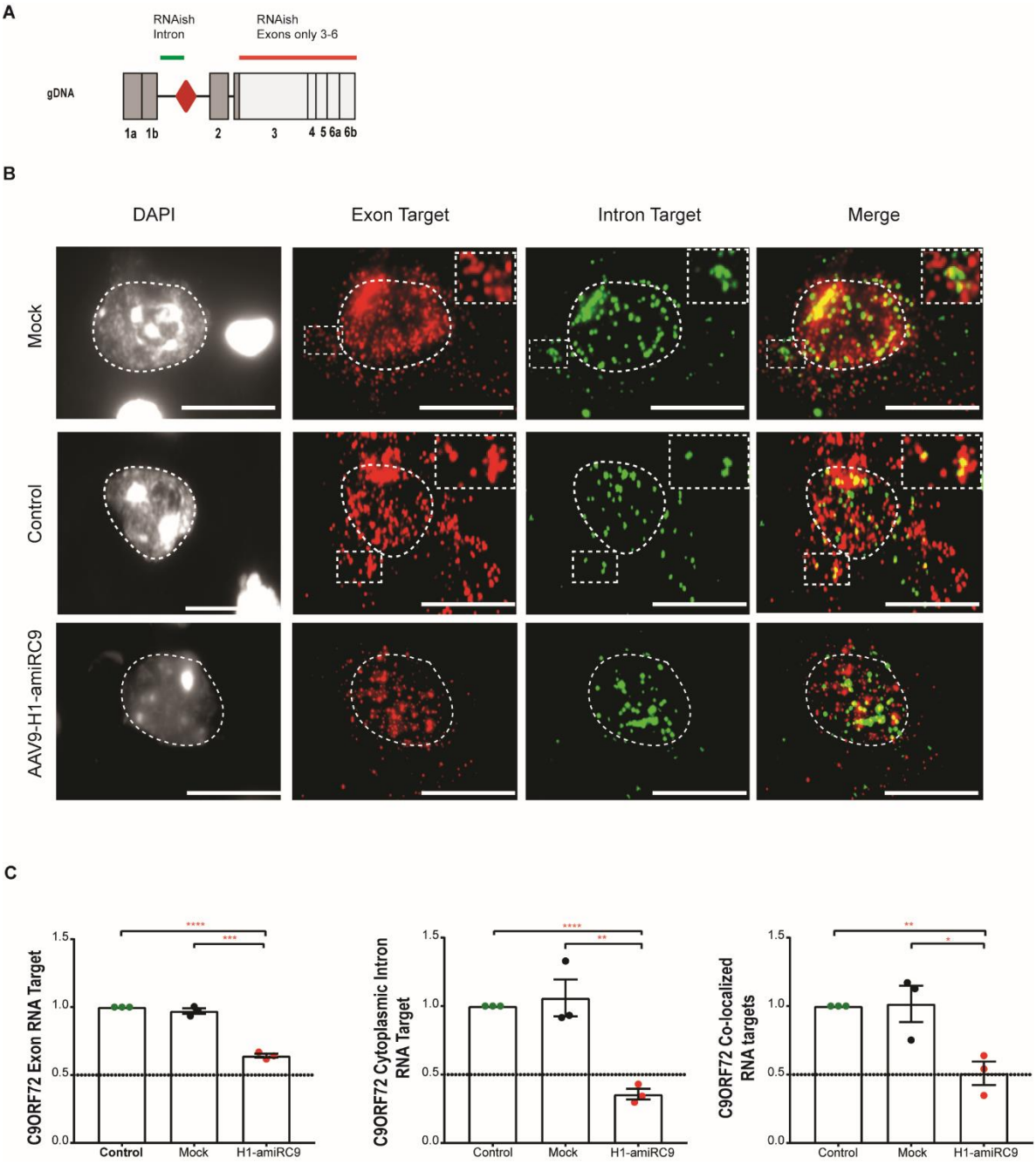

Figure 5.6: RNA in situ hibridazation staining and quantification of intronic and exonic RNA targets

(A) Representation of RNAish target location for Exon and Intron probes. (B) Cervical cord sections were cut at 7µm and stained with RNAish. Each row contains representative images from controls (GFP, PBS) and treated animals (AAV9-H1-amiRC9). Motor neurons were identified based on morphology, and position within the ventral horn. Slides were incubated with multiplex probes detecting *C9ORF72* intron1 (Cy3- Green), *C9ORF72* exons2-6 (Cy5-red). The nuclei are stained with DAPI. The final panel shows the co-localization of all channels and the merge in yellow. Quantification of each target RNA for independent channels shown in panel. The treated samples are distinguishable from controls, they show a significant decrease in RNA target signal for each channel. Scale bars indicate 100 µm (C) Quantification of RNA targets in motors neurons in the ventral horn of cervical cords. Total exon target quantification, cytoplasmic intron target and co-localization of both targets. (Mean ±SEM) Student-T test Student-T test (p** 0.001-0.01; p*** 0.0001-0.001; p****<0.0001)

Discussion

Recent publications from our group and others have shown that an AAV-mediated amiRs approach can be used to target neuro-muscular diseases such as Huntington's and ALS where the key factor is efficient transduction of the brain and spinal cord, as well as sustained silencing of said target [43, 46, 100, 102, 111-113]. Because the *C9ORF72-HRE* mutation accounts for most FALS and FTD, it is a prime target for therapy. Hence, we sought to use RNAi gene therapy to silence this gene and decrease its toxic products.

To achieve this, we designed multiple amiRs targeting exon regions within the *C9ORF72* gene. *A*fter screening in HEK293T cells, we selected the top silencing candidate and further validated its efficiency in primary cortical cultures and *in vivo* in a *C9ORF72* transgenic mouse model.

The transgenic model used throughout our experiments overexpr*esses C9O*RF72 by carrying multiple (18-20) tandem copies of the transgene. In a clinical setting, however,

most patients carry a single copy of the *C9ORF72*-HRE mutation, and only a few rare cases have been diagnosed as homozygous. Mindful of these differences, we set out to demonstrate that our therapeutic strategy could sil*ence C9ORF72* and its toxic counterparts in a safe and sustainable way.

The *in vitro* primary culture experiments confirmed the efficiency of rAAV9-H1-amiRC9 at transducing cortical neurons shown by eGFP expression, the proper processing of the mature H1-amiRC9, and the reduction of *C9ORF72 mRNA a*nd dipeptide levels. In order to assess the RNA foci presence in the nucleus, we used (FISH) to probe for the sense RNA aggregates. Quantification of these showed no significant differences compared to the untreated control. Although recent evidence shows that some microRNAs can shuttle back into the nucleus's for silencing [14, 107-109], that does not seem to be the case for H1-amiRC9 based on our foci quantification, Nonetheless, analysis of nuclear and cytoplasm fragments to assess whether H1-amiRC9 is present and silencing in the nucleus remains to be addressed. It would offer additional useful information regarding the silencing ability of this specific amiR.

As a proof of concept, we aimed to test the efficiency of our H1-amiRC9 *in vivo,* by performing stereotaxic striatal injections in adult mice, where we delivered a high dose of vector to a broad area of the brain. Although we can detect transduction thru eGFP expression 3-4 weeks after injection, we decided to age the mice 16 weeks post injection to allow for the accumulated or de novo GP dipeptides to be decreased by H1-amiRC9. We confirmed proper distribution of the vector into the striatum by eGFP expression, where medium spiny neurons compose most of the neuronal population transduced. All the assays showed a significant silencing of ~50% of *C9ORF72* mRNA, ~80% of protein and~50%

poly GP dipeptides, thereby supporting the notion that a local delivery to adult mice of AAV9-mediated H1-amiRC9 results in knockdown of *C9ORF72* and its products.

A relevant aspect of this research entailed comparing two different alternative delivery approaches in neonate mice: a local delivery with ICV injections, and a systemic delivery through the temporal (facial) vein. The intent was to learn which route is more efficient at silencing *C9ORF72* in the frontal lobe of the brain and in the spinal cord, and to determine if silencing at an early stage of life before the toxic dipeptide proteins accumulate yields higher silencing results. Since *C9ORF72* BAC112 produces detectable GP dipeptides by 2 months of age, we decided to age the mice from both ICV and facial experiments for 4 months post treatment, assuming an extra 2 months would be a good starting point to assay for GP decrease.

We first analyzed silencing in the frontal lobe. In the ICV-injected group. a significant reduction of *C9ORF72* variants and a slight decrease of the GP dipeptides in the treated group were detected. The facially-injected group, however, showed a non-significant mRNA and GP decrease **(Figure 5.4**). We detected low levels of silencing in the brain after a facial delivery, we assume this is due to a dilution factor explained by the nature of the delivery route which ensures the vector would spread systemically throughout the whole body, including crossing the weak BBB forming at P1 in the brain. The ICV route, in contrast, is a local injection closer to the frontal lobe.

Using the same ICV-injected brain sections, we sought to confirm the primary culture data and quantify foci aggregates *in vivo* in Layer V of the Frontal Lobe. Further supporting our previous results, the *in vivo* data showed no significant differences between the treated and

control animals. The only disparity observed between primary cultures and brain sections were the number of sense foci per nucleus. Foci were more abundant in primary cortical cultures ranging from 1-40 than the 1-10 in layer V.

Focusing on the cervical portion of the spinal cord, we used laser capture microdissection to collect motor neurons from the ventral horn of both ICV and temporal (facial) vein injected mice. Since high levels of eGFP expression were visible upon dissection, GFP negative neurons were not excluded for LCM to avoid compromising the RNA integrity and limited sample needed for proper quantification.Both routes showed significant silencing compared to controls; however, the facial vein route had 10-20% greater mRNA silencing effect.

Comparison across the different *in vitro* and *in vivo* experiments revealed a consistent silencing threshold of only 50% *C9ORF72* mRNA, ~70% protein, and Poly GP dipeptide decrease. Assuming 100% of cells are transduced and the majority of silencing is post-transcriptional, we hypothesized that ~50% leftover of *C9ORF72* mRNA should localize primarily to the nucleus where it cannot be targeted by H1-amiRC9. Similarly, with regard to dipeptide silencing, we examined the idea that missplicing results in a cytoplasmic species containing the both the intron-HRE, and the intron-HRE attached to correctly spliced exons 3-6. Only this intron-HRE-exon species allows for cytoplasmic H1-amiRC9 targeting.

These localization questions were addressed using in situ hybridization and specific probes targeting either the intron or the joint exons 3-6. We detected the exon RNA target in both

cellular compartments at a ~ ratio of 40 nuclear to 60 cytoplasmic. Quantification of the exon target showed it to be significantly reduced in the cytoplasm of treated mice only.

One would expect intron containing mRNA to be nuclear or perinuclear, yet their presence in the cytoplasm suggests missplicing is occurring. Lastly, the rare co-localized exon-intron transcript was significantly decreased in the cytoplasm of treated mice, hence the abnormal transcript containing intron-HRE-exon is available for H1-amiRC9 targeting. The cytoplasmic intron-HRE species that does not co-localize with the exon target may be the source for GP production that we are detecting and are unable to decrease. Our work, along with other publications [114, 115], reiterate the presence of the retained intron-HRE as well as a pseudo-start site (CUG) upstream of the intron, driving the translation of the *C9ORF72 (*HRE) [116]. The status of the expansion however, remains to be studied, and we cannot exclude the possibility of the HRE remaining within a lariat or as an unaccompanied intron-HRE transcript, If the latter is occurring it would be interesting to study how this transcript avoids degradation.

A summary of the mechanism by which our therapeutic approach is acting is proposed in (**Figure 5.6**) The first portion depicts the *C9ORF72* gene and the three different variants it produces, with variants 1 and 3 less abundant and carrying the (HRE), represented by the red diamond within the first intron. Splicing then removes the intron sequence and unifies the exons to form a mature mRNA, and each variant is translated to produce two proteins, a short 221 aa. (~24kDA) and a longer 481 aa. (~55 kDA). However, when missplicing occurs, variants 1 and 3 retain the intron beside the expansion, and the expansion is by some means exported to the cytoplasm. The presence of the expanded repeat in the cytoplasm allows for repeat associated non-ATG translation (RAN); resulting in the

production of toxic poly-dipeptides from six different reading frames, GP sense/antisense, GA, GR, PA, and PR [117]. The second portion depicts rAAV9-mediated delivery of H1-amiRC9, where the primary microRNA (pri-miR) enters the RNAi silencing pathway and it is exported to the cytoplasm to be further cleaved and enter the RISC complex, where it binds in perfect complementarity to the target mRNA. Since H1-amiRC9 targets exon 3, both properly spliced and intron-HRE-retaining *C9ORF72* mRNA will be targeted for silencing.

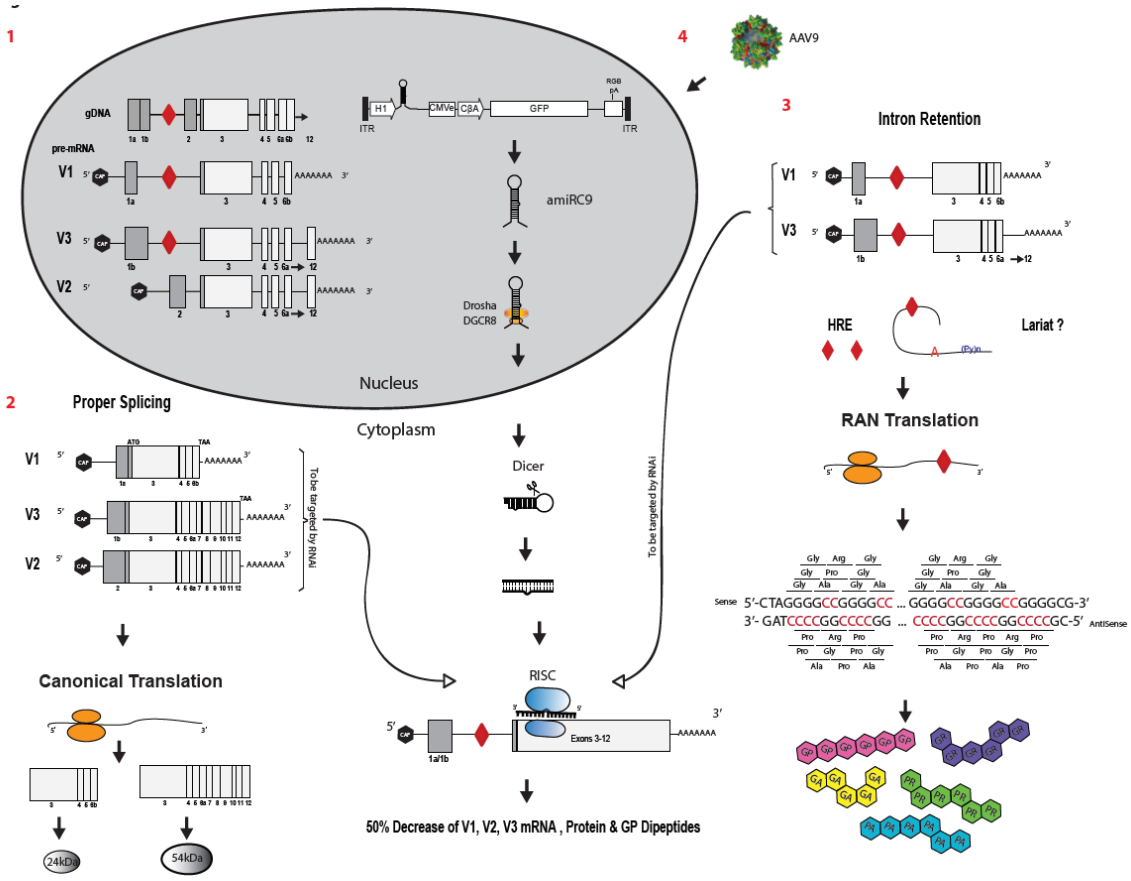

Figure 5.7: *C9ORF72* suggested mechanism

(1) The *C9ORF72* gene produces three different variants, variants 1 and 3 carry the hexanucleotide repeat expansion, depicted by the red diamond within the first intron. (2) When proper splicing takes place, each variant will follow the canonical translation and produce two proteins a short 221 aa. (~24kDA) and a long 481 aa. (~55 kDA) (3) When unconventional splicing is occurring, Variants 1 and 3 retain the intron along with the hexanucleotide expansion. The presence of the expansion in the cytoplasm allows for repeat associated non-ATG translation (RAN). Producing toxic poly-dipeptides. GP, GA, PR, PA, GR. (4) After rAAV9 mediated delivery of H1-amiRC9, the primary microRNA enters the RNAi silencing pathway. It is first trimmed by the microprocessor complex Drosha, and then exported to the cytoplasm to be further cleaved by Dicer. The mature microRNA will enter the RISC complex and bind in perfect complementarity to the target mRNA for cleavage. Since H1-amiRC9 specifically targets Exon 3, both properly spliced and intron retaining *C9ORF72* mRNA transcripts will be targeted for silencing, leading to *in vitro* and *in vivo* of ~ 50% of the *C9ORF72* mRNA, protein and GP Dipeptides.

Even though we have shown that there is intron retention of the HRE, the mechanism by which *C9ORF72* - HRE causes ALS remains a conundrum. While the formation of RNA foci is usually linked to sequestering of RNA-binding proteins that create a gain of function disease, this has not been shown to be the definitive source. Hence the cause of neuronal death could be an accumulation of all the toxic products from *C9ORF72*-HRE. A comparison where either the RNA foci or the dipeptides are individually silenced would provide greater clarity. Using AAV9-mediated H1-amiRC9 to silence C9 mRNA and dipeptides is a useful tool to address this problem.

Another similar approach involves amiRs designed to either target the expansion carrying variants 1-3, or the intron-HRE for both sense and antisense strands. These approaches would also be clinically advantageous, since variants V1-V3 represent a small fraction of total *C9ORF72* mRNA (sparing the abundant normal transcript V2). In addition, targeting the intron itself would lead to a decrease of all HRE-bearing transcripts and preserve

C9ORF72 mRNA. A group in the Netherlands recently published encouraging data using different amiR scaffolds, and AAV5 as a delivery vehicle [23, 118], supporting the use of AAV-mediated amiR silencing as a safe and reliable approach for the treatment of ALS.

Prior to moving forward with these therapeutics, testing in a mouse model that recapitulates not only the molecular but also the motor deficits seen in ALS is advised. If there is sufficient rescue of the motor deficit, then testing should advance to non-human primates. Our group has performed similar studies using AAV-mediated amiR for SOD1, which is the second most common mutation in ALS, yielding extended survival in the SOD1-G93 mouse model [111] as well as in non-human primates [112].

Other available strategies to target *C9ORF72* involve using antisense oligonucleotides (ASOs). ASO treatment in C9-ALS motor neurons derived from iPSCs reduce foci formation as well as gene expression alterations [90] [119]. Jiang et al. showed in their mouse model that they can not only reduce foci but also toxic dipeptides and overt behavioral aspects [89, 99, 110]. Though ASOs have certain delivery and long-term expression setbacks, they have been widely used to target gene silencing and have begun to move into the clinical setting for trials for multiple CNS diseases (SMN2, Huntington's, ALS-SOD1) [29].

While an AAV9- H1-amiRC9-mediated approach may not reach the nuclear foci, the main therapeutic advantage in this instance is that neurons are non-dividing cells, so a single dose can decrease C9O*RF72* gene products, especially the toxic GP dipeptide; hence it can diminish overall cell toxicity which may be sufficient to prevent motor neuron death.

In addition to determining a safe vehicle for a therapeutic, the delivery route, dose, and timing is crucial for gene therapy. For sporadic ALS, if diagnosed at an early stage, it can provide protection and perhaps decelerate the progression of the disease. In Familial ALS, it can be considered a pre-treatment for carriers and ameliorate the symptoms caused by this disease.

Methods

MicroRNA design and cloning

A 22-nucleotide artificial miRNA against exon 3 of the *C9ORF72* gene was designed and cloned into the miR-155 backbone. The artificial miR was cloned into 2 entry plasmids. The first was in the 3'UTR of a GFP encoding AAV proviral plasmid under the control of the chicken beta actin (CB) promoter with a CMV enhancer. The second was in a plasmid containing H1 promoter driving the miR a CMV enhancer followed by a CB promoter diving the expression of GFP. Both were used to package into rAAV9 vectors.

Table 5.1: microRNA Target sequences

amiR	Oligo Sequence	Target Exon
amiR123	Top strand: 5'- TGCTGTTTGGAGCCCAAATGTGCCTTGTTTTGGCCACTGACTGACAAGGCACATGGGCTCCAAA -3' Bottom strand: 5'- CCTGTTTGGAGCCCATGTGCCTTGTCAGTCAGTGGCCAAAACAAGGCACATTTGGGCTCCAAAC -3'	3
amiRC9	Top strand: 5'- TGCTGTATAGCACCACTCTCTGCTAAGTTTTGGCCACTGACTGACTTAGCAGAGTGGTGCTATA -3' Bottom strand: 5'- CCTGTATAGCACCACTCTGCTAAGTCAGTCAGTGGCCAAAACTTAGCAGAGAGTGGTGCTATAC -3'	3
amiR228	Top strand: 5'- TGCTGTTTACATCTATAGCACCACTCGTTTTGGCCACTGACTGACGAGTGGTGATAGATGTAAA -3' Bottom strand 5'- CCTGTTTACATCTATCACCACTCGTCAGTCAGTGGCCAAAACGAGTGGTGCTATAGATGTAAAC -3'	3
amiR496	Top strand: 5'- TGCTGAATACTCTGACCCTGATCTTCGTTTTGGCCACTGACTGACGAAGATCAGTCAGAGTATT -3' Bottom strand: 5'- CCTGAATACTCTGACTGATCTTCGTCAGTCAGTGGCCAAAACGAAGATCAGGGTCAGAGTATTC -3'	4-5

In vitro plasmid screening in HEK293T

HEK293T cells were seeded (1.2 E5 cell/ml) in a 24 well plate, maintained with DMEM media (11995-073; Gibco), 10% Fetal Bovine Serum FBS (F-0926 Sigma-Aldrich) and 1% Penicillin- Streptomycin (30-001-CI; Corning). Twenty-four hours after the cells were transfected using jetPRIME Reagent (Polyplus) and 1µg of each plasmid DNA (CB-GFP, CB-GFP-amiRs) (**Table 5.1**). Forty-eight hours post-transfection, GFP expression was visually assessed; cells were rinsed with PBS and collected using Trizol Reagent (Gibco BRL, Life Technologies, NY, and USA) for RNA isolation. Complementary DNA (cDNA) was generated using (High capacity RNA-to-cDNA Kit, Life Technologies). cDNA was diluted to 20ng/µl and a master mix was prepared for ddPCR.

Droplet Digital PCR (ddPCR) was run as a 20µl reaction containing ddPCR Supermix for Probes (no dUTP) (Bio-Rad, Gladesville, NSW, Australia), 1µl of diluted cDNA, 1µl of each primer/probe (20x), human HPRT with a HEX label was used as an endogenous control, and *C9ORF72* assays with FAM labels that detect each variant (**Table.5. 2**) . The 20µl sample, along with 70µl of ddPCR-oil was loaded into a DG8 cartridge and covered with a gasket according to manufacturer's instructions; the cartridge was then placed in a QX100 droplet generator. Into a 96 well PCR plate 40µl of sample were transferred and then placed in a PCR thermocycler (Eppendorf, North Ryde, NSW, and Australia). The plate was then placed in the QX100 ddPCR reader (Bio-Rad, Gladesville, NSW, Australia) for absolute quantification. Ratios were obtained by dividing absolute values from each variant to human HPRT. Samples were normalized in respect to GFP controls. GraphPad Prizm Program was used to graph and run Student- T test statistical, for three biological replicates.

Table 5.2: Primer and Probes

Probe		Location	Sequence
	Gene Expression		
V1 Life Technologies	GEX: Hs00331877_m1	1a-3	AGATGACGCTTGATATCTCCGGAGC
V2 Life Technologies	GEX: Custom	2-3	Fwd: AGGCGGTGGCGAGTGGATA Rev: TTGGAGCCCAAATGTGCCTTA Probe: CGACTCTTTGCCCACCG
V3 Life Technologies	GEX: Custom	1b-3	Fwd: GCGGGGTCTAGCAAGAGCAG Rev: TTGGAGCCCAAATGTGCCTTA Probe: CCACCGCCATCTC
Vall Life Technologies	GEX: HS00376619	3	AGAATATGGATGCATAAGGAAAGAC
HPRT hum: Bio-Rad	GEX: qHsaCIP0030549		Chromosome location X:133627547-133632465
HPRT mus: Bio-Rad	GEX: qMmuCEP0054164		Chromosome location X:53021117-53021221
	Copy Number Variation		
C9ORF72 genomic	CNV: Custom	4 -intron	Fwd: AAGGCACAGAGAGAATGGAAG REV: AGGCTTATTCGTATGTCTCCAAG Probe: AGGTTGATGGCTACATTTGTCAAGGC
mEIF2C1	CNV: Custom		Fwd: CCTGCCATGTGGAAGATGAT Rev: GAGTGTGGTTGGCTGGATTTA Probe: TGGGGAGAGCTGGAGCCAG

Copy number variation (CNV)

C9ORF72 BAC 112 mouse brains were fresh frozen and cut in a sagittal section to extract DNA. The tissue was lysed overnight at 55^0C, RNAse treated and eluted following

manufacturer's instructions (Gentra Puregene Tissue Kit, Qiagen). The DNA was diluted to 20ng/µl and 2µl were added to the ddPCR master mix along with 1µl of each primer /probe (Genomic *C9ORF72* and mouse EIF2C1 or RPP30 diploid genome). Droplets were generated followed by PCR and absolute quantification. CNV is determined by dividing the absolute value of *C9ORF72* by the absolute value of mEIF2C1 divided by 2 for diploid genome (**Table 5.2**). GraphPad Prism Program was used to graph the values. Homozygote mice have a CNV of 38-40, and heterozygote mice 18-20.

Mouse cortical cells

All murine experiments were conducted at UMASS medical school following strict protocols approved by the Institutional review board. Homozygotes BAC112 mice JAX Stock# 023099 were crossed with Female WT C57BL/6 mice to generate heterozygous embryos. Cortical cells were dissected at embryonic day 15 and pooled from multiple embryos. Mouse cortical cells were seeded at 50,000 cells/cm^2 in six well plates treated with poly-lysine (P4707; Sigma-Aldrich) and four well chamber slides (154917; Thermo Scientific). Cells were maintained with Neurobasal media (21103049; Invitrogen), Glutamax (35050-061; Invitrogen), 2% Penicillin- Streptomycin (15110122; Invitrogen), B27 supplement (17504-001; Invitrogen).

At day, *in vitro* four (DIV4) cells were infected with vectors (rAAV9-CB-GFP; rAAV9-H1-amiRC9-CB-GFP) at MOI of 50,000. At DIV10, cells were rinsed with PBS and collected for RNA or Protein isolation. For total RNA extraction samples were collected in Trizol reagent (Gibco, Life Technologies), the aqueous phase was added to a Zymo column for RNA purification following the Zymo Direct-zol (Zymo research R2050)

extraction protocol. cDNA was made using High-Capacity RNA-to-cDNA Kit, Life Technologies). cDNA was diluted to 20ng/µl and a master mix was prepared for Digital PCR. Ratios were obtained by dividing absolute values from each variant to mouse HPRT. Samples were normalized in respect to GFP controls. GraphPad Prizm Program was used to graph and run Student- T test statistical.

Mature H1-amiRC9 detection

In order to detect the mature H1-amiRC9 product of rAAV9-H1-amiRC9-CB-GFP, the RNA extracted from cells or tissue was further diluted to 10ng/µl. We generated complementary DNA using the TaqMan microRNA reverse transcription kit (4366597; Life Technologies). We used a custom TaqMan small RNA assay that detects the mature artificial microRNAC9 (**Table 5.3**) and used small nuclear RNA 135 as an endogenous control. For comparing the expression levels expressed by our amiRC9 with an endogenous microRNA. We used miR128a (**Table 5.3**) shown to be highly expressed in the brain.

Table 5.3: microRNA assays

Probe	**Assay ID**	**Sequence**
amiRC9: Life Technology	custom	ATAGCACCACTCTCTGCATT
snoRNA135: Life Technology	001230	CTAAAATAGCTGGAATTACCGGCAGATTGGTAGTGGTGAGCCTATGGTTTTCTGAAG
Hsa-miR-128a: Life Technology	002216	UCACAGUGAACCGGUCUCUUU

Bilateral Striatal injections:

Heterozygous BAC112 mice were age 4-6mo, gender and CNV matched into three groups. (PBS, rAAV9-CB-GFP, rAAV9-H1-amiRC9-CB-GFP). Mice were anesthetized with an intraperitoneal injection with a cocktail of Ketamine (100mg/kg), Xylazine (10mg/kg). Mice were positioned in a stereotaxic frame following (Stoica, Lorelei et al. "AAV-Mediated Gene Transfer to the Mouse CNS." Current protocols in microbiology 0 14 (2013): Unit14D.5. PMC. Web. 20 Apr. 2018.). Sterile disposable scalpels (Dynarex # 4111) were used to cut through the skin. Following Stereotaxic Atlas coordinates for the striatum the skull was drilled at positions (AP+1, ML+-2, DV-2.5). The mice were injected at a.5nl/ml flow a volume of 5 µl per side. At a final dose of 5E10 GC/ml per mouse. Mice were collected 16 weeks post injections. The animals were PBS perfused and the brain dissected. Brains were placed in an acrylic 1MM mouse Matrix (CP68-1175-1 SouthPoint surgical supply) and sections 2-6 were taken. A GFP positive 3mm punch encompassing the injection site was taken and used for either RNA or protein. The samples were fresh frozen in liquid nitrogen and stored in a -80 freezer for tissue processing.

ICV injections in Neonates

Postnatal day 1 pups were separated from their mother and individually anesthetized with isoflurane and placed in a heated pad. Prior to the injection's special adaptors RN Compression fitting 1mm Catalog # 55750-01, were used to attach to the Hamilton Syringe 10µl, gastight model: 1701 RN, and Micro-capillary FHC: Borosil 1.0 mm OD x 0.5mm ID/Fiber (100mm, 250 pack) were pulled in a Sutter Instrument: P-97 Flaming/Brown Micropipette puller. The pup was injected with 2µl of vector, into the lateral ventricle of each hemisphere, 2mm from the transverse sinus and 1mm to either side of the superior sagittal sinus, to a depth of 2 mm. It was then placed in a heating pad until it regained

consciousness. The pups were then rubbed against the bedding and placed back with the mother. Multiple litters were injected with the vectors: AAV9-CB-GFP~ 8.5E12 GC/ml; AAV9-CB-GFP-amiRC9~ 1E13 GC/ml; AAV9-H1-amiRC9-CB-GFP~ 5E12 GC/ml. Animals were aged and culled 16 weeks post injection. Following a 3-minute PBS perfusion, the whole brain and spinal cord were extracted, and the frontal lobe was dissected. The left side was fresh frozen, and the right side was embedded in OCT for cryo-sectioning and staining.

Temporal vein injections in Neonates

Postnatal day 1 pups were separated from their mother and individually anesthetized with isoflurane and placed in a heated pad. A Hamilton Syringe 10µl, gastight model: 1701 RN was used to inject 50µl of vector at a dose of 2E11GC/ml. We used the same vectors as previously mentioned for the ICV treatment. After injection the pups were rubbed against their bedding to prevent rejection from their mother and placed back in the cage. Mice were culled 16 weeks post injection following the same collection procedure as for the ICV samples.

Western Blot

Samples were lysed in RIPA buffer and a complete inhibitor tablet (Roche), at 4˚C and the supernatant collected. Then, 5µg of protein lysate was run on Novex 12% Tris-Glycine gels (Life Technologies, USA) using Tris-Glycine SDS running buffer (Invitrogen, USA). Protein was transferred to nitrocellulose membranes using an i-Blot transfer device (Invitrogen, USA). Membranes were blocked for 1 hour at room temperature with Odyssey Blocking Buffer (LiCor, USA) before being probed overnight with primary antibodies

(SiGMA ABN 1644-1645). IR labeled secondary antibodies were applied, and blots visualized, and the band intensity was quantified using the Odyssey Infrared imaging system (LiCor, USA).

Poly (GP) ELISA

Samples were lysed in RIPA buffer and a complete inhibitor tablet (Roche), using lysing Matrix D Beads (MP Bio). 3x 3min 30HZS in a Tissuelyser II (Qiagen 85300), samples were placed in a new Eppendorf 1.5ml tube and sonicated. After sonication, samples were centrifuged at 16,000 x g for 20 min and supernatants collected. The protein concentration of lysates was determined by BCA assay (Thermo Scientific, USA). Poly (GP) levels in lysates were measured using a previously described sandwich immunoassay that utilizes Meso Scale Discovery (MSD) electrochemiluminescence detection technology [29]. Lysates were diluted in Tris-buffered saline (TBS) and tested using 35µg of protein per well in duplicate wells. Serial dilutions of recombinant $(GP)_8$ in TBS were used to prepare the standard curve. Response values corresponding to the intensity of emitted light upon electrochemical stimulation of the assay plate using the MSD QUICKPLEX SQ120 were acquired and background corrected using the average response from lysates obtained from non-transgenic mice prior to interpolation of poly (GP) levels using the standard curve.

Fluorescent in situ hybridization

Cryosections of 20µm were serially collected (1/20) through the motor cortex and Cervical spinal cord. Sections were fixed in 4% PFA for 20 min, followed by five 20 min washes in DEPC-treated PBS containing 0.1% Tween and 50µg/ml of Heparin. Sections were pre-hybridized for 1 hour at 55^0C in 2x Sodium citrate (SSC) containing 0.1% Tween 20, 50%

of dextran sulfate, water, 50µg/ml heparin, 1mg/ml heat-denatured salmon sperm and 40% deionized sulfate. For hybridization, samples were incubated overnight at 55^0C in pre-hybridization buffer containing a 1:500 dilution of 1µM DNA probe (Sense: $GGGGCC_4$) with a Cy3 label. After hybridization, the samples were washed in a pre-warmed mix 1:1 of hybridization buffer and 2XSSC for 30 mins at 55^0C. Followed by 2 washes in pre-warmed 2XSSC for 30 mins at 55^0C, 2 washes with 0.2XSSC for 30 min at 55^0C, and 2 washes in 1XPBS+ 0.1%Tween +50µg/ml Heparin for 30 min, at room temperature. Sections were stained with DAPI (1:10,000) for 5 min, and auto fluorescence quenched by incubation in 0.5% Sudan Black in 70% ethanol for 5 min. Glass coverslips were mounted using Lab Vision™ PermaFluor™ Aqueous Mounting Medium (Thermo Scientific Shandon, USA)

For quantification of frontal lobe layer V neurons nuclei 10- 15µm z-stack images were collected from three sections per animal. 100-200 nuclei assessed from 3 sections per animal. The number of foci per nucleus was counted manually, with each nucleus categorized as containing 0 foci, 1-5 foci, 6-10 foci or >10.

Laser Capture microdissection of motor neurons and RNA isolation

Fresh frozen cervical cords were cryo-sectioned at 7µm of thickness. Using the Arcturus XT laser capture microdissection system. Slides were stained with histogene kit, fixed and dehydrated with 70-95-100% Ethanol followed by Xylenes. Approximately ~200 ventral horn Motor neurons per cap were collected and a total of 3 caps per animal. The samples were then processed for RNA using the PicoPure RNA extraction kit following

manufactures instructions and sent to a bio-analyzer for RNA concentration and quality. RNA from 2 out of 3 caps were individually run on ddPCR for quantification.

RNAscope Fluorescent Multiplex Assay

Cervical cords were embedded in OCT, frozen and 7µm cryosections were placed in plus/plus slides for staining. Sections were fixed in 10% NBF for 1 hour, followed by two washes in 1X PBS and four 5 min washes in ethanol (50%, 70%, 100%, and 100%) at room temperature. The fixed sections were covered with 5 drops of Protease IV for 30 min at room temperature followed by two washes in 1X PBS prior to proceeding to the RNAscope Fluorescent Multiplex Assay protocol. Probes were warmed for 10 min at 40^0C, cooled to room temperature, and a 1:50 C2:C1 and C3:C1 hybridization mixture was prepared. Approximately 180µl of hybridizing probe mixture was used to cover the sections completely and incubated for 2 hours at 40^0C. Two 2 min washes in 1X Wash Buffer (2.94 L distilled water to 1 Bottle (60mL) RNAscope Wash Buffer Reagents) with minor agitation preceded all of the Fluorescent Multiplex Detection Reagent additions. Approximately 180µl of each of the fluorescent detection reagents was added to completely cover all sections within the hydrophobic barrier prior to incubation in the HybEZ™ Oven at 40^0C. A 30 min incubation was used for Amp 1-Fl, 15 min for Amp 2-Fl, 30 min for Amp 3-Fl, and 15 min for Amp 4-Fl-Alt C. Sections were counterstained with Dapi for 30 sec at room temperature and glass coverslips were mounted using Prolong Gold Antifade Mountant and stored in 4ºC.

RNAscope Imaging and Quantification

All images were taken using a Leica DM5500 B microscope with a Leica DFC365 FX camera. A total magnification of 100.8X (63X oil lens * 1.6X camera) was used to generate the images, while using the acquisition settings **(Table 5.4**) for the various probes. A maximum projection of z-stacks with a range of 1-3µm was used for quantification.

Table 5.4 Fluorescent Microscope Acquisition and Filter Settings (AMP 4 Alt-C-FL)

Probe Channel	Excitation[nm]	Emission[nm]	Filter Set	Exposure[ms]	Gain	Intensity
C1	Atto 550 nm	580 ± 10nm	Cy3	645.00	3.2	5.0
C2	Atto 647 nm	690 ± 10nm	Cy5	466.00	3.2	5.0
	358 nm	461 nm	DAPI	36.00	1.2	3.0
	~488 nm	~509 nm	EGFP	300.00	3.0	4.0

Approximately 15 images were taken from three different cervical spinal cord sections for each animal, each with at least one motor neuron present. The quantification of intron, exon, and co-localized targets was conducted manually for motor neurons in the ventral horn. Cervical spinal motor neurons were identified by location, morphology, and larger nuclei. All RNA targets were characterized with respect to size (**Table 5.4**) as measured by the scale bar annotation tool in Leica Application Suite X (LAS X). Intron RNA targets were additionally classified as inside or outside of the nucleus by the presence of puncta within the DAPI signal. Co-localization of intron and exon puncta was determined using the z-stack and spectral color change as observed by light color properties of the RGB additive color model. RNA targets corresponding to an overlap of GFP signal were attributed to background and were not included in the quantification.

CHAPTER VI

Discussion

ALS is a fatal neurodegenerative disease, for which only 5-10% of familial cases could benefit from genetic screening. For most cases the irreversible effects of neuronal death become evident when the patient first shows signs of weakness, with either a bulbar onset, affecting primarily the facial muscles, speech and swallowing reflex, or a non-bulbar form affecting the extremities, neither following a specific degeneration pattern. The goal is to employ the therapeutic developed here as an early intervention to slow or halt the disease progression and improve the patient's quality of life.

For *C9ORF72* linked ALS however, haploinsuffiency, gain of function, RAN translation and nucleocytoplasmic transport seem to be key mechanisms by which *C9ORF72* -HRE is causing toxicity. Although the main issue seems to be the expansion itself, we and others have shown that targeting other areas within the gene can also lead to decreased cytotoxicity [23, 89, 90, 99, 118-121]. Due to the lack of a model that recapitulates all of the ALS hallmarks in which to test this approach, our group generated a human *C9ORF72* BAC transgenic model. For unknown reasons we[121] and others[99, 122] were unable to generate a model with both motor and molecular phenotype seen in ALS/FTD patients [101]. With the exception of a later model generated by Liu, Y. J. *et a*l, 2016 [122] for which a small percentage of females and at a later time point males , develop the motor

and molecular *C9ORF72*-ALS phenotype. To date no one has elucidated why this and not the other models recapitulated the motor deficits.

After characterizing the C9BAC mouse model we sought to test the artificial microRNAs targeting *C9ORF72* in primary cortical cultures and demonstrated a statistically significant decrease of *C9ORF72* mRNA variants and GP dipeptides in the treated samples when compared to controls. We then decided to further validate the artificial microRNA in a different mouse model produced by O'Rourke *et al*,[99], to confirm that the decrease was not just specific to our mouse model. In this model we tested our therapeutic reagent using both adult and neonate mice and multiple dosing routes. We were able to show different levels of *C9ORF72* mRNA, protein and dipeptide silencing in the frontal lobe of the brain and in the spinal cord depending on the delivery route. More importantly, we have identified a new transcript produced by missplicing of the intron bearing the HRE. This new cytoplasmic species is accessible for amiR targeting leading to the decreased dipeptide levels. Based on this preclinical screening, *in vivo* work in non-human primates to test safety and toxicity of AAV mediated H1-amiRC9 is currently underway.

Although we have yet to understand the complete mechanism of action for *C9ORF72*. An ideal approach would entail using AAV to deliver two artificial microRNAs targeting both the sense and antisense intron bearing the-HRE. This approach would decrease the levels of only the intron- HRE transcripts sparing the correctly spliced *C9ORF72*.

Moreover, recent studies using RNAse-H based technology have shown antisense oligonucleotides (ASOS) targeting both exonic and intronic *C9ORF72* nuclear RNAs can decrease mRNA, foci and dipeptides with the only caveat of having to be continuously re

delivered depending on the ASO's chemistry and half-life. Another concern with this therapeutic strategy envolves the risk of repeated injections for delivery of the ASO. Until the chemistry allows for longer, sustained persistance of ASOs, this therapeutic can be successful but at a health risk to the patient. Even so, the efficiency and lack of toxicity seen in animal models have lead to the commencement of clinical trials using ASOs for *SOD1*-ALS and *SMN2* for SMA [29, 123] among others. Both AAV and ASO approaches have shown significant therapeutic advantages, with differences which may or may not vary from patient to patient. Nonetheless, historical data from AAV clinical trials [36, 49, 124, 125] have shown that this approach if successful could be a permanent cure for *C9ORF72* linked ALS patients.

In addition to demonstrating that an AAV mediated RNAi approach is a sound and powerful tool to target ALS, I have also provided a methodology and approach to targeting other diseases with similar mechanisms. For different cases, such as in spinal muscular atrophy (SMA), where a mutation causes haploinsuffiency, AAV-mediated replacement therapy of the SMN gene has rapidly advanced to human clinical trials with groundbreaking results [126]. However, some diseases may require a combination of both silencing and replacement therapy to rescue normal cell function [48, 49] , such as in the case of hereditary sensory neuropathy (HSAN1), for which we have designed a therapeutic approach described in appendix II.

APPENDIX I

A *C9ORF72* BAC mouse model recapitulates key epigenetic perturbations of ALS/FTD

Introduction

A pathological GGGGCC hexanucleotide repeat expansion mutation located within the non-coding portion of the *C9ORF72* gene has been identified as the cause of chromosome 9p21-linked ALS and frontotemporal dementia (FTD),[127, 128]. The *C9ORF72* HRE is hypothesized to confer cytotoxicity, in part, via RNA gain of function whereby sense and antisense transcripts harboring the repeat sequester RNA binding proteins resulting in ribonucleoprotein foci [119, 129], preventing the proteins from carrying out their normal function. In addition, expanded RNAs and dipeptide-repeat proteins (DPRs) that arise from aberrant translation of mutant RNAs disrupt nucleocytoplasmic transport [24, 130, 131]. Given that mutant RNAs and the DPRs derived from them are the primary source of pathology in C9-ALS and epigenetic mechanisms regulate their production, it follows that epigenetic regulation of expanded *C9ORF72* alleles is of particular significance.

Epigenetic alterations occur in many repeat expansion disorders and there is now definitive evidence that epigenetic perturbations associated with the *C9ORF72* HRE contribute to C9-ALS pathophysiology [132-134]. Expanded *C9ORF72* alleles have reduced transcription rates, are depleted of active histone marks with concomitant enrichment of repressive epigenetic marks, including DNA hypermethylation in some cases. Specifically, the levels of all three *C9ORF72* transcript variants are reduced in C9-ALS, including variant 2 which does not contain the repeat sequence due to alternative transcription start

site (TSS) utilization [119, 127, 135]. Enriched repressive epigenetic marks include tri-methylation of histone 3 at lysine positions 9 and 27 (H3K9me3, H3K27me3) and histone 4 lysine 20 (H4K20me3) [135]. In addition, DNA methylation of cytosine residues within CpG islands near the *C9ORF72* promoter occurs in approximately 30% of patients [136-138]. Notably, promoter hypermethylation is theorized to be protective due to decreased production of toxic products in patient cells [139] leading to reduced neuronal loss in the brain [140]. Mechanistically, DNA hypermethylation is counteracted by active DNA demethylation [141] while repeat instability is conferred by highly stable GC-rich RNA-DNA duplex formation across the HRE [142]. In addition to repeat instability, RNA-DNA hybrid structures, or R-loops, may also contribute to *C9ORF72* hypermethylation. Indeed, R-loops are known to regulate DNA methylation at CpG islands of gene promoters including those affected by repeat expansion mutations [143, 144]. Taken together, these observations indicate that the *C9ORF72* HRE alters the local epigenetic environment such that the rate of transcription, DNA methylation, histone modification and R-loop formation are all perturbed by the expansion mutation.

Two independent groups were first to develop transgenic mouse models of C9-ALS carrying the pathogenic *C9ORF72* HRE [121, 145]. The human repeat expansion sequence was introduced into the mouse genome using a bacterial artificial chromosome (BAC). The C9-BAC mice displayed typical histopathological gain-off-function features of C9-ALS including RNA foci and DPR aggregates, yet no motor or cognitive phenotypes were observed. Subsequently, two additional groups generated C9-BAC mice that exhibit reduced survival, motor deficits and cognitive dysfunction [120, 122]. While these previous reports focused on the production of toxic HRE products, none have described

epigenetic features of the *C9ORF72* transgene. Notably, the number of toxic mRNA foci and DPR abundance in C9-BAC mice was observed to significantly decline as a function of age [121]. This is somewhat counter-intuitive since ALS/FTD are age-related disorders. Therefore, we hypothesized that partial epigenetic repression of the *C9ORF72* transgene could potentially attenuate the severity of phenotypes in C9-BAC mice, limiting their applicability to human disease. Herein, we performed a post-natal developmental study using transgenic BAC mice reported by Peters et al. [121] to systematically investigate whether characteristic epigenetic features of the HRE in C9-ALS are recapitulated in this mouse model system.

Results

Expression of the human *C9ORF72* transgene decreases while H3K9 tri-methylation increases in C9-BAC mice during the first post-natal weeks

Tissue samples from mice of 7 different age groups were assessed in this study: post-natal week 0 (n=5), 2 (n=4), 7 (n=5), 17 (n=4), 30 (n=9), 36 (n=4) and 93 (n=9). The activity and epigenetic status of the human *C9ORF72* transgene was assessed by quantifying levels of mRNAs and histone methylation within the promoter of the human gene. First, we measured human *C9ORF72* mRNA levels in the neocortex of C9-BAC mice across all age groups using quantitative real-time (qPCR). Three primer sets were used to amplify different human *C9ORF72* mRNA transcript variants (V1, V2, and V3) as well as three endogenous controls (beta-actin, GAPDH and 18S). Due to the observed variability in beta-actin expression levels across age groups (**Figure A1.1A**), we used the average values of GAPDH and 18S for normalization. We found that levels of all three *C9ORF72* transcript

variants are significantly reduced, starting within the first post-natal weeks of age (**Figure A1.1B, C, D**). To confirm our findings, we performed digital droplet quantitative PCR (ddPCR) for absolute quantification of the human *C9ORF72* levels and observed a similar trend (**Figure A1.1F**). This observation suggests that partial epigenetic repression of the transgene in the brain of post-natal C9-BAC mice is age-dependent. Next, we utilized chromatin immunoprecipitation (ChIP) to isolate H3K9me3-bound DNA fragments from brain samples of 0 and 7 weeks-old C9-BAC mice. H3K9me3 is a repressive epigenetic mark that negatively correlates with transcription rates and is enriched within the promoter region of expanded *C9ORF72* alleles as compared to unexpended alleles [135, 146, 147]. Using two different primer sets (C9.A and C9.B), we found that H3K9me3 levels within the promoter of the human *C9ORF72* transgene were significantly increased in the brain of C9-BAC mice by week 7 (**Figure A1.1E**). Increased H3K9me3 indicates partial epigenetic repression of the mutant gene locus occurs in the first post-natal weeks of life.

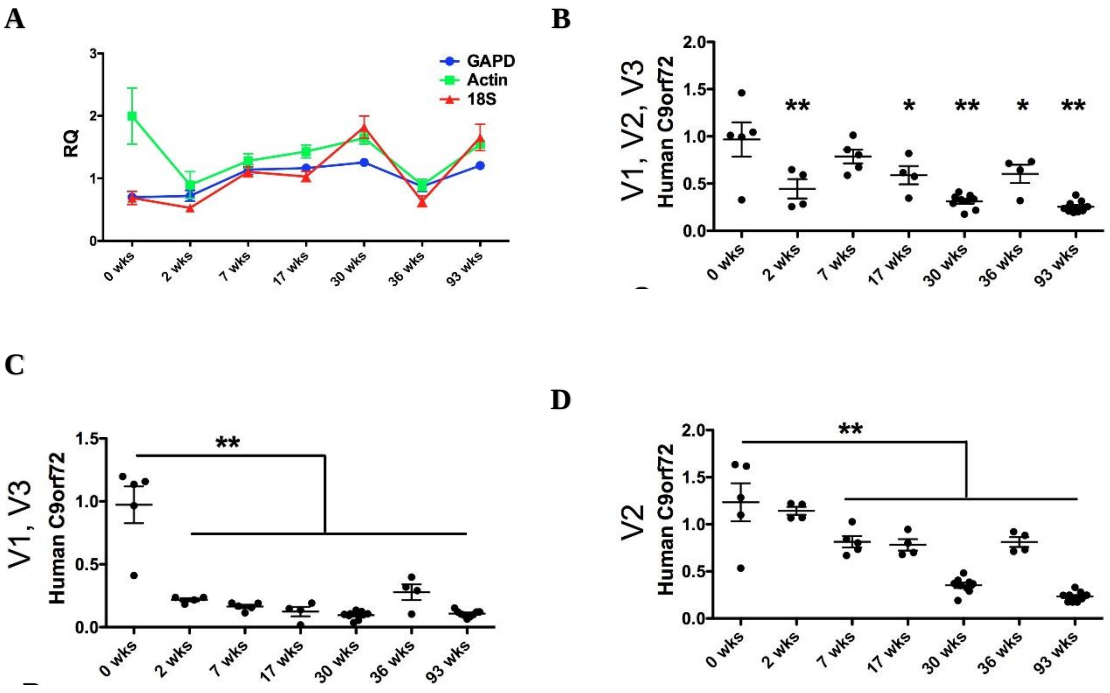

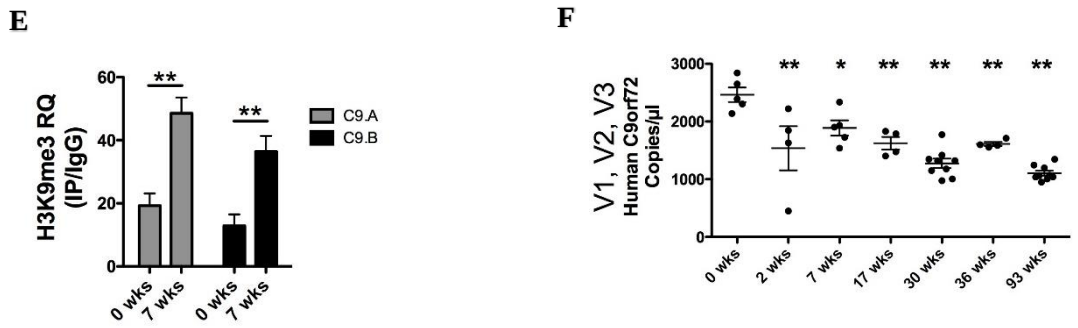

Figure A1.1 *C9ORF72* transcription decreases while a repressive histone methylation mark increases in the brain of C9-BAC mice during the first post-natal weeks

Relative quantification (RQ) values of mouse beta-actin, GAPDH and 18S endogenous controls in C9-BAC mouse cortex across different age groups are shown (A) Values of human *C9ORF72* in the BAC mouse cortex, normalized to the average of GAPDH and 18S, are shown for primers amplifying transcript variants V1, V2, V3 (B); V1, V3 (C) and V2 (D). Age groups are indicated on the x-axis in weeks (wks.). Mean and standard error of the mean (SEM) are indicated by long and short bars respectively. For each primer set, a one-way analysis of variance was performed ($p<0.001$). Bonferroni's multiple comparison test was performed between neonatal (0wks) and the rest of the age groups, significance is indicated by $p<0.05$ * and $p<0.01$ **. H3K9me3 levels were assessed by chromatin immunoprecipitation in brain tissues from 0 and 7-week-old C9-BAC mice (n=5). Two different primer sets were used: C9.A and C9.B amplifying regions within the human *C9ORF72* promoter. Relative enrichment of H3K9me3 was calculated by real-time PCR amplification of immunoprecipitants (IP) relative to inputs and an IgG negative control IP, $p<0.01$ ** (E). Absolute copy number of human *C9ORF72* transcripts per microliter in C9-BAC mice as determined by digital droplet PCR (F), one-way ANOVA ($p<0.001$) and Bonferroni's multiple comparison test was performed between neonatal (0wks) and the remaining age groups, significance is indicated by $p<0.05$ * and $p<0.01$ **.

DNA hypermethylation within the promoter of the human *C9ORF72* transgene occurs in a subset of C9-BAC mice, similar to the human C9-ALS patient population

In about 30% of all C9-ALS cases, methylated CpG dinucleotides within the *C9ORF72* promoter occur more frequently [136, 138]. This promoter hypermethylation is associated

with a modestly attenuated phenotype indicating that epigenetic repression is clinically relevant [139, 140]. To assess levels of DNA methylation within the promoter of the *C9ORF72* transgene, we extracted DNA from the cortex of C9-BAC mice and performed methylation-sensitive PCR as previously reported [147]. Interestingly, we found that in three adult mice, the *C9ORF72* promoter was hypermethylated, similar to what occurs in a subset of human C9-ALS patients (**Figure A1.2A**). Similar to C9-ALS patients, *C9ORF72* promoter hypermethylation in C9-BAC mice was stable across different brain regions (cortex and cerebellum) and somatic tissues (blood and tail clippings) (**Figure A1.2B**). To confirm these findings, we utilized a secondary method to assess DNA methylation. Using bisulfite pyrosequencing, we measured DNA methylation across 8 different CpG dinucleotides located both upstream and downstream of the transcription start site (TSS) of the human *C9ORF72* promoter (**Figure A1.2C**). Furthermore, we have eliminated the possibility that increased methylation levels are due to the abnormal copy number of the human C9ORF72 transgene by CNV analysis (**Figure A1.2E**). Our data demonstrate that adult mice from the same age group can have differential DNA methylation levels within the *C9ORF72* promoter, mirroring a phenomenon observed in C9-ALS patients. To determine whether promoter hypermethylation affects the production of toxic DPRs, we next measured levels of glycine-proline (GP) repeat proteins in the brains of 3 hypermethylated and 9 unmethylated C9-BAC mice (**Figure A1. 2D**).

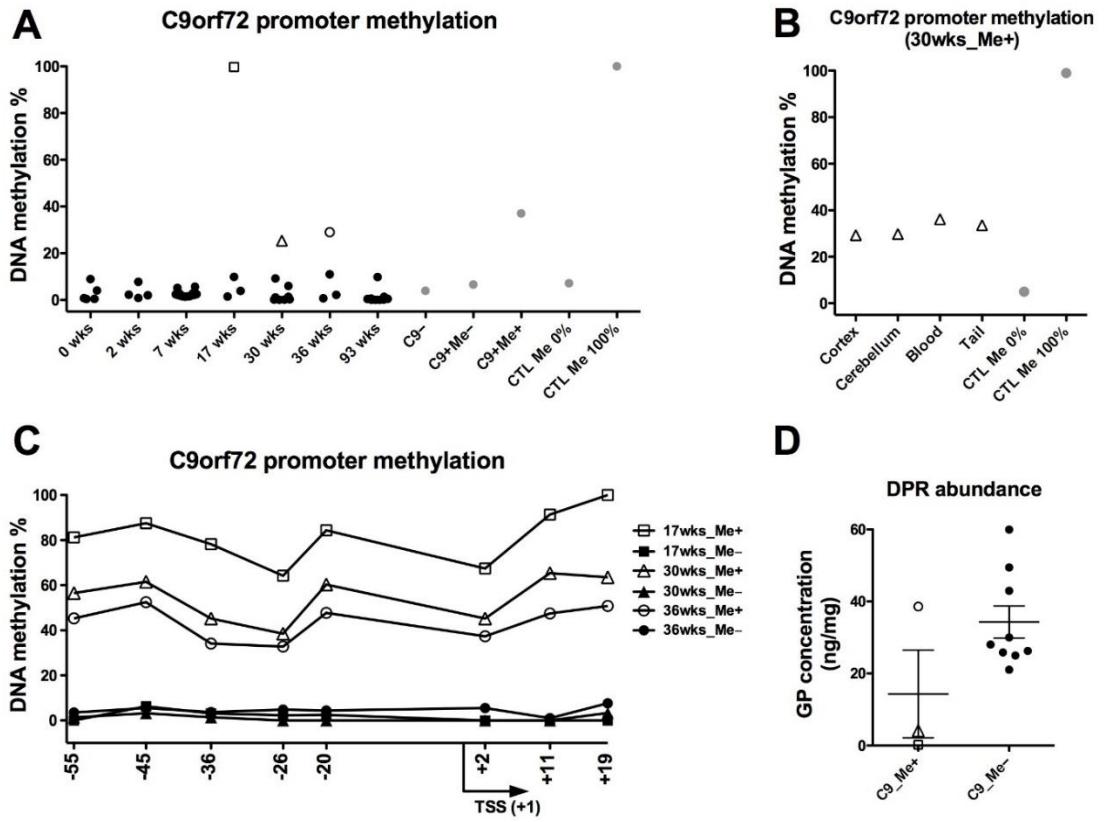

Figure A1.2 DNA hypermethylation at the expanded *C9ORF72* promoter appears in a fraction of adult mice

A) Site-specific DNA methylation sensitive PCR assessment of the human *C9ORF72* promoter in the cortex of C9-BAC mice at seven time points, indicated in weeks (wks) of age. Two HhaI restriction sites located at -215 and -109 base pairs from the transcriptional start site were interrogated; three hypermethylated animals are indicated by open shapes (17wks square, 30wks triangle and 36wks circle). Assay controls (grey circles on right) include DNA isolated from post mortem brain tissues of ALS patients with the hexanucleotide repeat expansion (C9+) with (me+) or without (me-) promoter hypermethylation, an unaffected healthy control (C9-) individual, and synthetic DNA enriched (CTL Me 100%) or depleted of 5mC (CTL Me 0%). Values are plotted relative to the synthetic high control, which is set to 100%. (B) *C9ORF72* promoter methylation assessment from brain cortex, cerebellum, blood and tail clippings of a 30-week-old hypermethylated mouse using HhaI methylation sensitive PCR. (C) Bisulfite pyrosequencing of brain cortex from 17, 30 and 36 weeks old C9-BAC mice (n=2 per age group) across 8 CpG dinucleotides within the human *C9ORF72* promoter, positions relative to TSS are shown on the x-axis. Filled symbols indicate samples from hypermethylated (me+) animals, open symbols are samples from unmethylated (me-) animals (D) Glycine-Proline DPR assessment of whole brain tissue samples from 3 hypermethylated animals (open symbols) and representative unmethylated samples (filled

symbols) from 17, 30 and 36-week-old C9-BAC mice (n=3 per age group). (E) Copy number variation analysis for human *C9ORF72* transgene in C9-BAC mouse brain cortex with hypermethylated (me+), unmethylated (me-) promoter and wild-type mouse (WT).

Our data indicate that there is a trend towards decreased GP levels in hypermethylated mice. Nevertheless, further studies with more animals are required to fully investigate the effect of DNA hypermethylation at the *C9ORF72* promoter on DPR production in these mice. Notably, GP levels in hypermethylated mice negatively correlated with the DNA methylation percentile as determined by bisulfite pyrosequencing analysis of 8 CpG dinucleotides (**Figure A1.3**). The goodness of fit (R^2) was similar for each of the 8 CpGs suggesting none have a more prominent regulatory role than others.

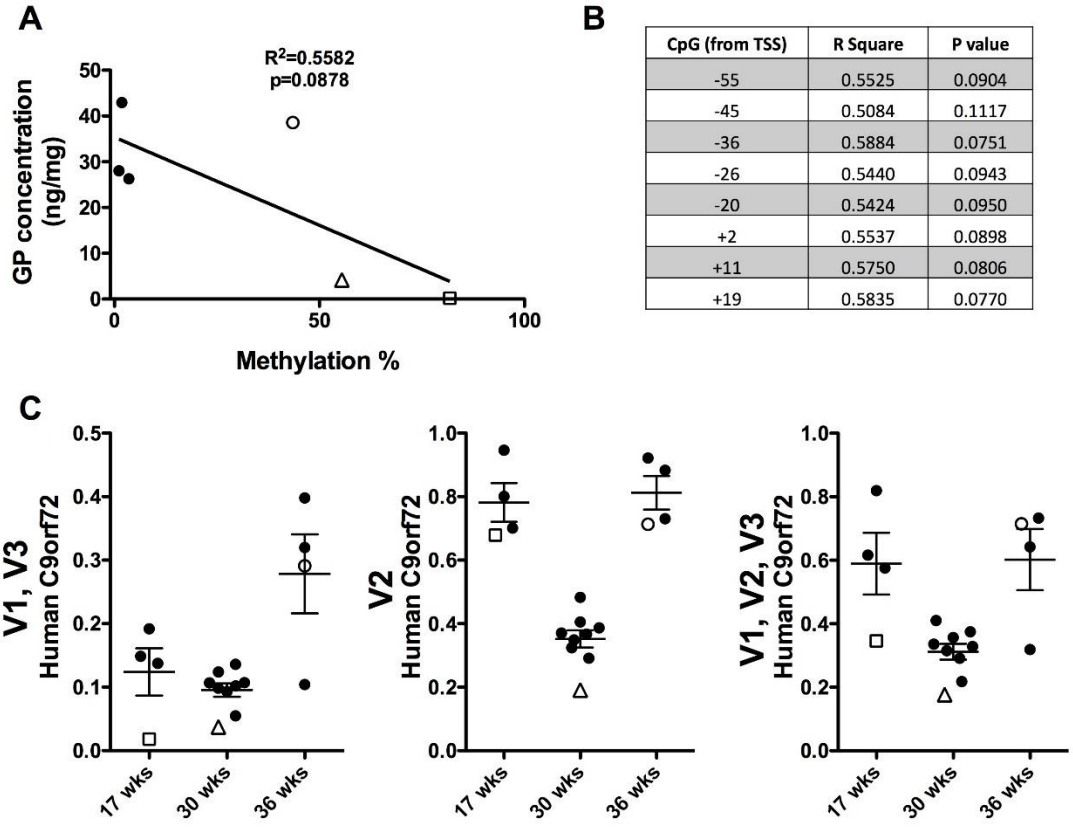

CpG (from TSS)	R Square	P value
-55	0.5525	0.0904
-45	0.5084	0.1117
-36	0.5884	0.0751
-26	0.5440	0.0943
-20	0.5424	0.0950
+2	0.5537	0.0898
+11	0.5750	0.0806
+19	0.5835	0.0770

Figure A1.3 GP levels in hypermethylated mice negatively correlated with the DNA methylation

A) Linear regression analysis of the mean *C9ORF72* promoter methylation percentile (as determined by bisulfite pyrosequencing) and glycine-proline dipeptide abundance (B) R square and p values for individual CpG dinucleotides. (C) Quantitative PCR assessment of *C9ORF72* expression in hypermethylated C9-BAC mice indicated by open shapes (17wks square, 30wks triangle, 36wks circle) and their age group counterparts, error bars represent SEM

Methylation of GGGGCC repeat expansion mutation increases with age in C9-BAC mice

Previously, Xi et al. reported that the HRE itself is methylated in every C9-ALS patient with the pathogenic repeat number [148], indicating a protective cellular response. Interestingly, the authors argue that the origin of DNA hypermethylation initiates within the HRE, but in some individuals, methylation spreads upstream to the promoter region. Therefore, we sought to determine if HRE hypermethylation is recapitulated in a C9-BAC mouse model of ALS. To quantitatively assess DNA methylation levels at the HRE in C9-BAC mice, we developed a novel assay that combines the HpaII methylation-sensitive restriction digest, which recognizes CCGG sequence, with repeat-primed PCR and capillary electrophoresis (**Figure A1.4A**). Given our finding that expression of the human *C9ORF72* transgene decreases within the first weeks of life (**Figure A1.1**), we quantified DNA methylation of the HRE at 0, 2 and 7 weeks of age (**Figure A1.4B**). We observed that HRE methylation was present in all three age groups but increased with age, reaching significance between 0 and 7 weeks. Representative graphs from one animal per group are shown in **Figure A1.4C**. These findings suggest that methylation of cytosine residues within the HRE sequence itself occurs within the first weeks of the C9-BAC mouse lifespan.

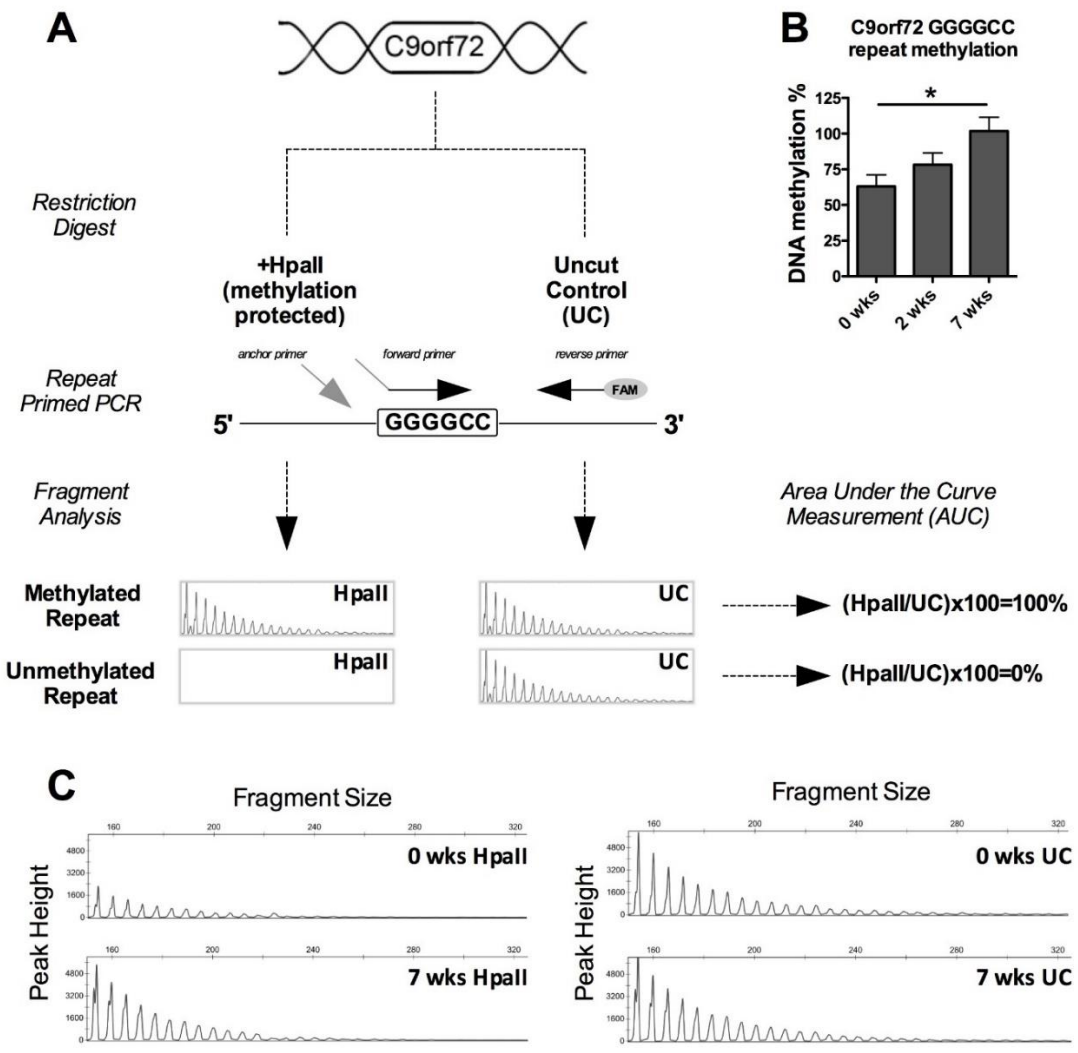

Figure A1.4 Hexanucleotide (GGGGCC) repeat methylation increases with age in C9-BAC mice

A) An illustration of the HRE methylation assessment method. For each sample, two repeat-primed PCR reactions are performed, one using DNA subjected to HpaII digest and one using uncut control (UC). DNA methylation percentage is calculated based on the area under the curve values following capillary fragment analysis of HpaII digested samples normalized to the uncut control sample. (B) HRE methylation levels were assessed at 0 (n=5), 2 (n=4) and 7 (n=5) weeks of age, significance is indicated by *$p<0.05$. (C) Representative electropherograms from 0 and 7-week-old C9-BAC mouse brain cortex DNA treated with HpaII as well as uncut control.

Hydroxymethylcytosine is observed at the expanded *C9ORF72* promoter in the brain of C9-BAC mice

We previously reported that 5-hydroxymethylcytosine (5hmC), a stable intermediate of the DNA demethylation pathway, is a novel epigenetic feature of repeat expansions mutations in Fragile X Syndrome and C9-ALS [141, 149]. Here, we sought to determine whether 5hmC is present at the *C9ORF72* promoter of hypermethylated BAC mice as well. We performed DNA hydroxymethylation assessment as previously described [141, 149]. We found that similar to C9-ALS patients, hypermethylated C9-BAC mice show elevated levels of 5hmC at the *C9ORF72* promoter sites both upstream and downstream of the TSS in the cortex (**Figure A1.5A, B**). Furthermore, we assessed peripheral tissues from the 30-week-old hypermethylated mouse. We found that 5hmC enrichment was unique to brain tissues (**Figure A1.5C, D**). This indicates more pronounced DNA demethylation in the brain of hypermethylated C9-BAC mice which is consistent with the highest abundance of the global 5hmC levels occurring in the central nervous system as compared to other tissue types, presumably due to the higher ten-eleven-translocation (TET) enzyme activity [150, 151].

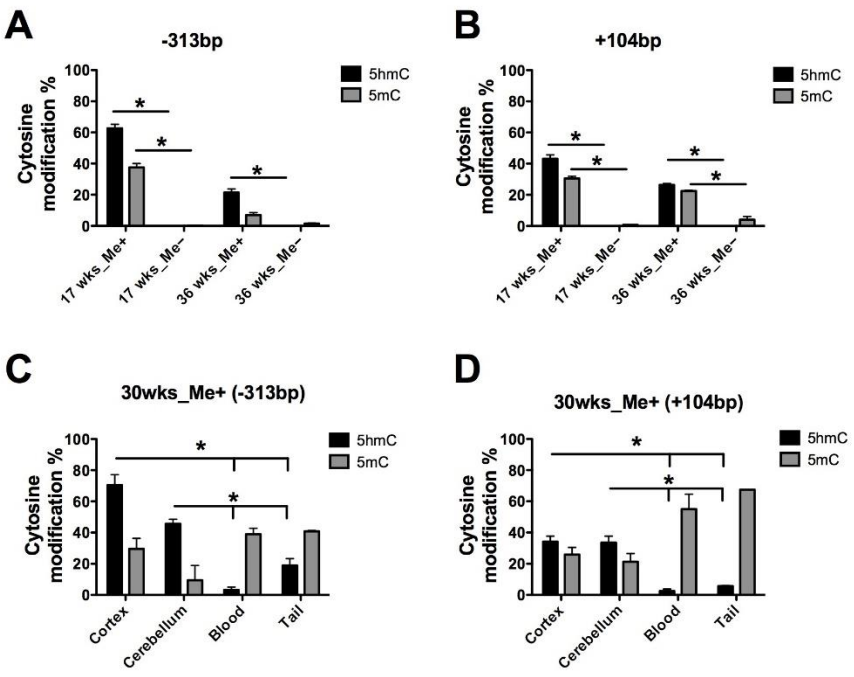

Figure A1.5 DNA demethylation is observed at the expanded *C9ORF72* promoter distinctively in the brain

A, B) Two CpG dinucleotides located within MspI/HpaII restriction sites at positions − 313 and + 104 base pairs from the *C9ORF72* transcriptional start site were interrogated by 5-methylcytosine (5mC) and 5-hydroxymethylcytosine (5hmC) sensitive PCR. The y-axis indicates percent 5hmC (black) and 5mC (grey) from brain cortex samples for a subset of C9-BAC mice, error bars represent standard deviation, experiments were performed in duplicates. Assessment of 5hmC enrichment at two restriction sites across tissue types of a 30-week-old hypermethylated mouse are illustrated in C and D. Student's t-test was performed to determine significance, indicated by $p<0.05$ *

DNA hypermethylation is acquired independently of RNA-DNA hybrid formation at the *C9ORF72* locus

We next sought to investigate one possible mechanism of DNA methylation acquisition at the *C9ORF72* promoter of ALS patients. By analogy to other repeat expansion disorders, such as Fragile X Syndrome and Freidriech's Ataxia [144, 152], we hypothesized that DNA-RNA hybrids or R-loops formed by an expanded *C9ORF72* transcript lead to

epigenetic silencing. In our previous report, we demonstrated that iPSC lines from a hypermethylated ALS patient can be used as a tool to investigate the acquisition of DNA methylation at the *C9ORF72* promoter [141]. In particular, we showed that DNA methylation at the *C9ORF72* promoter is erased during iPSC generation and then re-acquired during neuronal differentiation. To determine whether *C9ORF72* promoter DNA hypermethylation occurs via DNA-RNA hybrid formation, we created a stable iPSC line from a hypermethylated ALS patient expressing a small hairpin RNA targeting all three *C9ORF72* transcript variants (shC9) or a scrambled control (shCTL). We reasoned that disrupting R-loop formation by depleting *C9ORF72* mRNAs in iPSCs would prevent DNA hypermethylation upon neuronal differentiation, similar to what was previously shown in Fragile X Syndrome [152]. We generated stable iPSC cell lines expressing either the shC9 or shCTL constructs then differentiated the cells into motor neurons using our previously published protocols [141]. We confirmed efficient depletion of *C9ORF72* in shC9 iPSC lines using qPCR (**Figure A1.6A**). We then confirmed efficient disruption of R-loop formation at the C9ORF72 locus in shC9 motor neurons using DNA-RNA immunoprecipitation (DRIP) followed by qPCR with primers to amplify regions upstream and downstream the HRE (**Figure A1.6B, C**). Finally, DNA methylation at the *C9ORF72* promoter in motor neurons was assessed across 16 individual CpG dinucleotides using bisulfite pyrosequencing (**Figure A1.6D**). Patient-derived motor neurons from an individual with the Fragile X Syndrome that does not harbor *C9ORF72* repeat expansion were used as a negative control. Despite efficient knockdown of *C9ORF72* RNAs and disruption of R-loops, we did not observe significant differences in DNA methylation levels at the *C9ORF72* promoter between shC9 and shCTL motor neurons. These results

suggest that R-loops may not be required for the acquisition of DNA hypermethylation associated with the *C9ORF72* HRE.

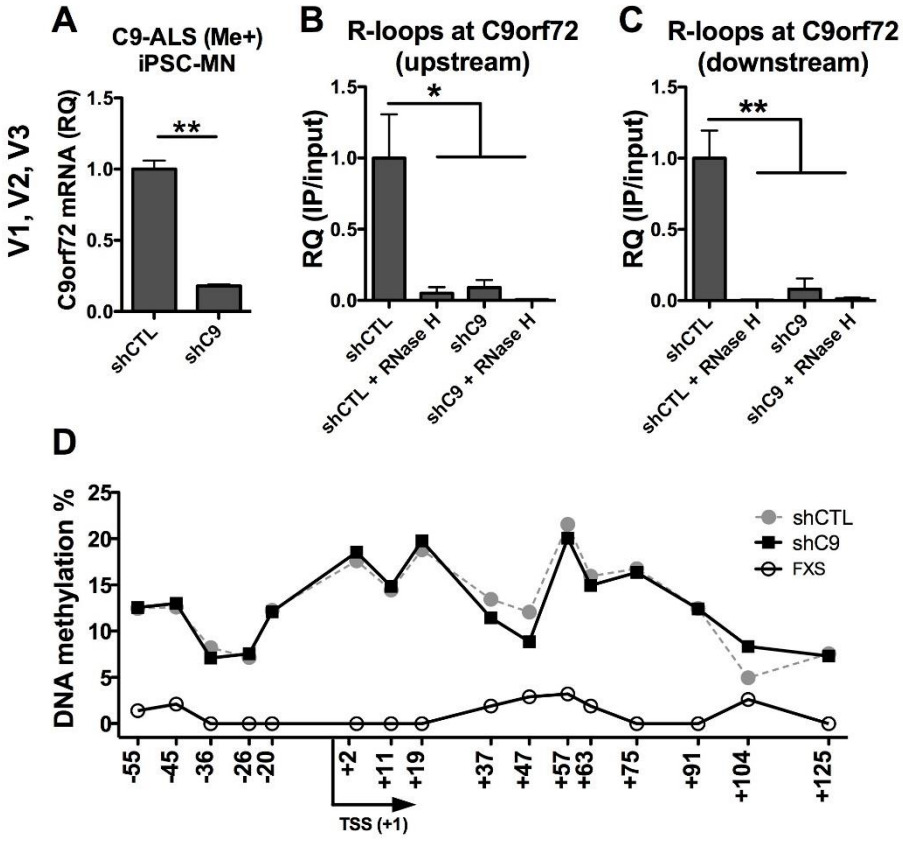

Figure A1.6 DNA methylation is acquired independently of RNA-DNA hybrid formation at the *C9ORF72* locus

A) Relative quantification of all three *C9ORF72* transcript variants in iPSC-derived motor neurons stably expressing a *C9ORF72*-specifc shRNA (shC9) or a scrambled CTL (shCTL) (A). DNA-RNA immunoprecipitation at the *C9ORF72* promoter of shC9 and shCTL motor neurons, relative quantification was measured using two sets of primers, designed upstream (B) and downstream (C) of the repeat expansion, RNase H treatment was performed prior to pull-down as a negative control. (D) DNA methylation levels at the *C9ORF72* promoter were assessed using bisulfite pyrosequencing across 16 CpG dinucleotides; positions relative to the transcription start site are indicated on the x-axis.

Fragile X patient-derived iPSC-neurons (FXS) were used as a negative control. Significance is indicated by $p<0.05$ * and $p<0.01$ **.

Discussion

Here we report that C9-BAC mice from Peters and Toro et al. [121] recapitulate epigenetic perturbations seen in *C9ORF72*-associated ALS and FTD patients. We observed enrichment of the repressive epigenetic mark H3K9me3 in the promoter of the human transgene, which corresponded to decreased transcription rates. We also observed DNA methylation within the HRE repeat sequence itself for all mice tested and in 3 mice, this methylation had spread to the promoter region. Our data show that HRE-mediated epigenetic repression occurs during the first few weeks after birth in C9-BAC mice and likely occurs at about the time of birth in humans (2 weeks in the mouse), although the unavailability of human tissues makes this difficult to assess. It will be important to determine whether epigenetic features of the HRE are shared among different C9-BAC lines. Of particular interest will be to determine whether phenotypic severity is associated with levels of epigenetic repression, in cases where a phenotype is observed, and whether the epigenetic repression is lost (even relatively) as animals continue to age and develop a clinical phenotype.

Our findings demonstrate that epigenetic features of the HRE in humans are mirrored in the C9-BAC mouse, and in some cases, appear at a similar levels and frequencies. For example, DNA hypermethylation of the HRE itself in C9 ALS/FTD patients occurs at a rate of 97% [148]. Using a quantitative assay to assess HRE methylation, we found that all C9-BAC mice assessed exhibit hypermethylation of the repeat sequence. This HRE

methylation increases with age, although P0 mice also show elevated levels of methylation within the repeat. These observations support the hypothesis that increased levels of DNA methylation within the repeat precede promoter hypermethylation and is a common feature of the HRE that serves a protective role to impede transcription across the mutation [139, 140, 148, 153]. The *C9ORF72* promoter hypermethylation on the other hand, is less common in C9-ALS patients, and is only observed in a fraction (~30%) of individuals with a pathogenic repeat number [136, 138]. Interestingly, we found that to be true for C9-BAC mice as well, where only a small fraction of the adults show DNA hypermethylation at the *C9ORF72* promoter, across different tissues. This is particularly poignant given the neuroprotective effect of the *C9ORF72* promoter hypermethylation *in vivo* [140]. Hence, we suggest that it may be important to stratify C9-BAC mice based on their epigenetic status while conducting phenotypic assessments and performing pre-clinical testing of experimental therapeutics.

Despite increased levels of repressive histone and DNA methylation marks, expanded *C9ORF72* alleles sustain sufficient transcriptional activity to produce toxic levels of mutant RNAs and DPRs. We have recently identified enrichment of 5hmC, an active DNA demethylation intermediate, as a novel epigenetic alteration common to at least two repeat expansion disorders: Fragile X Syndrome and C9-ALS [141, 149]. Given the high abundance of 5hmC at the *C9ORF72* promoter of hypermethylated patients and C9-BAC mice, we postulate that active DNA demethylation counteracts the protective hypermethylation of the promoter. Active DNA demethylation is a process facilitated by the ten-eleven translocation (TET) family proteins and acts as a switch between transcriptionally inactive and active gene states [154]. Our data demonstrate that active

DNA demethylation is most pronounced in the brain of C9-BAC mice, in concordance with the literature indicating that TET activity and global 5hmC levels are highest in neurons [150, 155]. Future studies are warranted to investigate the possibility of leveraging epigenetic equilibrium, perhaps by using small molecules, in such way that it favors DNA hypermethylation to more completely repress the expanded locus. This would be hypothesized to reduce the production of toxic products in C9-BAC mice.

The mechanism by which DNA hypermethylation is established at the *C9ORF72* promoter has been studied by our group and others [141, 146, 156]. These studies suggest that RNA-DNA hybrids or R-loops are key mediators of epigenetic repression [157]. Recent discoveries in other repeat expansion disorders, including Fragile X Syndrome and Freidriech's Ataxia support this reasoning [144, 152]. Here we investigated this possibility using iPSC-derived motor neurons, a method that we have successfully utilized in our previous report to model the acquisition of DNA hypermethylation in C9-ALS [141]. We show that despite their presence at the *C9ORF72* promoter of C9-ALS patient derived cells, reducing R-loop formation by depleting HRE RNAs is not sufficient to prevent the acquisition of DNA hypermethylation. Future studies could investigate alternative mechanisms leading to the epigenetic repression of HRE promoters. Though we did not address this issue here, it would also be interesting to see whether *C9ORF72* knockdown in C9-BAC mice will have any effect on the levels of DNA methylation associated with the expanded locus.

In conclusion, we have determined that epigenetic perturbations seen in C9-ALS patients are also observed in C9-BAC mice and that R-loops are unlikely to be initiators of DNA methylation at the expanded *C9ORF72* locus. Since many repeat expansion mutations,

including C9-ALS, have an epigenetic component that is directly linked to pathology, our observations are of significant importance for understanding the mechanism of disease and are of consequence for therapeutic development efforts utilizing C9-BAC mouse models.

Methods

C9-BAC mice

Animals used in the present study have previously been described [121]. Briefly, a BAC containing human sequence from a C9-ALS patient, spanning the gene promoter to exon 6, was inserted into the mouse genome using standard transgenic methods. All experimental procedures involving transgenic mice were performed in accordance with the guidelines of Institutional Animal Care and Use Committee of the University of Massachusetts Medical School.

DNA and RNA extraction

Genomic DNA and total RNA extractions were performed from 30mg of mouse brain tissues using a kit (AllPrep DNA/RNA Mini Kit®, Qiagen #80204) as per manufacturers' instructions.

Quantitative PCR (qPCR)

Reactions were performed using TaqMan® assays that amplify *C9ORF72* transcript variants V1, V2, V3 (Hs00376619_m1), *C9ORF72* V1, V3 (Hs00331877_m1), *C9ORF72* V2 (NM_018325.3, L/R/Probe: 5’CGGTGGCGAGTGGATATCTC / 5’TGGGCAAAGAGTCGACATCA/ 5’TAATGTGACAGTTGGAATGC), mouse Glyceraldehyde 3-phosphate dehydrogenase (*GAPDH*) (Mm99999915_g1), beta-actin

(Mm00607939_s1), eukaryotic 18S ribosomal RNA (Hs99999901_s1) and human GAPDH (Hs02758991_g1). Relative quantification values were calculated using a standard curve method, normalized to the average of GAPDH and 18S endogenous control genes.

Digital droplet PCR (ddPCR)

For gene expression, 500ng of total RNA was used in a 20µl reaction to generate complementary DNA (cDNA) using random hexamer primers and MultiScribe reverse transcriptase (High capacity RNA-to-cDNA Kit, Life Technologies). After diluting the cDNA 1:1.25, 2µl were loaded into a 20µl reaction containing ddPCR Supermix for Probes (nodUTP) (Bio-Rad, Gladesville, NSW, Australia), and 1µl of primers amplifying all three *C9ORF72* transcripts (Hs00376619_m1, Life Technologies). The 20µl sample, along with 70µl of ddPCR-oil was loaded into a DG8 cartridge and covered with a gasket according to manufacturer's instructions; the cartridge was then placed in a QX100 droplet generator. 40µl of sample were then transferred to a 96-well PCR plate and put in a normal PCR thermocycler (Eppendorf, North Ryde, NSW, Australia). The plate was then placed in the QX100 ddPCR reader (Bio-Rad, Gladesville, NSW, Australia) for absolute quantification.

Methylation-sensitive quantitative PCR

DNA methylation at the *C9ORF72* promoter was assessed using previously reported methods [147]. Briefly, 100ng of genomic DNA was used for methylation-sensitive restriction digest with 4 units of HhaI endonuclease. Two sets of primers were used for subsequent quantitative PCR: C9me (L/R: 5'CGGTAAAAACAAAATTTCATCCA / 5'GGGCAACTTGTCCTGTTCTT) spans two HhaI restriction sites within the *C9ORF72*

promoter, and C9ec (L/R: 5’AGGAAAGAGAGGTGCGTCAA / 5’TCCTAAACCCACACCTGCTC) was used as an endogenous control.

Bisulfite pyrosequencing

Genomic DNA (2µg) was treated with bisulfite and analyzed by pyrosequencing (EpigenDx Inc.) as previously reported [141]. The DNA methylation assessment was performed using the PSQTM96HS system and custom assays developed by EpigenDx (ADS3232-FS1 and ADS3232-FS2). The assay covers 16 cytosine residues within the *C9ORF72* promoter from −55 to +125 base pairs relative to the *C9ORF72* transcriptional start site.

Copy Number Variation (CNV) analysis

C9ORF72 mouse brains were fresh frozen and cut in a sagittal section to extract DNA. The tissue was lysed overnight at 55°C, RNAse treated and eluted following manufacturer’s instructions (Gentra Puregene Tissue Kit, Qiagen). The DNA was diluted to 20ng/µl and 2µl were added to the ddPCR master mix along with 1µl of each primer/probe. Primer and probe sequences used for human genomic *C9ORF72* (L/R/Probe: 5’AAGGCACAGAGAGAATGGAAG / 5’AGGCTTATTCGTATGTCTCCAAG / 5’AGGTTGATGGCTACATTTGTCAAGGC) and for mouse EIF2C1 diploid genome (L/R/Probe: 5’CCTGCCATGTGGAAGATGAT / 5’GAGTGTGGTGGCTGGATTTA / 5’TGGGGAGAGCTGGAGCCAG) quantification are indicated. Droplets were generated followed by PCR and absolute quantification.

Poly (GP) immunoassay

C9-BAC whole brain tissues were lyzed in buffer containing 50 mM Tris–HCl, pH 7.4, 300 mM NaCl, 1% Triton X-100, 2% sodium dodecyl sulfate, 5 mM EDTA, as well as protease (EMD Millipore) and phosphatase inhibitors (Sigma-Aldrich). After sonication, samples were centrifuged at 16,000 x g for 20 min at 4°C and supernatants collected. The protein concentration of lysates was determined by BCA assay (Thermo Scientific). Poly (GP) levels in lysates were measured using a previously described sandwich immunoassay that utilizes Meso Scale Discovery (MSD) electrochemiluminescence detection technology [158]. Lysates were diluted in Tris-buffered saline (TBS) and tested using 43 µg of protein per well in duplicate wells. Serial dilutions of recombinant $(GP)_8$ in TBS were used to prepare the standard curve. Response values corresponding to the intensity of emitted light upon electrochemical stimulation of the assay plate using the MSD QUICKPLEX SQ120 were acquired for interpolation of poly (GP) levels using the standard curve.

Generation of *C9ORF72* depleted induced pluripotent stem cell lines

Previously, we generated several patient-derived iPSC lines from *C9ORF72* ALS patients [141]. One of these lines was transduced with a lentiviral vector (Sigma-Aldrich, SHCLNV-NM-018325, clone TRCN0000148881) expressing a puromycin resistance gene and a small hairpin RNA (shRNA) targeting all three *C9ORF72* transcript variants. Transduction of iPSCs (MOI=3) was carried out in the absence of polybrene. Selection was performed in the presence of puromycin (1µg/ml) for 10 days; surviving colonies were expanded and used for motor neuronal differentiation. Depletion of *C9ORF72* RNAs was confirmed by qPCR.

Motor neuron differentiation

Motor neuronal differentiation was performed according to our previously published protocol [147]. Briefly, neural precursor spheres were differentiated from iPSC colonies using neural induction medium and cultured in ultra-low attachment flasks. Afterwards, spheres were seeded onto poly-L-ornithine and laminin-coated plates with neuronal induction medium and cultured for four weeks to obtain terminally differentiated motor neurons.

DNA-RNA immunoprecipitation (DRIP)

The DRIP protocol was adapted from Loomis et al. [159] with some modifications. Here, $5x10^6$ cells were lysed with 0.5% SDS and treated with 400 units of proteinase K at 37°C overnight. The next day, DNA extraction was performed using standard phenol/chloroform/isopropanol precipitation. Fifty micrograms of DNA were digested with EcoR1, HindIII, BsrGI, and XbaI (20 units each) at 37°C for 1 hour. Next, samples were incubated in the presence of the S9.6 antibody (Kerafast ENH001) for 2 hours at 4°C with inversion. As a control, samples were treated with 25 units of RNase H (ThermoFisher Scientific #EN0201) for 6 hours at 37°C. Following DRIP, DNA was precipitated with isopropanol and used for quantitative PCR with primers amplifying a region upstream (L/R: 5'AAGAGCAGGTGTGGGTTTAG / 5'GAGTACTGTGAGAGCAAGTAGTG) and downstream (L/R: 5'CTCAGAGCTCGACGCATTT / 5'CAATTCCACCAGTCGCTAGA) of the *C9ORF72* hexanucleotide repeat expansion.

C9ORF72 GGGGCC repeat methylation assessment

To measure *C9ORF72* HRE methylation, we combined HpaII methylation-sensitive restriction digest with the repeat-primed PCR assay in the presence of 5% dimethyl sulfoxide and complete substitution of 7-deaza-2-deoxy GTP for dGTP as previously described [141]. PCR fragments were analyzed using the ABI3730 DNA Analyzer and GeneMapper software. The area under the curve (AUC) values were calculated for peaks higher than 150 base pairs. The AUC of digested samples were normalized to AUC of uncut controls to calculate the percent DNA methylation of the HRE sequence.

DNA hydroxymethylation assessment

To quantify 5hmC and 5mC levels at the *C9ORF72* promoter, we utilized the EpiMark® 5-hmC and 5-mC Analysis Kit (New England Biolabs E3317), according to the manufacturer's protocol as previously reported [141]. Briefly, 2µg of genomic DNA was subjected to glycosylation by T4 β-glucosyltransferase, converting 5hmC to 5ghmC residues. Glucosylated DNA was then digested with MspI or HpaII endonucleases for 6 hours at 37°C and subsequently amplified by quantitative PCR using the -313bp primer set (L/R: 5'AGGAAAGAGAGGTGCGTCAA / 5'TCCTAAACCCACACCTGCTC) and +104bp primer set (L/R: 5'AAATTGCGATGACTTTGCAG / 5'ACTGCAAACCCTGGTAGG), each of which spans one CCGG MspI/HpaII restriction site.

Chromatin immunoprecipitation (ChIP)

Immunoprecipitation of H3K9me3 was performed as we previously reported [147]. Briefly, 50mg of brain tissue was sliced into small pieces and crosslinked in 1%

formaldehyde for 10 minutes and quenched with 0.125 M glycine for 5 minutes at room temperature. Sonication was performed for 5 minutes using the Bioruptor UCD200 sonication system set to the high setting. Lysates were then transferred to a tube containing Protein G Dynabeads prepared with an anti-H3K9me3 antibody (Abcam ab8898), or control rabbit IgG, and incubated overnight at 4°C with rotation. The following day, stringency washes were performed, and samples were re-suspended in 150 µL elution buffer consisting of 1% SDS, 0.1M $NaHCO_3$, 0.2M NaCl and incubated at 65°C overnight. The next day, samples were de-crosslinked by treatment with 50µL proteinase K and incubated at 42°C for 2 hours. De-crosslinked genomic DNA was isolated using the QiaQuick PCR purification kit (Qiagen #28104) according to the manufacturer's instructions. Quantitative PCR was performed using two primer sets: C9.A (L/R: 5'ACTCGCTGAGGGTGAACAAG / 5'TCCTGAGTTCCAGAGCTTGC) and C9.B (5'AAGAGCAGGTGTGGGTTTAG / 5'GAGTACTGTGAGAGCAAGTAGTG).

Appendix II

RNAi gene therapy for hereditary sensory neuropathy 1 (HSAN1)

Introduction

Hereditary sensory autonomic neuropathy 1 (HSAN1) is a rare subtype of sensory neuropathy with a low prevalence of <200,000 individuals in the US population [160]. This autosomal dominant disease is associated with missense mutations in the serine palmitoyltransferase (SPT), long chain base subunit 1 (*SPTLC*1) gene. Mutations in the *SPTLC1* gene lead to progressive degeneration of dorsal root ganglion (DG) and motor neurons. Studies have shown demyelination of said neurons causes loss of sensory and temperature sensation in hands and feet along with muscle atrophy and weakness. Due to loss of sensation patients commonly present ulcers which can become infected and result in amputation[160, 161].

SPT is the main enzyme involved in sphingolipid biosynthesis, it drives the conversion of L-serine and palmitoyl CoA to 3-oxosphinganine. It is a major component in the formation of lipid rafts in cell membranes that enable signal transduction [162]. Mutations in this gene alter the substrate specificity allowing the formation of 2 atypical deoxy-sphingoid bases (DSB). 1-deoxy-sphinganine (doxSA) and 1-deoxymethyl-sphinganine (doxmethSA), both lack a C (1) hydroxyl group of sphinganine, making them unsuitable for conversion to complex sphingolipids or degradation. Hence, they accumulate in the cells, becoming neurotoxic[161, 162]

Eichler et al., 2009 showed that overexpression of the wild type SPT1 subunit can lower (DSB) levels and rescue the HSAN1 phenotype in mice [162]. Henceforth, recent research

in mice and humans showed that an oral supplementation of L-serine could decrease neurotoxic DSBs and could be used as a temporary initial treatment for this disease [163]. Human clinical trials to evaluate the safety and efficacy of l-serine supplementation to HSAN1 patients revealed a slowed progression of the disease [164]. Although encouraging, oral supplementation L-serine is not a permanent solution. Given that this disease results from a gain- of- function mutation in *SPTLC1*, a silencing approach would be the best therapeutic strategy. By using AAV mediated artificial microRNAs to silence the *SPTLC1* gene we can target the mRNA and consequently reduce the production of the toxic DSB.

Prior to designing the microRNAs, we sought to find existing mouse models that could aid us in testing the efficacy of our therapeutic *in vivo*. The only available model to date is a transgenic mouse which has the Chinese hamster *SPTLC1* gene carrying the C133W mutation [165]. Since our end goal is to design microRNAs that will target either human and/or hamster *SPTLC1* we verified that the gene sequence was conserved across these different species. [165]. In order to screen for human targeting microRNAs, we used human embryonic kidney cells (HEK293T), to screen for hamster targeting we used Chinese hamster ovary cells (CHO) and to verify the specificity of the microRNAs in targeting human and hamster but not mouse we screened in a neuroblastoma mouse cell line (N2A). We began by testing multiple primers and probes for *SPTLC1* and *HPRT* cross-reactivity prior to *in vitro* validation and for future proof of concept studies. **(Table A2.1)**

Table A2.1: ***SPTLC1*** **and HPRT crossreactivity**

		Crossreactivity		
		human	mouse	hamster
Hamster specific SPTLC1	taqman	no	no	yes
Mouse specific SPTLC1	taqman	low	yes	no
Human SPTLC1	taqman	yes	no	no
human HPRT	ddpcr	yes	no	no
ctrl HPRT 1	taqman	no	yes	yes

In **Figure A2.1** ddPCR mRNA data of the assay specificity screen shows we can accurately detect each intended target and can move forward to testing the microRNAs in cultures.

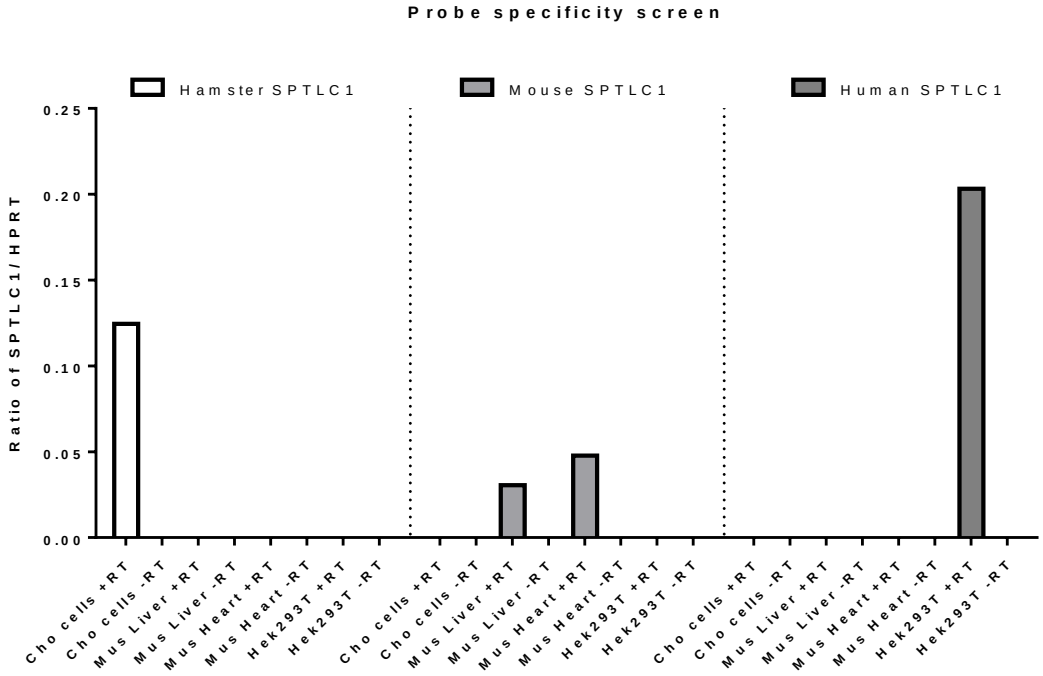

FigureA2.1: Probe specificity screen

TaqMan and ddPCR probes were used to test the cross reactivity in human (HEK293T), mouse (tissues heart-liver) and hamster (CHO) samples. Plus, and minus transcription were

run using ddPCR and HPRT as an endogenous control. Ratios to HPRT are graphed for each probe showing no crossreactivity.

Results

We have designed microRNAs that target human, hamster or both SPTLC1 simultaneously **(Table A2.2**), all microRNAs were cloned into the same entry plasmid containing Flanking ITRs for AAV packaging and a strong (Polymerase III) H1 promoter driving the microRNA, followed by Chicken Beta Actin (CB) driving the expression of enhanced green fluorescent protein (eGFP) (**Figure A2.2A**). An example of the microRNA with its 2-8 nucleotide seed is depicted **(Figure A2.2B)** and an illustration of an artificial microRNA targeting both human and hamster sequences is shown in **(Figure A2.2C)**

A

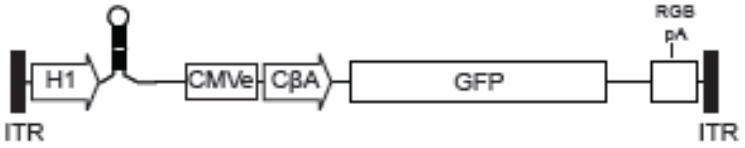

B

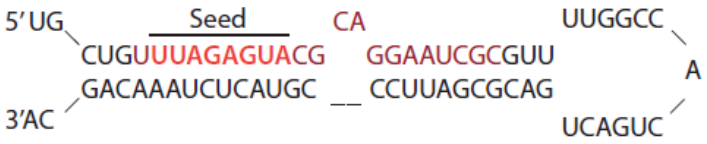

C

Figure A2.2: microRNA plasmid construct, illustration and sample sequence for amiR519

(A) Plasmid construct containing flanking ITRs, followed by an H1 promoter driving expression of microRNAs and a Chicken beta- actin (CB) promote driving GFP expression ending with a polyA tail. (B) Example of an artificial microRNA sequence with the 2-8 nucleotide seed highlighted in red. (C) amiR519 shown here targets both human and hamster SPTLC1. The targeting sequence is highlighted in green

Artificial microRNAS silence SPTLC1 *in vitro*

Human microRNAs were screened using HEK293T **(Figure A2.3)** cells, and hamster microRNAS were screened in a CHO cell line (**Figure A2.4**), RNA was extracted, and mRNA was quantified through digital PCR (ddPCR). Here we show in three independent biological replicates that we can significantly silence human and hamster SPTLC1, 48 hours after transfection with the microRNAS *in vitro.*

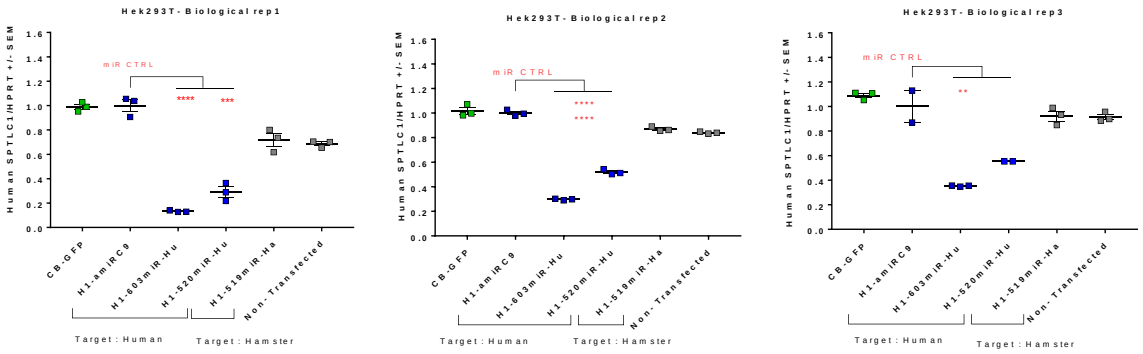

Figure A2.3: human microRNA screening in HEK293T cell line

HEK293T cells were transfected with 3 different artificial microRNAs cloned into the plasmid construct shown in (Figure A2.2). ddPCR analysis of expression of human SPTLC1 was normalized to Human HPRT and in reference to miR control. In addition, H1- amiRC9 a microRNA targeting the *C9ORF72* human gene was used as a microRNA control. miR603 and miR520 are human targeting and show significant mRNA silencing of~ 80%. miR 519 targets hamster and has a slight non-significant decrease of SPTLC1 (mean ±SEM, n=3, biological replicates, Student-T test ($p \geq 0.05$ not significant; p* 0.01-0.05; p** 0.001-0.01; p*** 0.0001-0.001; p****<0.0001).

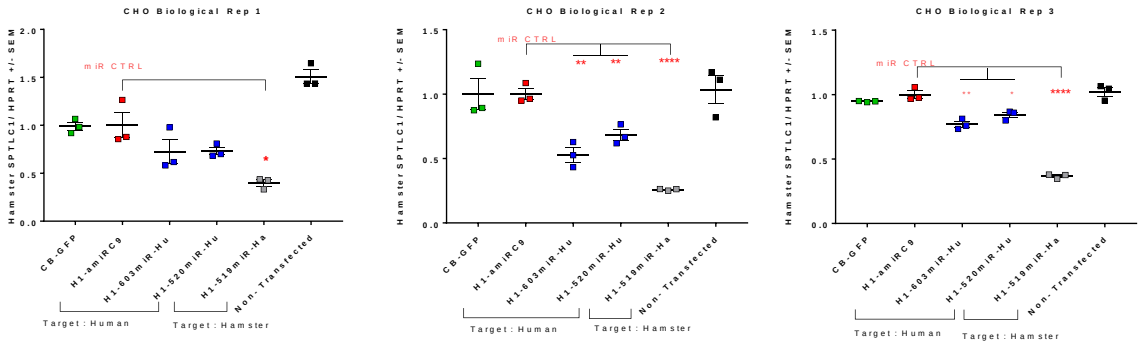

Figure A2.4: human microRNA screening in CHO cell line

CHO cells were transfected with 3 different artificial microRNAs cloned into the plasmid construct shown in (Figure A2.2). ddPCR analysis of expression of human SPTLC1 was normalized to Hamster HPRT and in reference to miR control. In addition, H1- amiRC9 a microRNA targeting the *C9ORF72*-ALS human gene was used as a microRNA control. miR603 and miR520 are human targeting and show slight mRNA silencing of~ 30%. miR 519 targets hamster and silences SPTLC1 by 80% (mean ±SEM, n=3, biological replicates, Student-T test ($p \geq 0.05$ not significant; p* 0.01-0.05; p** 0.001-0.01; p*** 0.0001-0.001; p****<0.0001).

Although these microRNAS are designed to target human and hamster specifically we first sought to verify that the microRNAS would not silence mouse SPTLC1 as well. Keeping in mind that future *in vivo* experiments would involve using the hamster transgenic mouse model and miss-targeting due to sequence similarity between hamster and mouse could lead to misleading data. To this end we used a mouse neuroblastoma cell line (N2A) and transfected the plasmids containing the microRNAs. ddPCR analysis in (**Figure A2.4)** illustrated only miR519 could slightly silence mouse SPTLC1 by 20%. All other microRNAs showed no silencing.

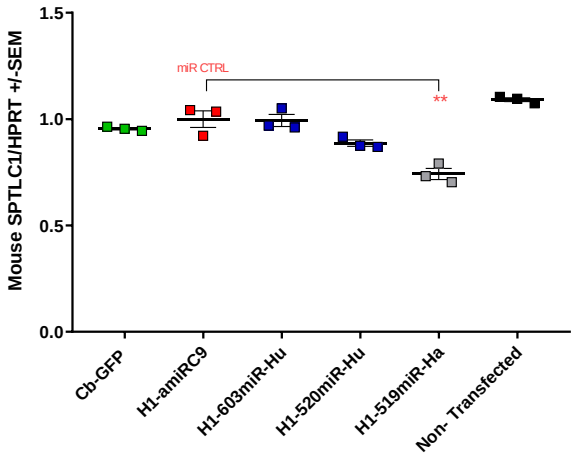

Figure A2.5: microRNA screening in N2A cell line

N2Acells were transfected with 3 different artificial microRNAs cloned into the plasmid construct shown in (Figure A2.2). ddPCR analysis of expression of human SPTLC1 was normalized to mouse HPRT and in reference to miR control. In addition, H1- amiRC9 a microRNA targeting the *C9ORF72*-ALS human gene was used as a microRNA control. miR 519 targets hamster and shows a slight silencing trend of 25% of mouse SPTLC1 (mean ±SEM, n=1, 3 technical replicates, Student-T test ($p \geq 0.05$ not significant; p** 0.001-0.01).

Discussion

Although HSAN1 is not a fatal disease, as a sensory neuropathy it does affect a patient's quality of life. Some patients, in addition to suffering from ulcers, infections and limb weakness, also experience hearing loss or are unable to walk due to pain. The need for a therapy that would permanently prevent mutant *SPTLC*1 from forming DSBs would be optimal. Knowing that an AAV mediated microRNA approach would silence both mutant and healthy alleles, a silence and replace approach is a more reasonable option. To this end both, a microRNA silencing *SPTLC1* and the healthy *SPTLC1 cDNA* would be delivered simultaneously. This healthy version of *SPTLC1* would be modified to be resistant to

microRNA targeting by having 2-3 mismatches while coding for the same amino acid protein.

Moving forward, these microRNAs will be packaged into AAVs for *in vivo* delivery to the CNS. An early intervention may be the best approach in patients, to prevent further demyelination of neuronal fibers. However, preliminary *in vivo* screening in mice would most likely entail either a direct intrathecal injection to the CSF in adult mice, or a systemic intravenous (IV) injection in neonate mice as a surrogate for a peripheral delivery in patients.

Future studies using a BAC transgenic mouse with the human SPTLC1 or a knock-In mouse would be a useful tool to validate the efficiency of this approach. Based on this preliminary data we hypothesize that decreasing the amount of SPTLC1 by 80% should be sufficient to delay disease onset at 10 months of age in the HSAN1 mouse model [165] and decrease peripheral axonal demyelination. This work remains to be done and we believe it will have promising results.

Methods

MicroRNA design and cloning

A 22-nucleotide artificial miRNA against human exons 6-7 and hamster SPTLC1 gene was designed and cloned into the miR-155 backbone [166]. Each microRNA in **Table A2.2** was cloned into an entry plasmid construct containing ITRs flanking a human H1 promoter driving the expression of the microRNA, followed by a CMV enhancer and a Chicken beta actin (CB) promoter driving the expression of eGFP (**Figure A2.2A**)

Table A.2.2: MicroRNA list

miR-520 (Human exon 6)	Top	5'- TGCTG**TTTAGAGTAAGCAGGAATAGC**GTTTTGGCCACTGACTGACGCTATTCCCTTACTCTAAA -3'
	Bottom	5'- CCTGTTTAGAGTAAGGGAATAGCGTCAGTCAGTGGCCAAAACGCTATTCCTGCTTACTCTAAAC -3'
miR-603 (Human exon 7)	Top	5'- TGCTG**AACTTAATGTCACTACGGGAT**GTTTTGGCCACTGACTGACATCCCGTAGACATTAAGTT -3'
	Bottom	5'- CCTGAACTTAATGTCTACGGGATGTCAGTCAGTGGCCAAAACATCCCGTAGTGACATTAAGTTC -3'
miR-519 (Hamster)	Top	5'- TGCTG**TTTAGAGTACGCAGGAATCGC**GTTTTGGCCACTGACTGACGCGATTCCCGTACTCTAAA -3'
	Bottom	5'- CCTGTTTAGAGTACGGGAATCGCGTCAGTCAGTGGCCAAAACGCGATTCCTGCGTACTCTAAAC -3'

In vitro plasmid screening in HEK293T, CHO cells and N2A cells

HEK293T and CHO cells were seeded (1.2 E5 cell/ml) in a 24 well plate, maintained with DMEM media (11995-073; Gibco), 10% Fetal Bovine Serum FBS (F-0926 Sigma-Aldrich) and 1% Penicillin- Streptomycin (30-001-CI; Corning). The plated cells were transfected using jetPRIME reagent (Polyplus) following the manufactures instructions and 1µg of each microRNA plasmid DNA (**Table A2.2**). Forty-eight hours post-transfection, GFP expression was visually assessed; cells were rinsed with PBS and collected using Trizol Reagent (Gibco BRL, Life Technologies, NY, and USA) for RNA isolation. Complementary DNA (cDNA) was generated using (High capacity RNA-to-cDNA Kit, Life Technologies). cDNA was diluted to 20ng/µl and a master mix was prepared for ddPCR.

Droplet Digital PCR (ddPCR) was run as a 20µl reaction containing ddPCR Supermix for Probes (no dUTP) (Bio-Rad, Gladesville, NSW, Australia), 1µl of diluted cDNA, 1µl of each primer/probe (20x), HPRT with a HEX label was used as an endogenous control, and

SPTLC1 assays with FAM labels (**Table A2.3**). The 20µl sample, along with 70µl of ddPCR-oil were loaded into a DG8 cartridge and covered with a gasket according to manufacturer's instructions; the cartridge was then placed in a QX100 droplet generator. Into a 96 well PCR plate 40µl of sample were transferred and then placed in a PCR thermocycler (Eppendorf, North Ryde, NSW, and Australia). The plate was then placed in the QX100 ddPCR reader (Bio-Rad, Gladesville, NSW, Australia) for absolute quantification. Ratios were obtained by dividing absolute SPTLC1 values to the absolute endogenous HPRT values. Samples were normalized in respect to miR controls. GraphPad Prism Program was used to graph and run statistical Student- T tests for three biological replicates.

Table A2.3: Primer and Probes

	Gene Expression Assay ID
SPTLC1 Hamster	GEX: Cg04422833_g1
SPTLC1 Mouse	GEX: Mm00447350_m1
SPTLC1 Human	GEX: Hs01116903_m1
HPRT Human	GEX: qHsaCIP0030549
HPRT hum: Bio-Rad	GEX: qHsaCIP0030549
HPRT Mm/Cg	GEX: Cg04448436_m1

Bibliography

1. Chio, A., et al., *Global epidemiology of amyotrophic lateral sclerosis: a systematic review of the published literature.* Neuroepidemiology, 2013. **41**(2): p. 118-30.
2. Flotte, T.R., S.A. Afione, and P.L. Zeitlin, *Adeno-associated virus vector gene expression occurs in nondividing cells in the absence of vector DNA integration.* Am J Respir Cell Mol Biol, 1994. **11**(5): p. 517-21.
3. Arthur, K.C., et al., *Projected increase in amyotrophic lateral sclerosis from 2015 to 2040.* Nature Communications, 2016. **7**: p. 12408.
4. Murros, K. and R. Fogelholm, *Amyotrophic lateral sclerosis in Middle-Finland: an epidemiological study.* Acta Neurologica Scandinavica, 1983. **67**(1): p. 41-47.
5. Byrne, S., et al., *Rate of familial amyotrophic lateral sclerosis: a systematic review and meta-analysis.* Journal of neurology, neurosurgery, and psychiatry, 2011. **82**(6): p. 623-627.
6. Kiernan, M.C., et al., *Amyotrophic lateral sclerosis.* Lancet, 2011. **377**(9769): p. 942-955.
7. Siddique, T. and S. Ajroud-Driss, *Familial amyotrophic lateral sclerosis, a historical perspective.* Acta myologica : myopathies and cardiomyopathies : official journal of the Mediterranean Society of Myology / edited by the Gaetano Conte Academy for the study of striated muscle diseases, 2011. **30**(2): p. 117-120.
8. Renton, A.E., et al., *A hexanucleotide repeat expansion in C9ORF72 is the cause of chromosome 9p21-linked ALS-FTD.* Neuron, 2011. **72**(2): p. 257-268.
9. DeJesus-Hernandez, M., et al., *Expanded GGGGCC hexanucleotide repeat in noncoding region of C9ORF72 causes chromosome 9p-linked FTD and ALS.* Neuron, 2011. **72**(2): p. 245-256.
10. Gijselinck, I., et al., *A C9orf72 promoter repeat expansion in a Flanders-Belgian cohort with disorders of the frontotemporal lobar degeneration-amyotrophic lateral sclerosis spectrum: a gene identification study.* Lancet Neurol, 2012. **11**(1): p. 54-65.
11. Boeynaems, S., et al., *Inside out: the role of nucleocytoplasmic transport in ALS and FTLD.* Acta Neuropathol, 2016. **132**(2): p. 159-73.
12. Zhang, K., et al., *Nucleocytoplasmic transport in C9orf72-mediated ALS/FTD.* Nucleus, 2016. **7**(2): p. 132-7.
13. Zhang, Y.J., et al., *Heterochromatin anomalies and double-stranded RNA accumulation underlie C9orf72 poly(PR) toxicity.* Science, 2019. **363**(6428).
14. Boeynaems, S., et al., *Drosophila screen connects nuclear transport genes to DPR pathology in c9ALS/FTD.* Sci Rep, 2016. **6**: p. 20877.
15. Shi, Y., et al., *Haploinsufficiency leads to neurodegeneration in C9ORF72 ALS/FTD human induced motor neurons.* Nat Med, 2018. **24**(3): p. 313-325.
16. Morris, H.R., et al., *Recent advances in the genetics of the ALS-FTLD complex.* Current neurology and neuroscience reports, 2012. **12**(3): p. 243-250.
17. Ciura, S., et al., *Loss of function of C9orf72 causes motor deficits in a zebrafish model of Amyotrophic Lateral Sclerosis.* Annals of Neurology, 2013.

18. Mackenzie, I.R., P. Frick, and M. Neumann, *The neuropathology associated with repeat expansions in the C9ORF72 gene.* Acta Neuropathol, 2014. **127**(3): p. 347-57.
19. Gao, F.B., S. Almeida, and R. Lopez-Gonzalez, *Dysregulated molecular pathways in amyotrophic lateral sclerosis-frontotemporal dementia spectrum disorder.* Embo j, 2017. **36**(20): p. 2931-2950.
20. Mori, K., et al., *Bidirectional transcripts of the expanded C9orf72 hexanucleotide repeat are translated into aggregating dipeptide repeat proteins.* Acta Neuropathol, 2013. **126**(6): p. 881-93.
21. Mori, K., et al., *The C9orf72 GGGGCC repeat is translated into aggregating dipeptide-repeat proteins in FTLD/ALS.* Science (New York, N.Y.), 2013. **339**(6125): p. 1335-1338.
22. Ash, P.E., et al., *Unconventional translation of C9ORF72 GGGGCC expansion generates insoluble polypeptides specific to c9FTD/ALS.* Neuron, 2013. **77**(4): p. 639-646.
23. Martier, R., et al., *Artificial MicroRNAs Targeting C9orf72 Can Reduce Accumulation of Intra-nuclear Transcripts in ALS and FTD Patients.* Mol Ther Nucleic Acids, 2019. **14**: p. 593-608.
24. Jovicic, A., et al., *Modifiers of C9orf72 dipeptide repeat toxicity connect nucleocytoplasmic transport defects to FTD/ALS.* Nat Neurosci, 2015. **18**(9): p. 1226-9.
25. Miller, R.G., et al., *Riluzole for amyotrophic lateral sclerosis (ALS)/motor neuron disease (MND).* Cochrane Database Syst Rev, 2002(2): p. Cd001447.
26. Takei, K., et al., *Post-hoc analysis of randomised, placebo-controlled, double-blind study (MCI186-19) of edaravone (MCI-186) in amyotrophic lateral sclerosis.* Amyotroph Lateral Scler Frontotemporal Degener, 2017. **18**(sup1): p. 49-54.
27. Cruz, M.P., *Edaravone (Radicava): A Novel Neuroprotective Agent for the Treatment of Amyotrophic Lateral Sclerosis.* P t, 2018. **43**(1): p. 25-28.
28. Hester, M.E., et al., *AAV as a gene transfer vector for the treatment of neurological disorders: novel treatment thoughts for ALS.* Current gene therapy, 2009. **9**(5): p. 428-433.
29. Schoch, K.M. and T.M. Miller, *Antisense Oligonucleotides: Translation from Mouse Models to Human Neurodegenerative Diseases.* Neuron, 2017. **94**(6): p. 1056-1070.
30. Fields, B.N., D.M. Knipe, and P.M. Howley, *Fields virology*. 2007, Philadelphia: Wolters Kluwer Health/Lippincott Williams & Wilkins.
31. De Jong, W.H. and P.J. Borm, *Drug delivery and nanoparticles:applications and hazards.* Int J Nanomedicine, 2008. **3**(2): p. 133-49.
32. Afione, S.A., et al., *In vivo model of adeno-associated virus vector persistence and rescue.* J Virol, 1996. **70**(5): p. 3235-41.
33. Berns, K.I., *The Gordon Wilson Lecture. From basic virology to human gene therapy.* Trans Am Clin Climatol Assoc, 1999. **110**: p. 75-85.
34. Berns, K.I. and N. Muzyczka, *AAV: An Overview of Unanswered Questions.* Hum Gene Ther, 2017. **28**(4): p. 308-313.

35. Flotte, T.R. and K.I. Berns, *Adeno-associated virus: a ubiquitous commensal of mammals.* Human Gene Therapy, 2005. **16**(4): p. 401-407.
36. Gruntman, A.M., et al., *Gene transfer in skeletal and cardiac muscle using recombinant adeno-associated virus.* Current protocols in microbiology, 2013. **Chapter 14**: p. Unit 14D.3.
37. McCarty, D.M., P.E. Monahan, and R.J. Samulski, *Self-complementary recombinant adeno-associated virus (scAAV) vectors promote efficient transduction independently of DNA synthesis.* Gene Ther, 2001. **8**(16): p. 1248-54.
38. Yan, Z., et al., *Trans-splicing vectors expand the utility of adeno-associated virus for gene therapy.* Proc Natl Acad Sci U S A, 2000. **97**(12): p. 6716-21.
39. Duque, S., et al., *Intravenous administration of self-complementary AAV9 enables transgene delivery to adult motor neurons.* Molecular therapy : the journal of the American Society of Gene Therapy, 2009. **17**(7): p. 1187-1196.
40. Foust, K.D., et al., *Intravascular AAV9 preferentially targets neonatal neurons and adult astrocytes.* Nat Biotechnol, 2009. **27**(1): p. 59-65.
41. Fu, H., et al., *Correction of neurological disease of mucopolysaccharidosis IIIB in adult mice by rAAV9 trans-blood-brain barrier gene delivery.* Molecular therapy : the journal of the American Society of Gene Therapy, 2011. **19**(6): p. 1025-1033.
42. Gray, S.J., et al., *Preclinical differences of intravascular AAV9 delivery to neurons and glia: a comparative study of adult mice and nonhuman primates.* Molecular therapy : the journal of the American Society of Gene Therapy, 2011. **19**(6): p. 1058-1069.
43. McLean, J.R., et al., *Widespread neuron-specific transgene expression in brain and spinal cord following synapsin promoter-driven AAV9 neonatal intracerebroventricular injection.* Neurosci Lett, 2014. **576**: p. 73-8.
44. Samaranch, L., et al., *Adeno-associated virus serotype 9 transduction in the central nervous system of nonhuman primates.* Human Gene Therapy, 2012. **23**(4): p. 382-389.
45. Schuster, D.J., et al., *Biodistribution of adeno-associated virus serotype 9 (AAV9) vector after intrathecal and intravenous delivery in mouse.* Front Neuroanat, 2014. **8**: p. 42.
46. Stoica, L., et al., *Adeno-associated virus-delivered artificial microRNA extends survival and delays paralysis in an amyotrophic lateral sclerosis mouse model.* Ann Neurol, 2016. **79**(4): p. 687-700.
47. Xie, J., et al., *MicroRNA-regulated, systemically delivered rAAV9: a step closer to CNS-restricted transgene expression.* Mol Ther, 2011. **19**(3): p. 526-35.
48. Mueller, C., et al., *Sustained miRNA-mediated knockdown of mutant AAT with simultaneous augmentation of wild-type AAT has minimal effect on global liver miRNA profiles.* Molecular therapy : the journal of the American Society of Gene Therapy, 2012. **20**(3): p. 590-600.
49. Mueller, C., et al., *5 Year Expression and Neutrophil Defect Repair after Gene Therapy in Alpha-1 Antitrypsin Deficiency.* Mol Ther, 2017. **25**(6): p. 1387-1394.
50. Wang, D., et al., *Adeno-Associated Virus Neutralizing Antibodies in Large Animals and Their Impact on Brain Intraparenchymal Gene Transfer.* Mol Ther Methods Clin Dev, 2018. **11**: p. 65-72.

51. Sathasivam, S., *Motor neurone disease: clinical features, diagnosis, diagnostic pitfalls and prognostic markers.* Singapore medical journal, 2010. **51**(5): p. 367-72; quiz 373.
52. Nowakowski, R.S., *Stable neuron numbers from cradle to grave.* Proc Natl Acad Sci U S A, 2006. **103**(33): p. 12219-20.
53. Harvey, R.J., M. Skelton-Robinson, and M.N. Rossor, *The prevalence and causes of dementia in people under the age of 65 years.* Journal of neurology, neurosurgery, and psychiatry, 2003. **74**(9): p. 1206-1209.
54. Mercy, L., et al., *Incidence of early-onset dementias in Cambridgeshire, United Kingdom.* Neurology, 2008. **71**(19): p. 1496-1499.
55. Ratnavalli, E., et al., *The prevalence of frontotemporal dementia.* Neurology, 2002. **58**(11): p. 1615-1621.
56. Williams, D.B., D.A. Floate, and J. Leicester, *Familial motor neuron disease: differing penetrance in large pedigrees.* Journal of the neurological sciences, 1988. **86**(2-3): p. 215-230.
57. Ferri, C.P., et al., *Global prevalence of dementia: a Delphi consensus study.* The Lancet, 2005. **366**(9503): p. 2112-2117.
58. de Lau, L.M. and M.M. Breteler, *Epidemiology of Parkinson's disease.* Lancet Neurol, 2006. **5**(6): p. 525-35.
59. Borel, F., M.A. Kay, and C. Mueller, *Recombinant AAV as a Platform for Translating the Therapeutic Potential of RNA Interference.* Mol Ther, 2013.
60. Davidson Bl Fau - McCray, P.B., Jr. and P.B. McCray, Jr., *Current prospects for RNA interference-based therapies.* (1471-0064 (Electronic)).
61. Napoli, C., C. Lemieux, and R. Jorgensen, *Introduction of a Chimeric Chalcone Synthase Gene into Petunia Results in Reversible Co-Suppression of Homologous Genes in trans.* Plant Cell, 1990. **2**(4): p. 279-289.
62. van der Krol, A.R., et al., *Flavonoid genes in petunia: addition of a limited number of gene copies may lead to a suppression of gene expression.* Plant Cell, 1990. **2**(4): p. 291-9.
63. Fire, A., et al., *Potent and specific genetic interference by double-stranded RNA in Caenorhabditis elegans.* Nature, 1998. **391**(6669): p. 806-11.
64. Vannini, A. and P. Cramer, *Conservation between the RNA polymerase I, II, and III transcription initiation machineries.* Mol Cell, 2012. **45**(4): p. 439-46.
65. Zamore, S.L.A.x.P.D., *Diversifying microRNA sequence and function.* Nature Reviews Molecular Cell Biology, 2013. **14**: p. 475-488.
66. Macrae, I.J., et al., *Structural basis for double-stranded RNA processing by Dicer.* Science, 2006. **311**(5758): p. 195-8.
67. Park, J.E., et al., *Dicer recognizes the 5' end of RNA for efficient and accurate processing.* Nature, 2011. **475**(7355): p. 201-5.
68. Zeng, Y., R. Yi, and B.R. Cullen, *Recognition and cleavage of primary microRNA precursors by the nuclear processing enzyme Drosha.* Embo j, 2005. **24**(1): p. 138-48.
69. Pan, Q., et al., *A dynamic perspective of RNAi library development.* Trends Biotechnol, 2012. **30**(4): p. 206-15.
70. Birmingham, A., et al., *3' UTR seed matches, but not overall identity, are associated with RNAi off-targets.* Nat Methods, 2006. **3**(3): p. 199-204.

71. Ossowski Stephan, F.J., Schwab Rebecca, Riester Markus and Weigel Detlef, personal communication. *WMD3 and AmiRNA*. 2005; Available from: http://wmd3.weigelworld.org/cgi-bin/webapp.cgi?page=About.
72. Grimm, D., *The dose can make the poison: lessons learned from adverse in vivo toxicities caused by RNAi overexpression.* Silence, 2011. **2**: p. 8.
73. Maczuga, P., et al., *Optimization and comparison of knockdown efficacy between polymerase II expressed shRNA and artificial miRNA targeting luciferase and Apolipoprotein B100.* BMC Biotechnol, 2012. **12**: p. 42.
74. Lorenz, R., et al., *ViennaRNA Package 2.0.* Algorithms Mol Biol, 2011. **6**: p. 26.
75. Auyeung, V.C., et al., *Beyond secondary structure: primary-sequence determinants license pri-miRNA hairpins for processing.* Cell, 2013. **152**(4): p. 844-58.
76. Han, J., et al., *The Drosha-DGCR8 complex in primary microRNA processing.* Genes Dev, 2004. **18**(24): p. 3016-27.
77. Zeng, Y. and B.R. Cullen, *Structural requirements for pre-microRNA binding and nuclear export by Exportin 5.* Nucleic Acids Res, 2004. **32**(16): p. 4776-85.
78. Chen, C.Z., et al., *MicroRNAs modulate hematopoietic lineage differentiation.* Science, 2004. **303**(5654): p. 83-6.
79. Gu, S., et al., *The loop position of shRNAs and pre-miRNAs is critical for the accuracy of dicer processing in vivo.* Cell, 2012. **151**(4): p. 900-11.
80. Lewis, B.P., et al., *Prediction of mammalian microRNA targets.* Cell, 2003. **115**(7): p. 787-98.
81. Siolas, D., et al., *Synthetic shRNAs as potent RNAi triggers.* Nat Biotechnol, 2005. **23**(2): p. 227-31.
82. Boudreau, R.L., A.M. Monteys, and B.L. Davidson, *Minimizing variables among hairpin-based RNAi vectors reveals the potency of shRNAs.* Rna, 2008. **14**(9): p. 1834-44.
83. Livak, K.J. and T.D. Schmittgen, *Analysis of relative gene expression data using real-time quantitative PCR and the 2(-Delta Delta C(T)) Method.* Methods (San Diego, Calif.), 2001. **25**(4): p. 402-408.
84. Mizielinska, S. and A.M. Isaacs, *C9orf72 amyotrophic lateral sclerosis and frontotemporal dementia: gain or loss of function?* Curr Opin Neurol, 2014. **27**(5): p. 515-23.
85. Therrien, M., et al., *Deletion of C9ORF72 results in motor neuron degeneration and stress sensitivity in C. elegans.* PLoS One, 2013. **8**(12): p. e83450.
86. Ciura, S., et al., *Loss of function of C9orf72 causes motor deficits in a zebrafish model of Amyotrophic Lateral Sclerosis.* Ann Neurol, 2013.
87. Almeida, S., et al., *Modeling key pathological features of frontotemporal dementia with C9ORF72 repeat expansion in iPSC-derived human neurons.* Acta Neuropathol, 2013. **126**(3): p. 385-99.
88. Donnelly, C.J., et al., *RNA toxicity from the ALS/FTD C9ORF72 expansion is mitigated by antisense intervention.* Neuron, 2013. **80**(2): p. 415-28.
89. Lagier-Tourenne, C., et al., *Targeted degradation of sense and antisense C9orf72 RNA foci as therapy for ALS and frontotemporal degeneration.* Proc Natl Acad Sci U S A, 2013. **110**(47): p. E4530-9.

90. Sareen, D., et al., *Targeting RNA foci in iPSC-derived motor neurons from ALS patients with a C9ORF72 repeat expansion.* Sci Transl Med, 2013. **5**(208): p. 208ra149.
91. Janssens, J. and C. Van Broeckhoven, *Pathological mechanisms underlying TDP-43 driven neurodegeneration in FTLD-ALS spectrum disorders.* Hum Mol Genet, 2013. **22**(R1): p. R77-87.
92. Rohrer, J.D., et al., *C9orf72 expansions in frontotemporal dementia and amyotrophic lateral sclerosis.* Lancet Neurol, 2015.
93. Geevasinga, N., et al., *Cortical Function in Asymptomatic Carriers and Patients With C9orf72 Amyotrophic Lateral Sclerosis.* JAMA Neurol, 2015: p. 1-7.
94. Alfieri, J.A., N.S. Pino, and L.M. Igaz, *Reversible behavioral phenotypes in a conditional mouse model of TDP-43 proteinopathies.* J Neurosci, 2014. **34**(46): p. 15244-59.
95. Filiano, A.J., et al., *Dissociation of frontotemporal dementia-related deficits and neuroinflammation in progranulin haploinsufficient mice.* J Neurosci, 2013. **33**(12): p. 5352-61.
96. Prudencio, M., et al., *Distinct brain transcriptome profiles in C9orf72-associated and sporadic ALS.* Nat Neurosci, 2015. **18**(8): p. 1175-82.
97. Mizielinska, S., et al., *C9orf72 frontotemporal lobar degeneration is characterised by frequent neuronal sense and antisense RNA foci.* Acta Neuropathol, 2013. **126**(6): p. 845-57.
98. Esanov, R., et al., *A C9ORF72 BAC mouse model recapitulates key epigenetic perturbations of ALS/FTD.* Mol Neurodegener, 2017. **12**(1): p. 46.
99. O'Rourke, J.G., et al., *C9orf72 BAC Transgenic Mice Display Typical Pathologic Features of ALS/FTD.* Neuron, 2015. **88**(5): p. 892-901.
100. Pfister, E.L., et al., *Safe and Efficient Silencing with a Pol II, but Not a Pol lII, Promoter Expressing an Artificial miRNA Targeting Human Huntingtin.* Mol Ther Nucleic Acids, 2017. **7**: p. 324-334.
101. Batra, R. and C.W. Lee, *Mouse Models of C9orf72 Hexanucleotide Repeat Expansion in Amyotrophic Lateral Sclerosis/ Frontotemporal Dementia.* Front Cell Neurosci, 2017. **11**: p. 196.
102. Peters, O.M., et al., *Human C9ORF72 Hexanucleotide Expansion Reproduces RNA Foci and Dipeptide Repeat Proteins but Not Neurodegeneration in BAC Transgenic Mice.* Neuron, 2015. **88**(5): p. 902-909.
103. Bak, M., et al., *MicroRNA expression in the adult mouse central nervous system.* Rna, 2008. **14**(3): p. 432-44.
104. Adlakha, Y.K. and N. Saini, *Brain microRNAs and insights into biological functions and therapeutic potential of brain enriched miRNA-128.* Mol Cancer, 2014. **13**: p. 33.
105. Bartel, D.P., *MicroRNAs: genomics, biogenesis, mechanism, and function.* (0092-8674 (Print)).
106. Ambros, V., *The evolution of our thinking about microRNAs.* Nat Med, 2008. **14**(10): p. 1036-40.
107. Hoffer, P., et al., *Posttranscriptional gene silencing in nuclei.* Proceedings of the National Academy of Sciences of the United States of America, 2011. **108**(1): p. 409-414.

108. Huang, V. and L.C. Li, *miRNA goes nuclear.* RNA biology, 2012. **9**(3): p. 269-273.
109. Nishi, K., et al., *Human TNRC6A is an Argonaute-navigator protein for microRNA-mediated gene silencing in the nucleus.* RNA (New York, N.Y.), 2013. **19**(1): p. 17-35.
110. Jiang, J., et al., *Gain of Toxicity from ALS/FTD-Linked Repeat Expansions in C9ORF72 Is Alleviated by Antisense Oligonucleotides Targeting GGGGCC-Containing RNAs.* Neuron, 2016. **90**(3): p. 535-50.
111. Borel, F., et al., *Therapeutic rAAVrh10 Mediated SOD1 Silencing in Adult SOD1(G93A) Mice and Nonhuman Primates.* Hum Gene Ther, 2016. **27**(1): p. 19-31.
112. Borel, F., et al., *Safe and effective superoxide dismutase 1 silencing using artificial microRNA in macaques.* Sci Transl Med, 2018. **10**(465).
113. Pfister, E.L., et al., *Artificial miRNAs Reduce Human Mutant Huntingtin Throughout the Striatum in a Transgenic Sheep Model of Huntington's Disease.* Hum Gene Ther, 2018. **29**(6): p. 663-673.
114. Niblock, M., et al., *Retention of hexanucleotide repeat-containing intron in C9orf72 mRNA: implications for the pathogenesis of ALS/FTD.* Acta Neuropathol Commun, 2016. **4**: p. 18.
115. Sznajder, L.J., et al., *Intron retention induced by microsatellite expansions as a disease biomarker.* Proc Natl Acad Sci U S A, 2018. **115**(16): p. 4234-4239.
116. Tabet, R., et al., *CUG initiation and frameshifting enable production of dipeptide repeat proteins from ALS/FTD C9ORF72 transcripts.* Nat Commun, 2018. **9**(1): p. 152.
117. Zhang, Y.J., et al., *Poly(GR) impairs protein translation and stress granule dynamics in C9orf72-associated frontotemporal dementia and amyotrophic lateral sclerosis.* Nat Med, 2018. **24**(8): p. 1136-1142.
118. Martier, R., et al., *Targeting RNA-Mediated Toxicity in C9orf72 ALS and/or FTD by RNAi-Based Gene Therapy.* Molecular Therapy - Nucleic Acids, 2019. **16**: p. 26-37.
119. Donnelly, C.J., et al., *RNA toxicity from the ALS/FTD C9ORF72 expansion is mitigated by antisense intervention.* Neuron, 2013. **80**(2): p. 415-28.
120. Jiang, J., et al., *Gain of Toxicity from ALS/FTD-Linked Repeat Expansions in C9ORF72 Is Alleviated by Antisense Oligonucleotides Targeting GGGGCC-Containing RNAs.* Neuron, 2016. **90**(3): p. 535-550.
121. Peters, O.M., et al., *Human C9ORF72 Hexanucleotide Expansion Reproduces RNA Foci and Dipeptide Repeat Proteins but Not Neurodegeneration in BAC Transgenic Mice.* Neuron, 2015. **88**(5): p. 902-909.
122. Liu, Y.J., et al., *C9orf72 BAC Mouse Model with Motor Deficits and Neurodegenerative Features of ALS/FTD.* Neuron, 2016. **90**(3): p. 521-534.
123. Evers, M.M., L.J.A. Toonen, and W.M.C. van Roon-Mom, *Antisense oligonucleotides in therapy for neurodegenerative disorders.* Advanced Drug Delivery Reviews, 2015. **87**: p. 90-103.
124. Flotte, T.R., et al., *Phase 2 clinical trial of a recombinant adeno-associated viral vector expressing alpha1-antitrypsin: interim results.* Hum Gene Ther, 2011. **22**(10): p. 1239-47.

125. Loring, H.S. and T.R. Flotte, *Current status of gene therapy for alpha-1 antitrypsin deficiency.* Expert Opin Biol Ther, 2015. **15**(3): p. 329-36.
126. Mendell, J.R., et al., *Single-Dose Gene-Replacement Therapy for Spinal Muscular Atrophy.* New England Journal of Medicine, 2017. **377**(18): p. 1713-1722.
127. DeJesus-Hernandez, M., et al., *Expanded GGGGCC hexanucleotide repeat in noncoding region of C9ORF72 causes chromosome 9p-linked FTD and ALS.* Neuron, 2011. **72**(2): p. 245-56.
128. Renton, A.E., et al., *A hexanucleotide repeat expansion in C9ORF72 is the cause of chromosome 9p21-linked ALS-FTD.* Neuron, 2011. **72**(2): p. 257-68.
129. Zu, T., et al., *RAN proteins and RNA foci from antisense transcripts in C9ORF72 ALS and frontotemporal dementia.* Proc Natl Acad Sci U S A, 2013. **110**(51): p. E4968-77.
130. Freibaum, B.D., et al., *GGGGCC repeat expansion in C9orf72 compromises nucleocytoplasmic transport.* Nature, 2015. **525**(7567): p. 129-33.
131. Zhang, K., et al., *The C9orf72 repeat expansion disrupts nucleocytoplasmic transport.* Nature, 2015. **525**(7567): p. 56-61.
132. Belzil, V.V., R.B. Katzman, and L. Petrucelli, *ALS and FTD: an epigenetic perspective.* Acta Neuropathologica, 2016. **132**(4): p. 487-502.
133. Evans-Galea, M.V., et al., *Epigenetic modifications in trinucleotide repeat diseases.* Trends in Molecular Medicine, 2013. **19**(11): p. 655-663.
134. Yandim, C., T. Natisvili, and R. Festenstein, *Gene regulation and epigenetics in Friedreich's ataxia.* Journal of Neurochemistry, 2013. **126**: p. 21-42.
135. Belzil, V.V., et al., *Reduced C9orf72 gene expression in c9FTD/ALS is caused by histone trimethylation, an epigenetic event detectable in blood.* Acta Neuropathol, 2013. **126**(6): p. 895-905.
136. Belzil, V.V., et al., *Characterization of DNA hypermethylation in the cerebellum of c9FTD/ALS patients.* Brain Res, 2014. **1584**: p. 15-21.
137. Xi, Z., et al., *Hypermethylation of the CpG-island near the C9orf72 G(4)C(2)-repeat expansion in FTLD patients.* Hum Mol Genet, 2014. **23**(21): p. 5630-7.
138. Xi, Z., et al., *Hypermethylation of the CpG island near the G4C2 repeat in ALS with a C9orf72 expansion.* Am J Hum Genet, 2013. **92**(6): p. 981-9.
139. Liu, E.Y., et al., *C9orf72 hypermethylation protects against repeat expansion-associated pathology in ALS/FTD.* Acta Neuropathol, 2014. **128**(4): p. 525-41.
140. McMillan, C.T., et al., *C9orf72 promoter hypermethylation is neuroprotective: Neuroimaging and neuropathologic evidence.* Neurology, 2015. **84**(16): p. 1622-30.
141. Esanov, R., et al., *C9orf72 promoter hypermethylation is reduced while hydroxymethylation is acquired during reprogramming of ALS patient cells.* Exp Neurol, 2016. **277**: p. 171-7.
142. Reddy, K., et al., *Processing of double-R-loops in (CAG).(CTG) and C9orf72 (GGGGCC).(GGCCCC) repeats causes instability.* Nucleic Acids Res, 2014. **42**(16): p. 10473-87.
143. Ginno, P.A., et al., *R-loop formation is a distinctive characteristic of unmethylated human CpG island promoters.* Mol Cell, 2012. **45**(6): p. 814-25.

144. Groh, M., et al., *R-loops associated with triplet repeat expansions promote gene silencing in Friedreich ataxia and fragile X syndrome.* PLoS Genet, 2014. **10**(5): p. e1004318.
145. O'rourke, J.G., et al., *C9orf72 BAC Transgenic Mice Display Typical Pathologic Features of ALS/FTD.* Neuron, 2015. **88**(5): p. 892-901.
146. Cohen-Hadad, Y., et al., *Marked Differences in C9orf72 Methylation Status and Isoform Expression between C9/ALS Human Embryonic and Induced Pluripotent Stem Cells.* Stem Cell Reports, 2016. **7**(5): p. 927-940.
147. Zeier, Z., et al., *Bromodomain inhibitors regulate the C9ORF72 locus in ALS.* Exp Neurol, 2015.
148. Xi, Z., et al., *The C9orf72 repeat expansion itself is methylated in ALS and FTLD patients.* Acta Neuropathol, 2015. **129**(5): p. 715-27.
149. Esanov, R., et al., *The FMR1 promoter is selectively hydroxymethylated in primary neurons of fragile X syndrome patients.* Human Molecular Genetics, 2016.
150. Globisch, D., et al., *Tissue distribution of 5-hydroxymethylcytosine and search for active demethylation intermediates.* PLoS One, 2010. **5**(12): p. e15367.
151. Kinney, S.M., et al., *Tissue-specific distribution and dynamic changes of 5-hydroxymethylcytosine in mammalian genomes.* J Biol Chem, 2011. **286**(28): p. 24685-93.
152. Colak, D., et al., *Promoter-bound trinucleotide repeat mRNA drives epigenetic silencing in fragile X syndrome.* Science, 2014. **343**(6174): p. 1002-5.
153. Bauer, P.O., *Methylation of C9orf72 expansion reduces RNA foci formation and dipeptide-repeat proteins expression in cells.* Neuroscience Letters, 2016. **612**: p. 204-209.
154. Kaas, G.A., et al., *TET1 controls CNS 5-methylcytosine hydroxylation, active DNA demethylation, gene transcription, and memory formation.* Neuron, 2013. **79**(6): p. 1086-93.
155. Kriaucionis, S. and N. Heintz, *The nuclear DNA base 5-hydroxymethylcytosine is present in Purkinje neurons and the brain.* Science, 2009. **324**(5929): p. 929-30.
156. Zamiri, B., et al., *Quadruplex formation by both G-rich and C-rich DNA strands of the C9orf72 (GGGGCC)8,Ä¢(GGCCCC)8 repeat: effect of CpG methylation.* Nucleic Acids Research, 2015. **43**(20): p. 10055-10064.
157. Wang, J., A.R. Haeusler, and E.A. Simko, *Emerging role of RNA center dot DNA hybrids in C9orf72-linked neurodegeneration.* Cell Cycle, 2015. **14**(4): p. 526-532.
158. Su, Z., et al., *Discovery of a biomarker and lead small molecules to target r(GGGGCC)-associated defects in c9FTD/ALS.* Neuron, 2014. **83**(5): p. 1043-50.
159. Loomis, E.W., et al., *Transcription-Associated R-Loop Formation across the Human FMR1 CGG-Repeat Region.* Plos Genetics, 2014. **10**(4).
160. Bejaoui, K., et al., *SPTLC1 is mutated in hereditary sensory neuropathy, type 1.* Nat Genet, 2001. **27**(3): p. 261-2.
161. Penno, A., et al., *Hereditary sensory neuropathy type 1 is caused by the accumulation of two neurotoxic sphingolipids.* J Biol Chem, 2010. **285**(15): p. 11178-87.

162. Eichler, F.S., et al., *Overexpression of the wild-type SPT1 subunit lowers desoxysphingolipid levels and rescues the phenotype of HSAN1.* J Neurosci, 2009. **29**(46): p. 14646-51.
163. Garofalo, K., et al., *Oral L-serine supplementation reduces production of neurotoxic deoxysphingolipids in mice and humans with hereditary sensory autonomic neuropathy type 1.* J Clin Invest, 2011. **121**(12): p. 4735-45.
164. Fridman, V., et al., *Randomized trial of l-serine in patients with hereditary sensory and autonomic neuropathy type 1.* Neurology, 2019. **92**(4): p. e359-e370.
165. McCampbell, A., et al., *Mutant SPTLC1 dominantly inhibits serine palmitoyltransferase activity in vivo and confers an age-dependent neuropathy.* Hum Mol Genet, 2005. **14**(22): p. 3507-21.
166. Toro Cabrera, G. and C. Mueller, *Design of shRNA and miRNA for Delivery to the CNS.* Methods Mol Biol, 2016. **1382**: p. 67-80.